STUDIES OF LOW ENERGY ANOMALOUS AND GALACTIC COSMIC RAYS IN NEAR-EARTH-SPACE

by

Anjan Dutta
Physical Research Laboratory
Ahmedabad-380009, India

A thesis
submitted to the
Gujarat University
for the degree of
Doctor of Philosophy

June 1991

Physical Research Laboratory
Ahmedabad 380 009, India

CERTIFICATE

I hereby declare that the work presented in this thesis is original and has not formed the basis for the award of any degree or diploma by any University or Institution.

Anjan Dutta

Anjan Dutta

(Author)

Certified by:

Rao M.N.

M.N.Rao

(Thesis Supervisor)

June , 1991

Dedicated

to my

Parents

Abstract

The interplanetary space in the vicinity of the earth have many components of energetic charged particles. The Solar Wind (SW) particles with energies ≤1 KeV/n, emitted continuously from the Sun, dominate at low energies. In the energy interval of ~ 1 - 100 MeV/n, the Solar Energetic Particles (SEP), emitted sporadically from the Sun during solar flares, are most abundant. Above 100 MeV/n and up to energies of TeV/n and more we have Galactic Cosmic Rays (GCR) coming from outside the solar system. In the energy range of 1-30 MeV/n, a new component of energetic particles was discovered in nearby interplanetary space during solar quiet period in the early seventies. The most characteristic feature of this component is the overabundance of He, N, O and Ne relative to C compared to their abundances in SEP and GCR. While the GCR energy spectrum in this low energy range show a positive power law index in energy, the spectra of this new component has a negative power law index. Because of these peculiar features and unknown source and origin, this new component was termed Anomalous Cosmic Rays (ACR).

The ionization states of the energetic particles of solar and extra-solar origin provide clues to the plasma conditions (*e.g* temperature, density etc.) prevailing at their source regions and at their acceleration sites and also of the processes occurring during their interstellar and interplanetary propagation. The ionization states of low energy SW and SEP particles are well studied earlier, using electrostatic charge analyzers, which revealed the presence of partially ionized particles in both SW and SEP. In the case of GCR, available data on the electron capture and stripping cross sections, and the large amount of matter traversal during their interstellar propagation, predict their equilibrium charge states to be fully ionized for energies >10 MeV/n. Although the ionization states of high energy (>1 GeV/n) GCR particles were inferred to be fully ionized from the measured dependence of their flux on the geomagnetic latitude, no attempt has been made so far to determine the ionization states of low energy (≤100 MeV/n) GCR particles. Such a determination is important as there could be differences in the

propagation histories of low and high energy galactic cosmic rays. The ionization state of the ACR component, which is one of the key parameter in all the models proposed for its source and origin, have also not been measured directly until recently. Indirect inferences for a partial ionization state of ACR particles have been drawn from several experiments. One such experiment was conducted in 1973 using the Skylab platform ($\lambda = \pm 50^0$, altitude = 435 km), which provided the first indirect hint that the ACR particles are in partially ionized states. This inference was based on the observation of high fluences of low energy CNO group particles that are geomagnetically forbidden at the Skylab orbit. The similarity in the composition of these particles with that of the ACR component led to the suggestion that they are indeed a part of ACR, and, these particles could be observed inside the magnetosphere only because of their partial ionization states and hence higher effective rigidities.

The direct determination of the ionization states of ACR particles as well as that of low energy GCR particles have been accomplished recently by us based on the data obtained from the Indian cosmic ray experiment '*Anuradha*' flown on board Space Shuttle Spacelab-3 during April-May,1985. This experiment takes advantage of the presence of the low energy ACR and GCR particles inside the earth's magnetosphere and use the geomagnetic field as a rigidity filter to determine their ionization states. The present thesis mainly deals with the results obtained from this experiment, and their implication towards understanding the source and origin of the ACR as well as the characteristics of the low energy GCR particles in the near-earth-space. Since the approach of using the geomagnetic field as a rigidity filter to determine the ionization states of low energy charged particles has not been utilized before, we have also made a special effort to check the validity of the geomagnetic transmission factor calculated using the International Geomagnetic Reference Field model and trajectory-tracing method.

The main topics on which results and discussion are presented in this thesis are :

1) GCR oxygen ion flux in the energy interval (50-250 MeV/n) inside the magnetosphere and a check on the validity of the calculated geomagnetic transmission factor.

2) Ionization states of anomalous cosmic rays (ACR) and the implications of the results concerning the source and origin of the ACR.

3) New results on the ionization states of low energy (<125 MeV/n) particles (6 <Z <28) of GCR origin and their implications.

The basic structure of the thesis is as follows:

The general features of the energetic particles in the near-earth-space *viz.* the SW, SEP, magnetospheric, ACR and GCR alongwith the present knowledge about their ionization states are discussed in the first chapter.

In the second chapter we discuss the method followed in the present work to determine the ionization state(s) of low energy particles and the Nuclear Track technique used to determine the atomic number, mass and energy of the charged particles based on the records left by them in the plastic (CR-39) detectors used in the *Anuradha* experiment. A brief description of the instrument is also given in this chapter.

Calibration of the detector, data acquisition procedures, error estimation etc. are outlined briefly in the third chapter.

In the fourth chapter we present the results on the calculated values of the orbit-averaged geomagnetic cutoff rigidity obtained by trajectory-tracing method and the deduced transmission factors at the Spacelab-3 orbit as a function of the rigidity of the charged particles. Results obtained on the orbit-averaged flux of the low energy (50-250 MeV/n) GCR oxygen at the Spacelab-3 orbit are presented alongwith a discussion on the validity of the calculated geomagnetic transmission factors. Finally, the method used to

calculate the threshold rigidity of individual ions is also discussed in this chapter.

In the fifth chapter we present new result on the observation of low energy (20-125 MeV/n) partially ionized iron group ions and discuss why we consider GCR as their most plausible source. We then present a plausible model for the origin of these partially ionized heavier ions assuming them to be of GCR origin. The results on the ionization state of ACR particles alongwith their implications are also presented in this chapter.

A summary of the results alongwith their implications and scope for further work are discussed in the sixth chapter.

The results presented in this thesis are summarized below.

We have measured the orbit-averaged GCR oxygen ion flux in the energy interval 50-250 MeV/n from an analysis of the track records in the detector stacks flown on the *Anuradha* experiment on board space shuttle Spacelab-3. To obtain the corresponding GCR oxygen flux in the interplanetary space we have calculated the Spacelab-3 orbit-averaged geomagnetic transmission factor by using the 1985 reference geomagnetic field model. The geomagnetic cutoff rigidities are obtained by the trajectory-tracing method. The average rigidities for 5^0 latitude x 5^0 longitude grids are calculated and the time spent by the Spacecraft in each of these grids were considered in calculating the orbit-averaged geomagnetic transmission factor. The interplanetary fluxes derived from the present experiment for three energy bands and the corresponding expected fluxes in units of $p/(m^2.sr.sec.MeV/n)$ are: $(1.73\pm1.00)\times10^{-3}$ and 2.2×10^{-3} (45±10 MeV/n), $(3.12\pm1.38)\times10^{-3}$ and 4.2×10^{-3} (121±37 MeV/n) and $(4.96\pm3.46)\times10^{-3}$ and 5.0×10^{-3} (235±72 MeV/n) respectively. These two sets of fluxes compare well within the error limits. We have also calculated the modulation parameter ϕ from the interplanetary oxygen flux derived by us, and compared this value with the ϕ values for proton and helium for the 1985-86 epoch. The normalized modulation parameter $\Phi = (\frac{A}{Z} * \phi)$ obtained for proton,

helium and oxygen are 650±20, 670±40 and 640±60 MV respectively. The close agreement between the derived and the expected interplanetary oxygen fluxes and in Φ values for p, He and O give us good confidence in the validity of the calculated orbit-averaged geomagnetic transmission factors and hence on the cutoff rigidity values obtained by the trajectory-tracing method using the 1985 geomagnetic reference field model.

Unambiguous determination of the ionization states of a total of 13 ACR events have been accomplished from the data obtained from the *Anuradha* experiment in this and earlier work. Out of these, nine events (1 nitrogen, 5 oxygen and 3 neon) have ionization states of 1^+. The ionization states of the other four ACR particles are also consistent with their being in 1^+ state. These results from the *Anuradha* experiment thus support the suggestion that the local interstellar neutrals are the source of ACR. In this model the neutral atoms from the nearby interstellar medium enter into the solar system and get singly ionized by solar ultraviolet rays and by charge exchange process with the solar wind. After ionization they propagate away from Sun alongwith the solar wind and are accelerated to the observed energies perhaps in the heliospheric boundary, before diffusing back into the heliosphere, where we observe them as Anomalous Cosmic Rays.

The experimental and analytical methods used for determining the ionization states of ACR particles were also used to determine the ionization states of low energy (≤125 MeV/n) heavier ions ($6 \leq Z \leq 28$) that were recorded in the *Anuradha* detector. A total of 26 events out of 46, for which the ionization states could be determined, are found to be in fully ionized state. An additional 4 events are most probably fully ionized, if we consider the extreme limits of experimental uncertainty. The remaining 16 events are definitely in partially ionized states. These include one Titanium (6^+), two Vanadium (10^+, 16^+), two Chromium (5^+, 8^+), one Manganese (4^+), eight Iron (3^+, 3^+, 10^+, 11^+, 14^+, 14^+, 20^+, 20^+) and two Nickel (8^+, 14^+) ions. We have good confidence in these new results because the use of the same experimental setup and analytical

procedures yielded results that showed that the ACR particles are singly ionized and most of the GCR particles are fully ionized, which are in good agreement with our present knowledge about the ionization states of these components. The results obtained by us therefore suggest that ~25- 30% of the low energy (<125 MeV/n) heavy ions are in partially ionized states. We, therefore believe that a new component of partially ionized low energy iron group particles is present in the near-earth-space.

Because of the entirely unexpected nature of the results we have made a detailed analysis for the possible sources of these particles viz. anomalous cosmic rays, solar energetic particles, magnetospheric particles and galactic cosmic rays, and, conclude that they are of GCR origin. We also present in the thesis a plausible model for the generation of partially ionized low energy galactic cosmic rays. We postulate the presence of a low energy (1-10 MeV/n) partially ionized GCR component outside the solar system. Such a component could simply represent the low energy steady-state local interstellar GCR spectra or could be produced through trapping of high energy (up to few hundred MeV/n) GCR particles in large molecular clouds in nearby interstellar space, where a fraction of them suffer degradation in energy to ~1-10 MeV/n and gets partially ionized through electron capture. Acceleration of this low energy partially ionized GCR component to the observed energies can take place in the heliospheric boundary. Further work will be needed to properly understand the different aspects of this new component.

Acknowledgements

I am grateful to my thesis supervisor Prof. M.N.Rao for fruitful discussions and many helpful comments on my work. I sincerely acknowledge his encouragement during the course of this work. It is a great pleasure to acknowledge my guide Prof. J.N.Goswami who has introduced me to the fascinating field of cosmic rays. His encouragement, valuable criticism and occasional blasting helped me in many ways. I thank him for carefully reading the manuscript and suggesting important changes.

I am fortunate to be associated with Prof. S.Biswas, principal investigator of the Anuradha experiment, and Prof N.Durgaprasad, both from the Tata Institute of Fundamental Research. I owe a great deal to them for many stimulating discussions, and sincerely thank them for constant encouragement and advice. My deep reverence to Prof. D.Lal for his encouragement. My sincere gratitude to Dr. D.P.Dewangan and Prof. N.Bhandari for many helpful discussions and to Dr. G.Subramaniam, Dr. S.K.Bhattacharya and Dr. R.Ramesh for critically evaluating this work and also for going through the manuscript.

I am grateful to NASA for providing the opportunity to conduct the Anuradha experiment onboard Space Shuttle Spacelab-3. I am also thankful to the following facilities: Variable Energy Cyclotron Center, Calcutta, Dubna Accelerator Facility, USSR and Bevalac of Lawrence Berkeley Laboratory, USA, for providing us with beams of energetic helium and heavy ions for calibration. I must thank our Electronics lab members, especially H.S.Mazumdar, D.V.Subhedar, S.N.Pradhan and N.Dutta for designing and fabricating the electronics for the experiment.

My thanks to Nirjhari and Deomurari for their help rendered during scanning and computation. They alongwith Srini and V.G.Shah provided a conducive atmosphere in the lab, where work was a pleasure.

I thank all the members of the Geocosmophysics group, with whom I have been continually associated over the last several years, for providing me a very congenial atmosphere for research. I would like to thank Prof. B.L.K.Somayajulu and Prof S.Krishnaswami for their constant encouragement. My special thanks to J.P.Bhavsar who was always ready to help me.

My sincere thanks to TIFR group members, namely P.J.Kajarekar, B.Mitra, R.K.Singh, M.N.Vahia and J.S.Yadav for many scientific help and also to R.B.Bulsara, S.P.Prabhudesai, V.M.Patel, P.K.Pawar, A.K.Samant, S.Savitri, P.H.Umadikar for skilled technical assistance.

I must mention about the PRL facilities, in particular the prompt, helpful and friendly atmosphere in the library. My thanks are due to Mr.Ranpura and Mr. S.C.Bhavsar for their efficient and skillful photography and drafting.

It is time I should take note of the nonsingular existence of my being which is largely due to the warmth and love of Bhushan, Navin, Sarkar and Pandey. I sincerely thank them who helped in many ways in expediting the completion of the thesis. I must thank all my friends in PRL who have helped me unfailingly in keeping mood and spirits high.

To my family members, without whose inspiration and moral support I might not have been able to cross the finishing line. To Jaya, whose deserted evenings are described in the following pages.

LIST OF CONTENTS

5. RESULTS AND DISCUSSION.

Part-I: ANOMALOUS COSMIC RAYS

Part-II: LOW ENERGY (20-125 MeV/n) GALACTIC COSMIC RAYS

6. CONCLUSIONS

LIST OF ILLUSTRATIONS

LIST OF TABLES

CHAPTER I

INTRODUCTION

The energetic charged particles observed in the interplanetary space in the vicinity of the earth have many components. At the lowest end of energy we have the Solar Wind (SW) plasma emitted continuously from the Sun with energies ≤1 KeV/n. In the energy interval ~1-100 MeV/n, the Solar Energetic Particles (SEP), emitted sporadically from the Sun during solar flares, is the major component. Above 100 MeV/n and up to energies of TeV/n and more we have Galactic Cosmic Rays (GCR) coming from outside the solar system. The main constituent of all these components is proton with a few percent helium. Heavier particles are also present but their abundance is extremely small (~1% of the total). A new component of energetic particles, in the energy range of 1-30 MeV/n, was discovered in nearby interplanetary space during the solar quiet period in early seventies (Hovestadt *et al.*,1973; Garcia-Munoz *et al.*,1973; McDonald *et al.*,1974). The most characteristic feature of this component is the overabundance of He, N, O and Ne relative to C compared to their abundances in SEP and GCR. While the GCR energy spectrum in this low energy range shows a positive power law index in energy, the spectrum of this new component has a negative power law index. Because of these peculiar features and unknown source and origin, this new component was termed Anomalous Cosmic Rays (ACR).

Much closer to the earth , within the earth's magnetosphere,

the entry of the low energy SEP and GCR is controlled by the geomagnetic field. Low energy SEP and GCR particles can have access only in the polar region, while the high energy GCR particles can reach the top of the earth's atmosphere at lower latitudes depending on their energy. In addition there are two zones within the magnetosphere which are populated with energetic protons and electrons. These zones are known as Van Allen radiation belts, and the particles are termed as geomagnetically trapped particles.

A very significant observation made in 1973, relates to the presence of high fluence of geomagnetically forbidden low energy (<30 MeV/n) C, N, O particles in an experiment conducted using the Skylab platform [Biswas *et al.*,1975; Chan and Price,1975; Biswas and Durgaprasad,1980]. The cutoff energy for the Skylab orbit ($\lambda = \pm 50^0$, altitude= 435 km), for fully ionized particles with mass to atomic number ratio (A/Z) of 2 was ~50 MeV/n. The observation of the forbidden particles, coupled with the fact that their composition resembles more with the newly discovered ACR component rather than solar or galactic cosmic ray composition , led Biswas *et al.*[1975] to suggest that this component is related to ACR. It was implicit in this suggestion, that the ACR component is partially ionized, which allowed these low energy particles to reach the Skylab orbit, due to their higher magnetic rigidities.

Fig 1-1 shows a composite spectra of the major components of energetic charged particles, observed in the near-earth-space. A brief description of each of these components is given in the following sections.

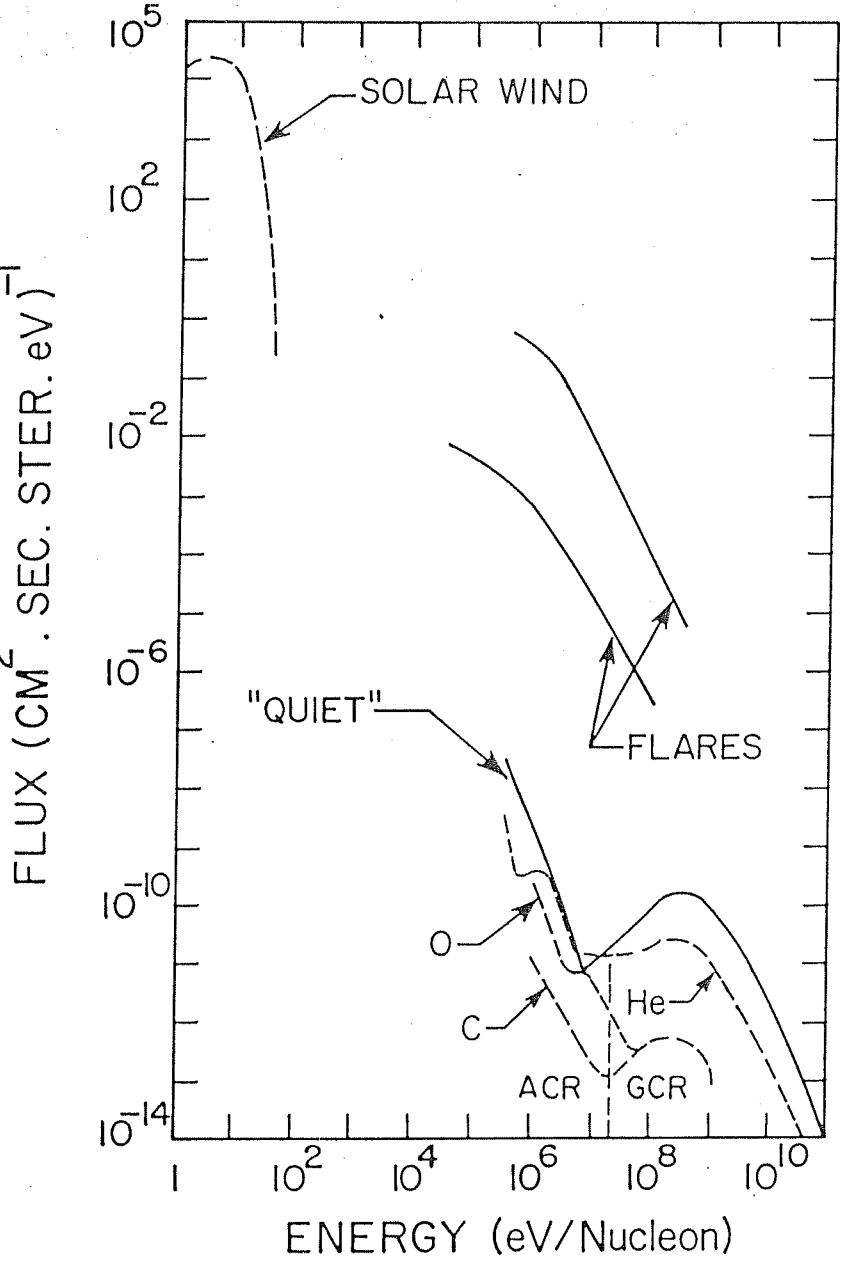

Fig.1-1 Energy spectra of Solar Wind, Anomalous Cosmic Rays, Galactic Cosmic Rays and Solar Flare particles measured at 1 AU. [From Lin, 1981]

1.1 Energetic Particles in the near-earth-space

1.1.1 Galactic Cosmic Rays

The energetic particle population in the interplanetary space at energies above a few hundred MeV/n is dominated by the galactic cosmic rays. 98% of these particles are nucleons and the remaining 2% are electrons and positrons [Simpson, 1983a]. The nucleonic component of GCR consists of 87% proton, ~12% helium and ~1% heavier nuclei from carbon to actinides. Detailed information on the composition and energy spectra of all the elements up to iron and the general features of trans-iron nuclei are available at present [Simpson,1983a; Binns *et al.*,1989]. In fig.1-2 we show the differential energy spectra of some of the major elements in GCR (proton, helium, carbon and iron) in the energy range 10 to 10^7 MeV/n at 1 AU (Astronomical Unit). All these spectra could be represented by a power law in energy of the form $dJ \propto E^{-\gamma}dE$, with a value of the spectral index $\gamma \simeq 2.6$. The deviation from this power law at < 5000 MeV/n is due to the loss in energy and consequent decrease in particle flux by the interaction of incoming GCR particles with the magnetic irregularities, carried by the outgoing solar wind. The decrease in flux of the GCR particles is higher during high solar activity when the magnetic irregularities of the solar wind increase. Thus GCR flux at energies below a few GeV/n is inversely correlated with the solar activity. This is termed as the solar modulation, which follows the well-known 11 year cycle; one finds a variation in the flux of GCR particles by a factor of ~2 (at

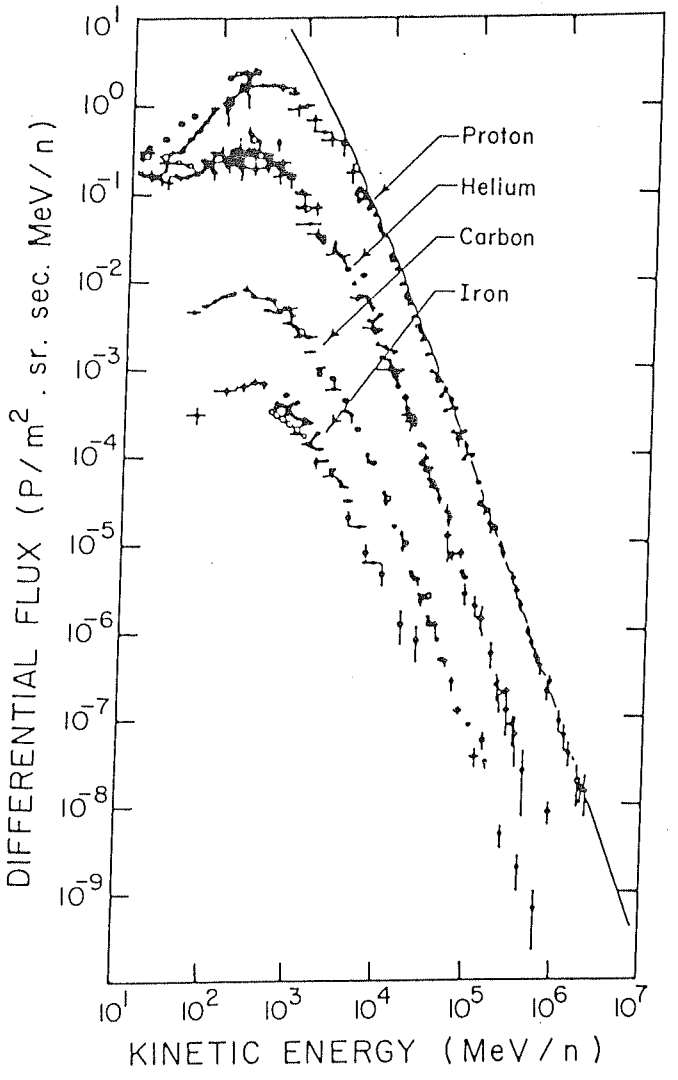

Fig.1-2 Energy spectra of H, He, C and Fe measured at 1 AU based on data from satellite and balloon borne experiments. The solid curve shows the hydrogen spectrum extrapolated to interstellar space by unfolding the effects of solar modulation. The "turn-up" of the helium flux below 60 MeV/n is due to the anomalous ^{4}He component. [Reproduced from Simpson, 1983a]

~1 GeV/n) between the period of solar maxima and minima.

The elemental abundances in GCR generally match with that of the solar system. However, there is a major difference. Elements and isotopes like ^{2}H, ^{3}He, Li, Be, B, F and several others elements between Si and Fe, ,which are nearly absent in the solar system , are present in GCR in significant amount. These particles are mostly produced by nuclear interactions or fragmentations of the primary cosmic rays, during their passage through interstellar medium, and are termed as secondary particles. The secondary particles can therefore be used as a probe to determine the amount of matter traversed by the GCR particles, before reaching the interplanetary space. In general, GCR particles traverse ~5-10 gm cm^{-2} of matter before reaching 1 AU [Garcia-Munoz *et al.*,1987a]. From the measurements of the ratio of the radioactive isotope ^{10}Be (half life ($T_{1/2}$) ~1.5 x 10^{6} yrs), to other stable beryllium isotopes, the containment life time of GCR particles in our galaxy is estimated to be ~2 x 10^{7} yrs .

The source of the GCR particles is not unambiguously known. The main difficulty in identifying their source is the isotropy in the observed flux, caused by the interaction of the GCR particles with the interstellar magnetic irregularities during their propagation. The GCR particles could be a representative sample of specific stellar objects (*e.g* supernova, pulsar etc.) or matter from the interstellar medium itself.

The acceleration of the galactic cosmic rays to the observed energies, could have taken place at one or more specific astrophysical sites. For example, they could gain their energy from stochastic processes through interaction with the interstellar magnetic field during their propagation [Fermi,1949]. Alternatively, shocks propagating in the interstellar medium (*e.g* of supernova origin) could be responsible for their acceleration [Axford *et al.*,1977; Eichler,1979; Blandford and Ostriker,1980; Volk,1981]. Also, according to Silberberg *et al.*[1983] the acceleration of cosmic rays is distributed over their propagation through interstellar space. They suggest that after the principal acceleration and during their galactic confinement, cosmic rays are further accelerated by weak shocks of widely distributed old supernova remnants. The distributed acceleration model has been successful in explaining certain peculiarities in cosmic ray composition [Wandel *et al.*, 1987; Cesarsky, 1987]. However, even if the acceleration sites for GCR are identical, it will not help in pinpointing their source. Measurement of isotopic and elemental compositions of different elements, at different energy range, and comparison of the measured elemental and isotopic compositions of GCR in the interplanetary space with that expected from specific source compositions, are needed to decide among the most plausible sources.

1.1.2 Solar Energetic Particles

Determination of the composition of solar energetic particles

gives us information on the elemental abundances in the Sun, and the processes which are responsible for the storage and acceleration of these particles from the solar atmosphere. The emission of energetic proton and helium particles from the Sun was studied in detail for the first time in balloon experiments during the solar flare events of September 1960 [Biswas *et al.*,1962]. The initial studies of SEP during early sixties was mainly restricted to large solar flare events, a summary of which was presented by Biswas and Fichtel [1965]. The relative abundances of SEP at energy ≥20 MeV/n is found to be similar to solar photospheric abundances.

Rocket and satellite borne experiments in 1970's revealed a very interesting feature of SEP during certain flare events; an enhancement of heavier ions relative to their abundances in the solar photosphere at energies ≤20 MeV/n. This enhancement was first reported by Price *et al.* [1971] for iron group ions, who also suggested an energy dependence in the enhancement factor. A recent summary [McGuire *et al.*,1986; Reams,1990] of data from a large number of solar flare events showed that there is a systematic departure of SEP abundances from photospheric abundances and in some events there exist a Z-dependent heavy ion enrichment or depletion. The enhancement factor increases almost linearly with Z and then becomes nearly a constant between Z=12 to Z=26 [Biswas *et al.*,1983 and references therein].

A further insight towards understanding the variability of solar flare composition was provided by Breneman and Stone [1985].

They have calculated the average SEP abundance by combining data from 10 solar flares that occurred during 1977-82. A systematic variation in abundance of individual flares relative to the average abundance was observed. Using the measured ionization states for different elements (see section-1.2.1 for a detail discussion) they found that flare-to-flare variability in composition exhibits a monotonic dependence on the ionic charge-to-mass ratio (Q/M) of the particles. This trend could be due to dependence of the acceleration and propagation processes on the rigidity of the particle which is inversely proportional to Q/M.

The relative abundance of ^{2}H, ^{3}H, and ^{3}He are rather small in normal solar flares ($^{2}H/^{1}H = 7(+10,-6).10^{-6}$, $^{3}H/^{1}H \sim 3.10^{-6}$, $^{3}He/^{4}He = (9\pm4).10^{-3}$), which indicates that the production of secondary particles in the solar atmosphere by nuclear spallation reactions is probably not significant [Mewaldt *et al.*,1979]. However, there are exceptions like ^{3}He-rich flares where the $^{3}He/^{4}He$ ratio reaches close to unity compared to the photospheric ratio of $\sim 4.10^{-4}$. At present it is firmly established that there exists a class of generally weak flare events where ^{3}He is highly enhanced relative to its normal solar abundance [Anglin *et al.*,1973; Balasubramanyan and Serelemitos,1973; Dietrich,1973; Garrard *et al.*,1973; Ramaty *et al.*,1980 and Kocharov and Kocharov,1984]. It is observed that there is an enhancement in heavier ions also, mostly iron, in association with the ^{3}He enhancement. The ratio Fe/O in ^{3}He-rich flares varies by almost three orders of magnitude from 0.01 to 10. The enhancement of ^{3}He and heavier ions in weak flares is now understood in terms of

their selective heating by wave particle interactions in the flare plasma and hence their preferential injection into the accelerating region [Fisk, 1978].

Average elemental abundances for solar particles with energy ≥1 MeV/n in large solar flare events (where peak intensities exceed ~100 protons/(cm^2.sr.sec.MeV)) are shown in fig.1-3. The energy range considered here are, 1-20 MeV/n for normal flares and 1-5 MeV/n for flares enriched in iron. The vertical extent of the solid bar and open rectangles in the figure shows the variation in composition from one solar flare to the other. Despite these variations the basic compositional features of SEP are similar to that of solar corona and solar photosphere, whose abundances are also shown in fig.1-3. An overall agreement is seen in the abundances in He, C, N and S through Fe. The elements like Li, Be, B, F and P are rare. The odd atomic number (Z) elements like N, F, Na, Al and P are comparatively much less abundant than their neighboring even-Z elements.

The energy spectra of protons for various solar flares are shown in fig.1-4. The spectral index γ varies between ~3 to ~6 from flare to flare. An alternative representation is in terms of the rigidity, that usually covers a much wider range. The rigidity spectra are expressed as $dJ/dR \alpha \exp(-R/R_0)$. The steepness of the spectrum is determined by R_0, which varies roughly between 40MV (steep) to 400MV (flat). McGuire *et al.*[1981] have shown that the spectral form based on a Bessel function of momentum/nucleon (p)

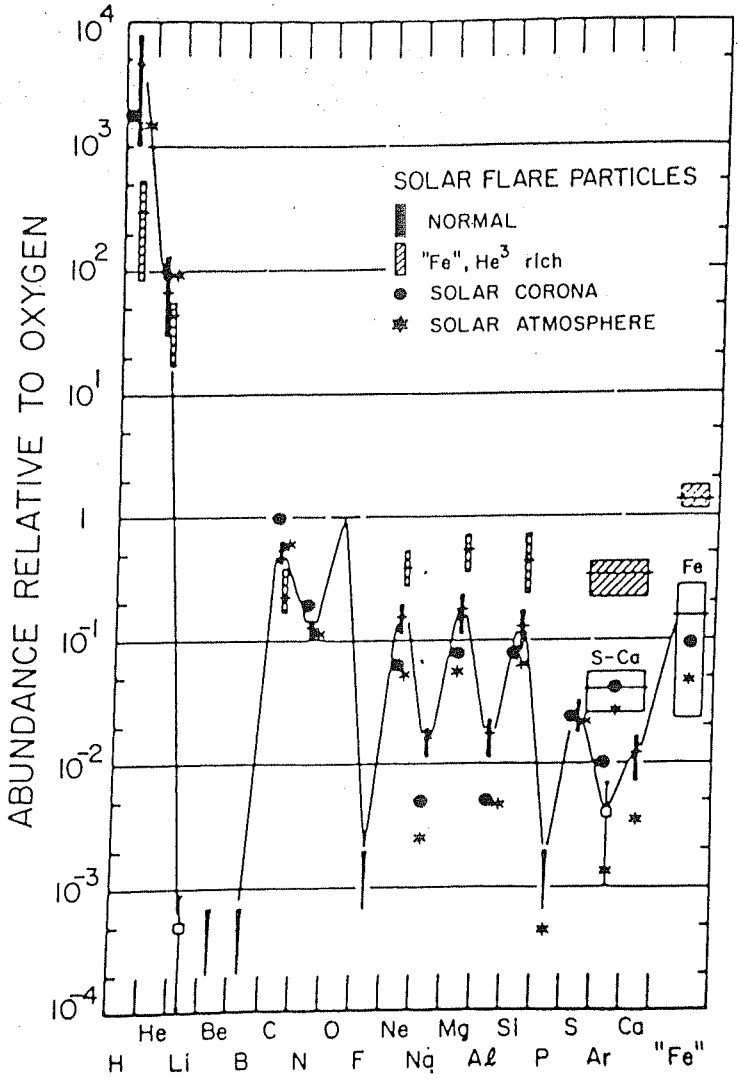

Fig.1-3 Abundances normalized to oxygen in the solar corona (filled circles), photosphere (stars) and in flare events. The abundances for relatively large flare events are indicated by solid vertical bars, solid triangles (upper limits), open squares (single measurement) and open rectangles (element groups). The composition for "Fe"-rich (also ^{3}He-rich) flare events are indicated by cross hatched bars and rectangles. The vertical extent of the bars represents the degree of variability in the composition between different solar flare events. [Reproduced from Gloeckler, 1979]

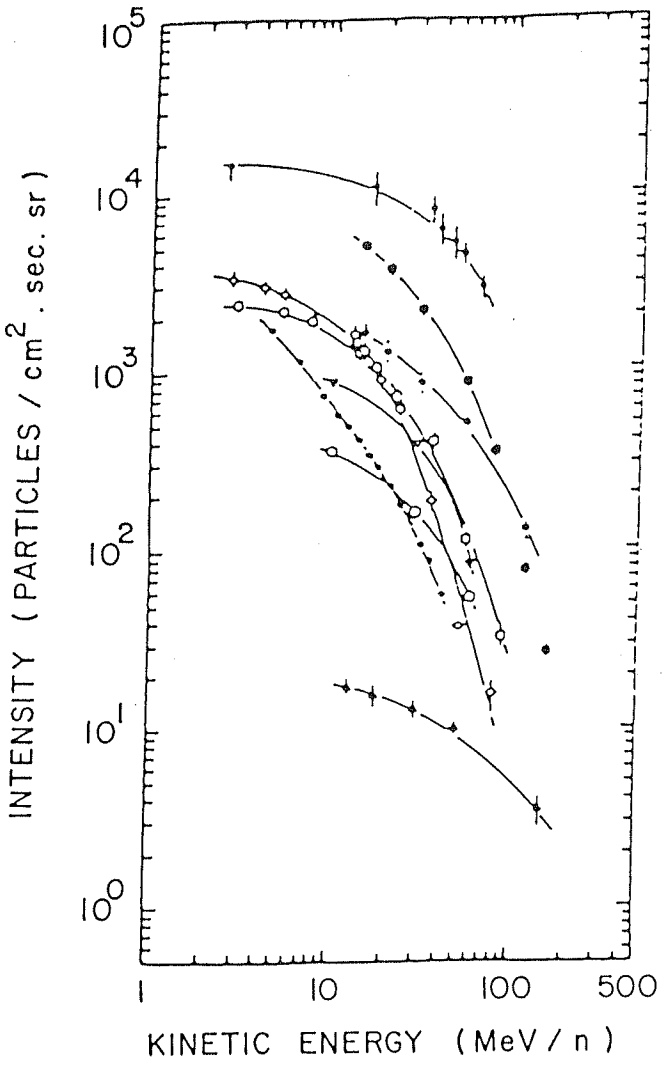

Fig.1-4 Proton spectra for nine different solar flare events measured over the time period 1960 to 1972. [Reproduced from Vahia and Biswas, 1983]

also represents the intensity of SEP quiet well. Such a spectrum ($dJ/dE \alpha p.K_2[2\{3(p/c)(1/aT)\}^{1/2}]$) can result from stochastic Fermi acceleration, where energy loss effects are neglected in the acceleration region. In this expression K_2 is a modified Bessel function of order 2, "a" is the acceleration rate and T is the escape time from the acceleration region.

1.1.3 Anomalous Cosmic Rays

Anomalous cosmic rays (ACR) were discovered during the early seventies in nearby interplanetary space in several satellite borne experiments [Garcia-Munoz *et al.*,1973; Hovestadt *et al.*,1973; McDonald *et al.*,1974]. This component of energetic particles are characterized by the overabundance of He, N, O and Ne relative to C in the energy range 1-30 MeV/n, compared to their abundances in SEP and GCR. Further, their energy spectra are also very different from those of GCR in this energy range, which has a negative power law index. The distinctly different energy spectra of ACR species (He, N, O, Ne) are shown in fig.1-5 along with the GCR spectra for different elements. A peak in the ACR intensities can also be noticed at ~10 MeV/n. Because of the lower flux level, the ACR components can be observed only in the absence of SEP *i.e* during solar quite time. It is evident from fig.1-5 that the ACR helium flux exceed that of GCR proton at E < 30 MeV/n, and ACR oxygen has much higher flux than GCR carbon. The elemental abundances of ACR relative to that of GCR and SEP are given in table-1.1

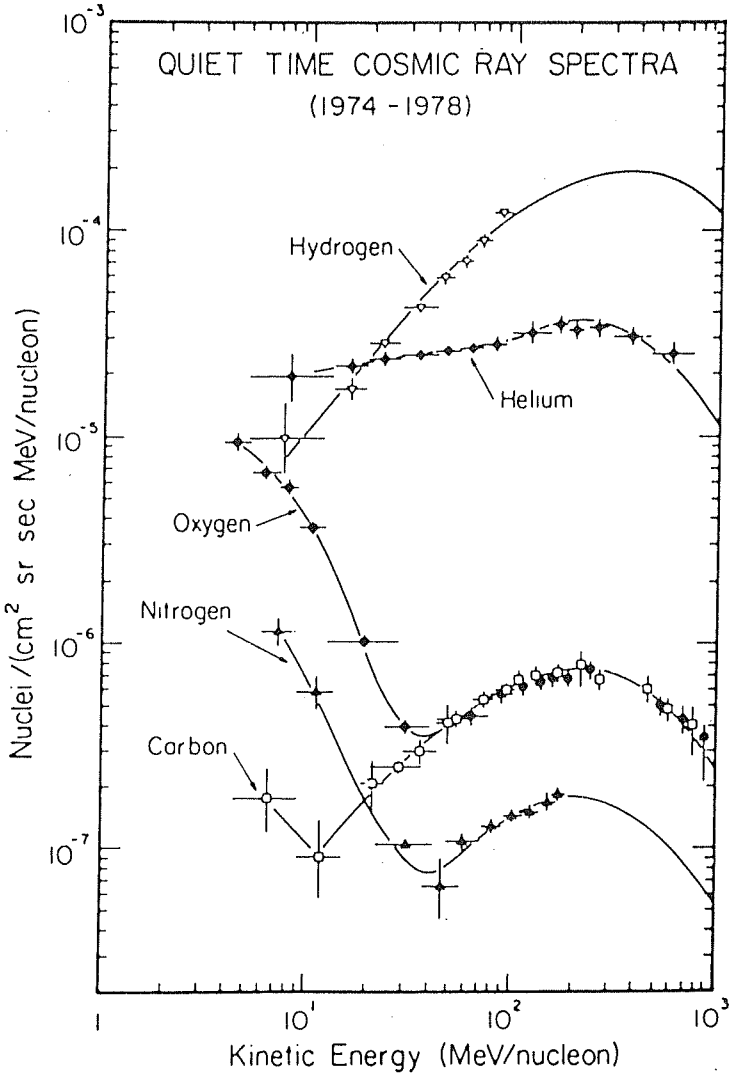

Fig.1-5 Quiet time energy spectra for H, He, C, N and O measured at 1 AU over the period from 1974 to 1978. The "anomalous" enhancement in the low energy spectra of He, N and O can be clearly seen. [Reproduced from Mewaldt et al., 1984]

Table-1.1 : Elemental abundance of ACR, GCR and SEP.*

Element	ACR	GCR	SEP †	Ratio
	(2-30) MeV/n	(>100) MeV/n	(1-20) MeV/n	$(ACR_{2-30}/GCR_{>100})$
He	90	50	130	1.8
C	≡ 1	≡ 1	≡ 1	1
N	3	0.255	0.25	11.8
O	18	1.0	1.85	18
Ne	1.3	0.175	0.30	7.4
Mg	<0.3	0.23	0.33	1.3
Si	<0.2	0.17	0.24	1.17
Fe	<0.03	0.12	0.28	0.25

* *From Gloeckler,1979*

† '^{3}He-rich' and 'Fe-rich' flares are not included.

Investigation until now have conclusively shown the presence of six elements in the ACR, namely He, C, N, O, Ne and Ar. The presence of H in ACR had been reported recently although this can not be considered as conclusive [Christian *et al.*,1990; Garcia-Munoz *et al.*,1990; McDonald *et al.*,1990; Mewaldt,1990].

Continuous monitoring of the ACR component in the interplanetary space by the Pioneer and Voyager Spacecrafts over the last two decades have provided a lot of data on the different characteristic features of the ACR, like its temporal and spatial variations inside the heliosphere [Christian *et al.*,1988; Cummings and Stone,1988; Cummings *et al.*, 1990a; Cummings *et al.*, 1990b, Garcia-Munoz *et al.*,1990; Mewaldt, 1990]. The temporal variations of ACR show an inverse correlation with solar activity, with maximum intensity during solar minimum and minimum intensity during solar maximum. The quite time ACR flux was near its maximum and had almost the same intensity during 1972-78 encompassing the solar minimum of 1976. During the 1980 solar maximum, the ACR intensity at 1 AU went below the detection limit, and returned again to the maximum level for a short period during 1987. We show in fig.1-6 the ACR oxygen intensity at 1 AU as measured by IMP-8 spacecraft over the period 1972-1988 along with the neutron monitor data for the same period. The data obtained from IMP-8, Voyager-2 and Pioneer-10 spacecrafts, all of which were monitoring the ACR component at different heliospheric distances near the ecliptic plane show that the ACR flux has a radial gradient of ~14%/AU between 1 to 20 AU and ~3%/AU between 20 to 40 AU from the Sun [Cummings *et al.*,1990b]. This is shown in fig.1-7. The latitudinal gradient for ACR oxygen component (E= 7-17 MeV/n) have also been estimated from the data obtained from Voyager-1, Voyager-2 and Pioneer-10 spacecrafts during 1984 to 1989, when Voyager-1 had sampled ACR particles away from the ecliptic plane [Cummings *et al.*,1990b]. The magnitude of the latitudinal gradient shown in fig.1-8 appears to have a good correlation with

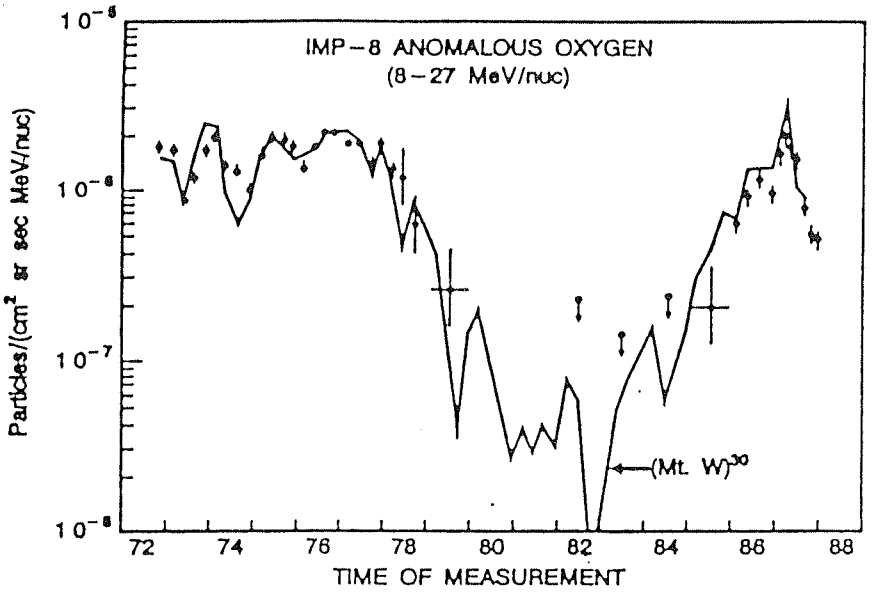

Fig.1-6 Variation in the flux of 8-27 MeV/n ACR oxygen ion at 1 AU during 1982 to 1988. The solid line represents the Mt. Washington neutron monitor data to the 30th power. [Reproduced from Mewaldt, 1990]

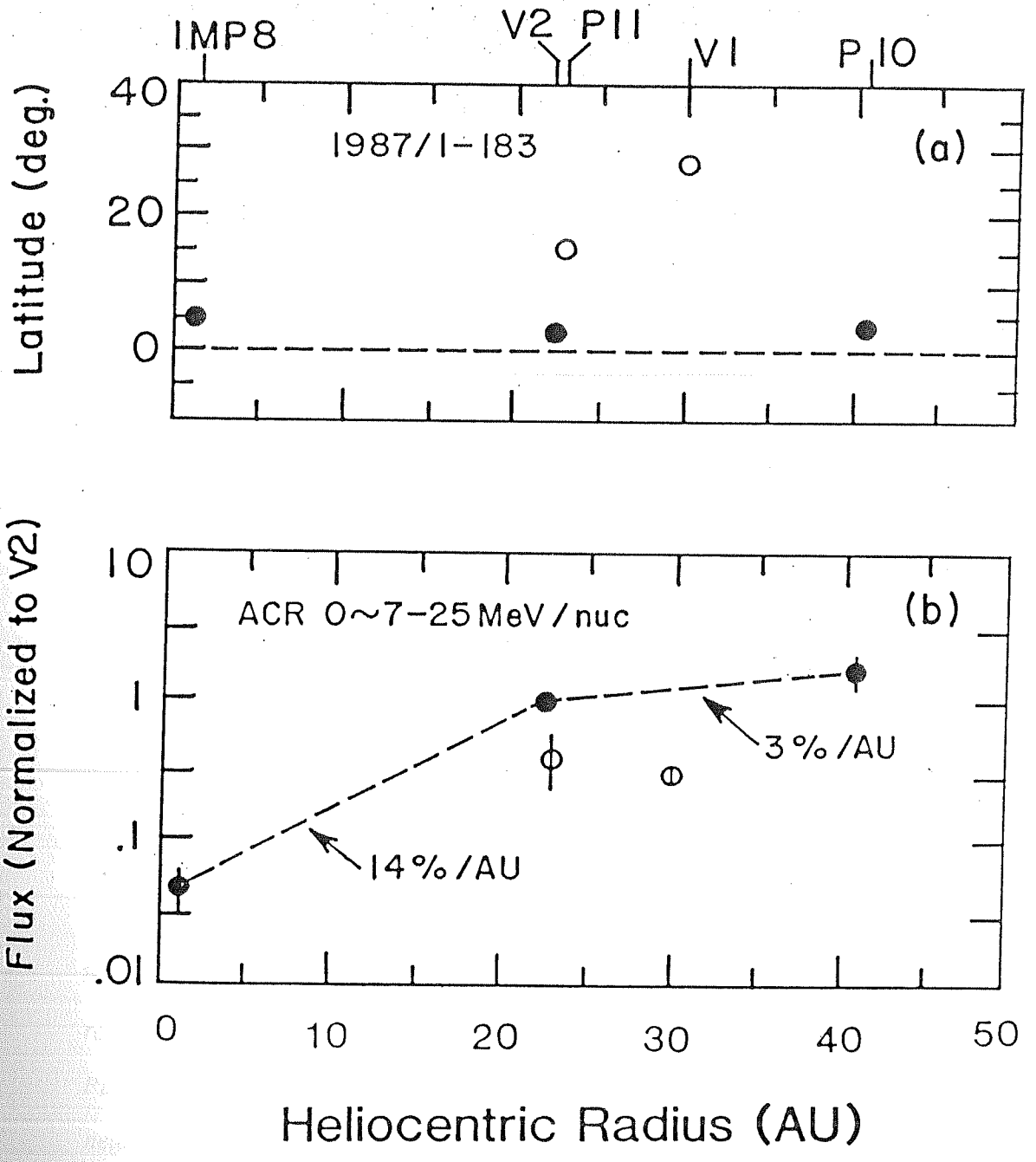

Fig.1-7 *(a) Heliographic latitude of the spacecrafts IMP-8, Voyager-2, Pioneer-11, Voyager-1 and Pioneer-10 versus heliocentric radius. (b) Flux of ACR oxygen ion (normalized to Voyager-2 data) versus heliocentric radius. The dashed line represents one of the possible radial dependence of the ACR oxygen flux in heliosphere. [Cummings et al., 1990b]*

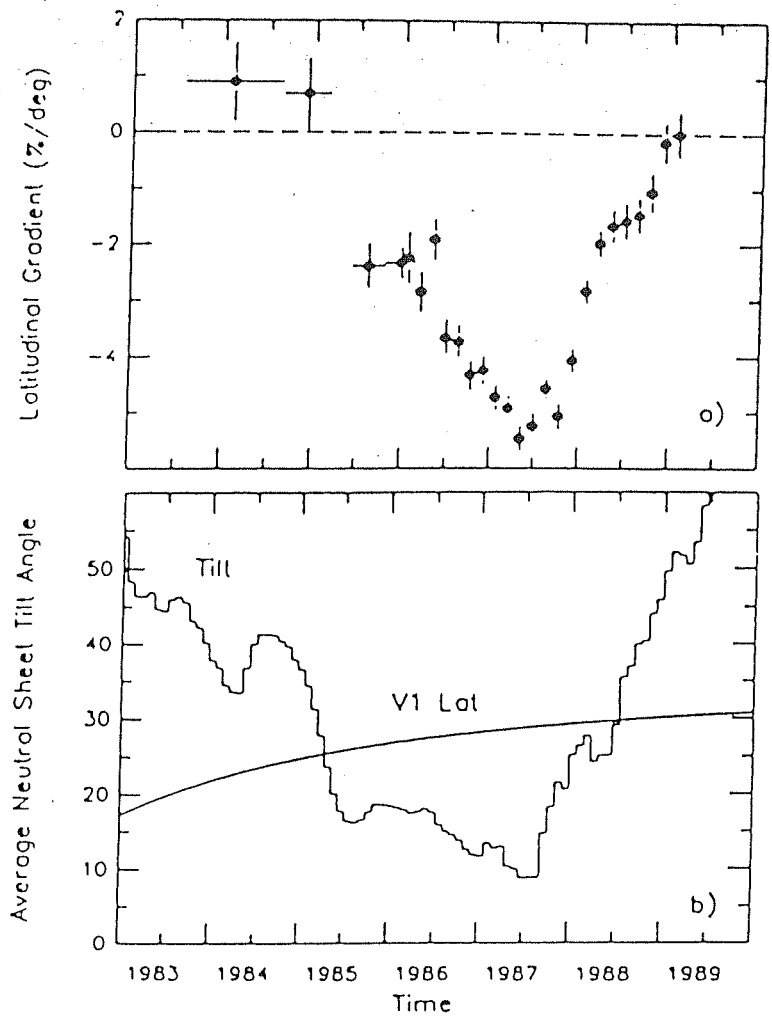

Fig.1-8 (a) Latitudinal gradients of ACR oxygen ions in the energy range 7.1-17.1 MeV/n computed from Voyager-1, Voyager-2 and Pioneer-10 data verses time. (b) Time-shifted and time averaged neutral sheet tilt angle versus time (histogram). The solid line is the heliographic latitude of Voyager-1. [Reproduced from Cummings et al., 1990a)

the tilt of the neutral current sheet from the heliographic equatorial plane. The latitudinal gradient for the ACR oxygen component first becomes negative when the neutral sheet tilt drops below the latitude of Voyager-1 and have a maximum value of -5.5%/deg during mid-1987 and becomes near zero by the end of 1988 when the tilt angle and the Voyager-1 latitude are same.

The isotopic composition of ACR has been mainly studied using the Caltech Heavy Isotope Spectrometer Telescope (HIST) experiment on ISSE-3 and Electron/Isotope experiment (EIS) on IMP-7 at 1 AU. The results of these studies are described in detail by Mewaldt *et al.*[1984] and Mewaldt [1988]. Summary of these results are given in table-1.2.

Table-1.2 : Isotopic composition in anomalous cosmic rays.

Isotope Ratio	Anomalous Cosmic Rays				Galactic Cosmic Rays (~100 MeV/n)
	IMP-7		ISSE-3		
	Energy range	Observed ratio	Energy range	Observed ratio	
$^{3}He/^{4}He$	5-15	≤ 0.02	-	-	~0.1
$^{13}C/C$	-	-	5-30	≤ 0.11	~0.06
$^{15}N/N$	6-13	≤ 0.19	5-30	$0.11^{+0.19}_{-0.11}$	~0.55
$^{17}O/^{16}O$	7-12	≤ 0.06	6-30	≤ 0.03	~0.02
$^{18}O/^{16}O$	7-11	$0.03^{+0.03}_{-0.01}$	6-30	≤ 0.03	~0.02
$^{22}Ne/^{20}Ne$	-	-	5-28	≤ 0.36	~0.6

It is clear from table-1.2 that the abundance of secondary particles like ^{3}He, ^{13}C, ^{15}N and ^{22}Ne in ACR is extremely small compared to those found in GCR. This suggests that the ACR particles have not travelled much amount of interstellar matter and might have originated from a nearby source *i.e* basically they are composed only of primary nuclei. The source of the ACR particles is proposed to be either solar and local galactic objects (comets/stars/novae) with peculiar composition, or neutral particles from local interstellar medium [Fisk *et al.*, 1974; Hoyle and Clayton, 1974; McDonald *et al.*, 1974; Durgaprasad, 1977; McDonald *et al.*,1977; Biswas *et al.*, 1981]. The presently available data as well as the data presented in this thesis support the latter hypothesis.

1.1.4 Solar Wind

Solar wind, the continuous emission of energetic protons, heavy ions and electrons from the Sun, is basically the outward expansion of the hot (~10^{6} deg K) solar corona into interplanetary space. Parker first considered the hydrodynamical equations for a hot plasma in the gravitational field of the Sun and predicted the existence of a general outflow of matter, which was named solar wind [Parker,1958; Parker,1963]. This prediction was verified by the Soviet satellite Lunik II during 1959 and US Venus Probe Mariner 2 during 1962, which measured the particle density, velocity and magnetic field strength in interplanetary space outside the earth's magnetosphere. The average characteristics of the solar wind in the vicinity of the earth are given in table-1.3.

Table-1.3: Average characteristics of the solar wind.*

Composition	Proton, electrons and a few percent of alpha and heavier particles
Flux	5×10^8 particles/cm^2 sec
Velocity	300 to 450 km per second†
Density	5 particles/cm^3 (range 1 to 20, generally of each sign)
Thermal energy	10 eV
Proton kinetic energy	1000 eV
Electron kinetic energy	10 eV
Magnetic field	5×10^{-5} gauss (range 3 to 15)

* *From Venkatesan, 1985*

† There are occasional high speed streams with velocity as high as 600 to 800 kms/sec and sometimes reaching 2000 km/sec

The magnetic field energy density of the solar wind is ~60 $eV.cm^{-3}$. Since this energy is a very small fraction of the proton energy present in the solar wind, one can conclusively say that the kinetic energy of proton carries most of the solar wind energy.

1.1.5 Magnetospheric Particles

Large population of energetic protons and electrons were first observed in two specific zones within the earth's magnetosphere during 1958 in satellite borne experiments [Van Allen *et al.*,1958]. The first zone, called the inner radiation belt, is situated at an altitude of ~3000 km and the second zone, the outer radiation belt is centered at ~16,000 km altitude. The geomagnetically trapped energetic particles gyrate across the magnetic field lines and bounce back and forth along the magnetic field lines. These particles drift around the earth on a magnetic L shell. The L shells are defined as the surfaces formed by rotating a magnetic field line around the earth's magnetic dipole axis. The distance of the L-shells are measured at the equator in terms of the earth's radius (R_E). The inner radiation belt is located at $L = 1.5R_E$ and the outer radiation belt has its center around $L = 3.5R_E$.

The main constituents of the energetic particles in the radiation belts are protons and electrons. The inner radiation belt contains high energy protons with energy up to ~1 BeV. The energy spectrum of proton in the inner radiation belt is shown in fig.1-9 [from Freden and White, 1960]. The outer radiation belt contains

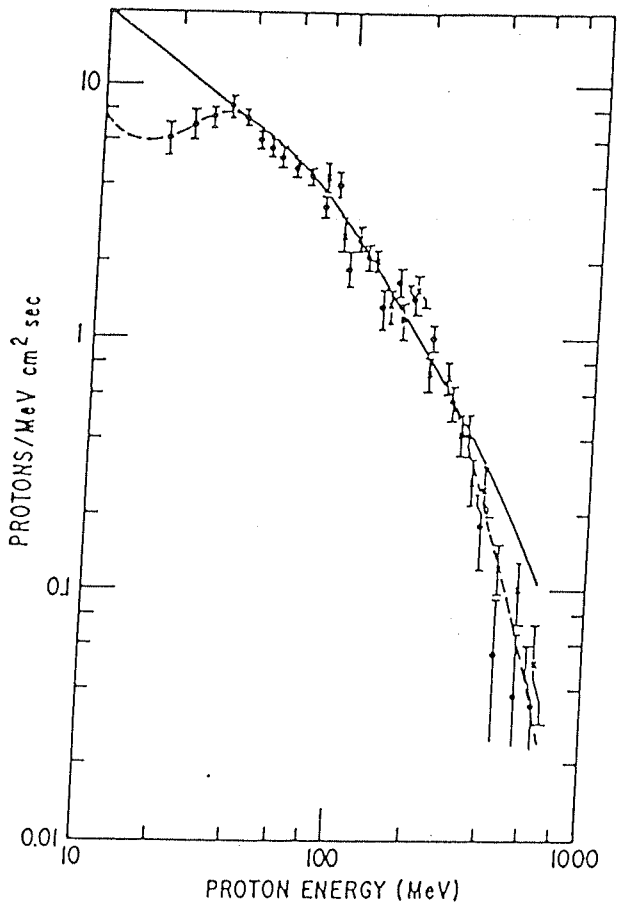

Fig.1-9 The trapped proton energy distribution as measured by Freden and White [1962]. The shape of this distribution is well fitted by cosmic ray albedo neutron decay injection and atmospheric ionization and nuclear collision losses.

much lower energy protons compared to those in the inner radiation belt. The low energy (~0.19 MeV) proton in the outer radiation belt has a maximum intensity at about $L=4.5R_E$, whereas the higher energy protons (~2.8 MeV) show peak at $L=2.5R_E$ [Mihalov and White,1966]. Relatively few measurements exist on the flux of the geomagnetically trapped particles heavier than proton. This is because of the experimental difficulties in their detection in the presence of a high background of protons. At energies above 0.6 MeV/n the alpha/proton ratio is fairly stable with a value of ~2 x 10^{-4}. In comparison, this ratio varies between ~2.5 x 10^{-3} to 2 x 10^{-4} at lower energies from one solar flare to the others [Vette,1971]. In the solar wind the alpha/proton ratio is ~0.04. The ratio of intensities of CNO/alpha particles in the outer radiation belt is ~3 x 10^{-3} [Van Allen *et al.*,1970] at an energy of 0.3 MeV/n, compared to the solar wind ratio of 0.01 [Bame *et al.*,1968]. Mogro-Campero [1972] have also reported the observations of the CNO group nuclei in the energy range 13-33 MeV/n with O/C ≈ 0.5.

The source of protons in the inner radiation belt is due to the cosmic ray albedo neutron decay (CRAND). Cosmic ray protons collide with the atmospheric nuclei and the product neutron stream back into the magnetosphere and decay into protons, electrons and anti-neutrinos ($n \Rightarrow p + e + \bar{\nu}_e$) [Singer,1958]. Predicted shape of the proton energy distribution from CRAND matches well with the measured data points shown in fig.1-9. Two leading candidates have been discussed [Mogro-Campero and Simpson,1970] as the possible source of heavy ions in the radiation belt. These are solar wind and

solar flare particles. Solar flare particles could enter the magnetosphere at low energies and get locally accelerated before residing as trapped particles. On the other hand, solar wind particles could be transported and accelerated into the radiation belt due to the violation of the third adiabatic invariant or the flux invariant. While neither of these two possibilities could be established conclusively, most of the heavy ions found in the radiation belt are basically considered to be of solar origin.

1.2 Ionization States of Energetic Particles in Near-Earth-Space.

The determination of the ionization states of the energetic particles of solar and extra-solar origin provides clues to the plasma conditions (*e.g* temperature, density etc.) prevailing at the source regions and at the acceleration sites as well as the processes occurring during their interstellar and interplanetary propagation. From the available data on the electron capture (σ_{cap}) and the electron stripping (σ_{loss}) cross section, GCR equilibrium charge state in the interstellar medium is predicted to be fully ionized at energies >10 MeV/n [Durgaprasad, 1977; Rule and Omidvar, 1979]. However, for the solar flare particles, their equilibrium charge state will depend upon the plasma conditions at the flare site [Luhn *et al.*,1987]. Similarly, the equilibrium charge state for SW particles depend on the physical conditions of the solar corona. Except for hydrogen and helium, most of the higher atomic number elements present in SW are predicted to be in partially ionized state [Allen and Dupree,1969; Cox and Tucker,1969; Jordan,1969].

Different techniques were used to measure the ionization states of energetic particles in SW, SEP, GCR, ACR and radiation belts. The ionization states of the solar wind particles are found to be similar to those of the solar energetic particles. The magnetospheric particles and the high energy galactic cosmic rays are found to be fully ionized. Recent studies including the present one show that the anomalous cosmic rays are predominantly in singly ionized state. A new observation presented in this thesis is the partially ionized state of low energy (20-125 MeV/n) GCR iron group ions. In the following sections we shall discuss our present understanding of the ionization states of energetic particles observed in the near-earth-space.

1.2.1 Ionization States of Solar Energetic Particles and Solar Wind

Direct and indirect measurements of the ionization states of the solar energetic particles indicate an incomplete stripping of the electron from the heavy ions over an energy range of up to ~5-10 MeV/n [Gloeckler,1979]. Direct measurements [Gloeckler *et al.*, 1976; Sciambi *et al.*,1977] have shown that, in general, ionization states of C, O and Fe in SEP with energy below 1 MeV/n are consistent with the ionization states of these elements in solar wind, which are 6, 6 and 12 respectively. These measurements were made using the ultra low energy telescope (ULET) and the electrostatic energy versus charge analyzer (EECA) on board IMP-8 satellite. The ULET determines the atomic number and energy of the incoming particles by E-dE/dX method, whereas, EECA determines the ionization states of the

particle from the amount of deflection in electrostatic field and the information on the kinetic energy of the particle. About 10 small to moderate flare events were studied during 1973-74, and the following results were obtained:

1. The mean ionic charge states of carbon, oxygen and iron are 5.7, 6.2 and 11.6 respectively for E < 1 MeV/n.
2. There is apparently little variation of ionization states with energy in any given event between E =37 KeV/n to 1 MeV/n.
3. There is apparently no variation of ionization states with time during any event.
4. There appear to be only statistical fluctuation of these ionization states from event to event.

Results from a similar experiment on board ISSE-3 during 1978-79 [Luhn *et al.*,1985] show more or less similar values of ionization states obtained from 12 solar flare events. The results obtained by them are given in table-1.4. Surprisingly, the ionization states measured for Si and Fe during ^{3}He-rich solar flare events are much higher than those given in the table-1.4 for normal flares [Luhn *et al.*,1987]. Si is found to have a mean charge close to 14 *i.e* compatible with fully ionized Si and Fe is found to have a mean charge 20.5 $\pm$ 1.2.

Table-1.4 : Ionization states of solar energetic particles.*

Elements	Energy range (MeV/n)	Ionization state
C	0.45-2.34	5.70±0.02
N	0.45-2.62	6.37±0.04
O	0.54-2.64	7.00±0.02
Ne	0.56-3.14	9.05±0.07
Mg	0.56-3.37	10.7±0.07
Si	0.55-2.97	11.0±0.10
S	0.55-3.17	10.9±0.24
Fe	0.34-1.78	14.9±0.09

* *From Luhn et al., 1985*

The first observations of ion species other than $^{1}H^{+1}$ and $^{4}He^{+2}$ in the solar wind (which were detected in a Mariner-2 experiment [Neugebauer and Snyder,1966]), were made by Bame *et al.* [1968] using electrostatic analyzer on board two Vela 3 spacecrafts. Further observations were carried out later by the two pairs of earth-oriented satellites Vela 5A and B, Vela 6A and B with improved instrumentation [Bame,1972]. The main assumption made in these experiments was that all ion species have the same mean velocity, which was assumed to be 440 Km/sec, which is equivalent to 1 KeV/n. With this assumption, the ion species position in E/Q spectrum are expected to be at $m/m_p q$, where m is the ion mass, q is the ion charge and m_p is the proton mass. Hence, the peak expected in E/Q for $^{1}H^{+1}$, $^{3}He^{+2}$ and $^{14}N^{+6}$ are at 1.00, 1.50 and 2.32 respectively and similarly for other ions. In fig.1-10 the results obtained from Vela 3A are shown. It is clear from the figure, that the main

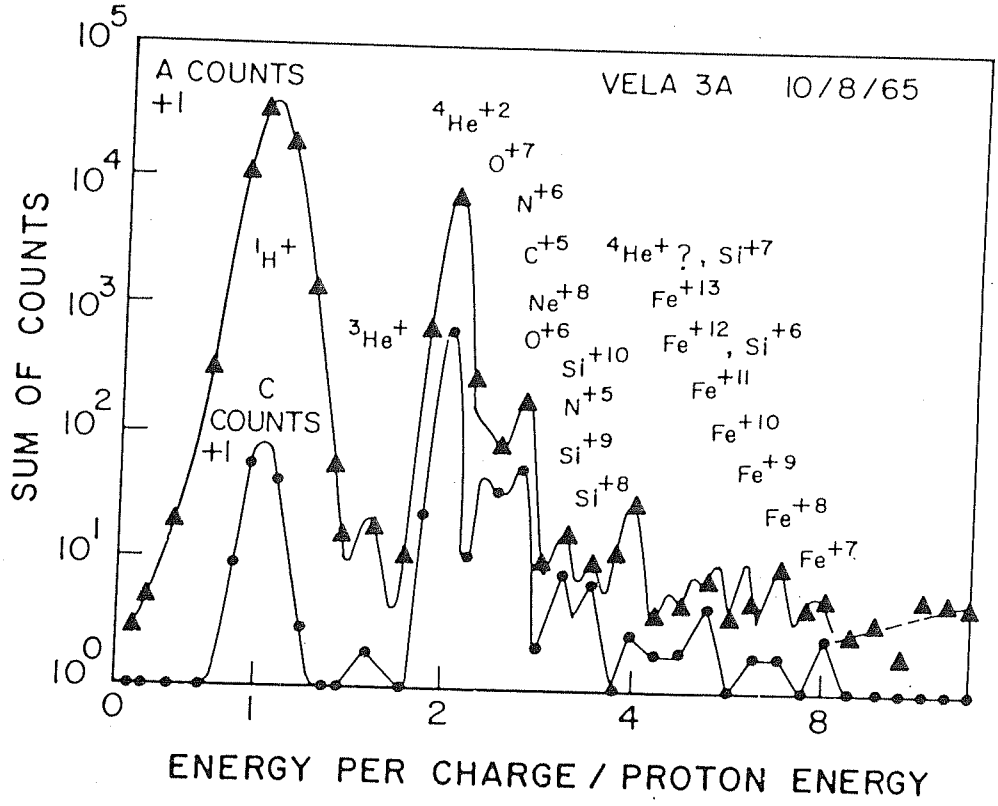

Fig.1-10 Solar wind E/Q spectra from Vela 3A spacecraft obtained simultaneously at two different sensitivity levels. The peak at 4.0 is anomalously high to be explained as only due to $^{28}Si^{+7}$ ions. [Reproduced from Bame, 1972]

constituents of SW are $^{1}H^{+1}$, $^{3}He^{+2}$, $^{4}He^{+2}$, $^{14}N^{+6}$, $^{16}O^{+6}$ to $^{16}O^{+7}$, $^{28}Si^{+7}$ to $^{28}Si^{+9}$, $^{56}Fe^{+7}$ to $^{56}Fe^{+12}$. Presence of $^{4}He^{+1}$ is not very certain, but there seems little doubt that the ion species like $^{12}C^{+5}$, $^{20}Ne^{+8}$, $^{24}Mg^{+10}$, $^{28}Si^{+9}$ and $^{32}S^{+10}$ are present in solar wind.

1.2.2 Ionization States of Geomagnetically Trapped (Radiation Belt) Particles

H, He and heavy ions with energies ≥ 0.12 MeV/charge were detected in the magnetotail and in the magnetosheath of earth. Measurement of the energy spectra for H, He and heavier ions were carried out by Fan *et al.*[1975] who have also inferred the ionization states of these particles. The instrument used for this experiment was an electrostatic deflection spectrometer , designed for the measurement of low energy particles. The principle to determine the ionization state was simple: a particle is first selected by means of an electrostatic analyzer according to its energy per charge and its energy is then measured from the pulse height generated by the energy deposited in an Au-Si solid state detector. The ionization state is determined by combining these two sets of data. In the experiment of Fan *et al.*[1975], the particles are first selected according to their energy per charge in the range 0.12-0.16, 0.17-0.28 and 0.38-0.65 MeV/charge, and plotted as a function of their energy. Combining the results from all the three energy ranges, spectra of each species are calculated and these are shown in fig.1-11. When expressed in terms of power law, the intensity (in p/ {cm^2. sr. sec. (MeV/charge)}) for H^{+1} is seen to be

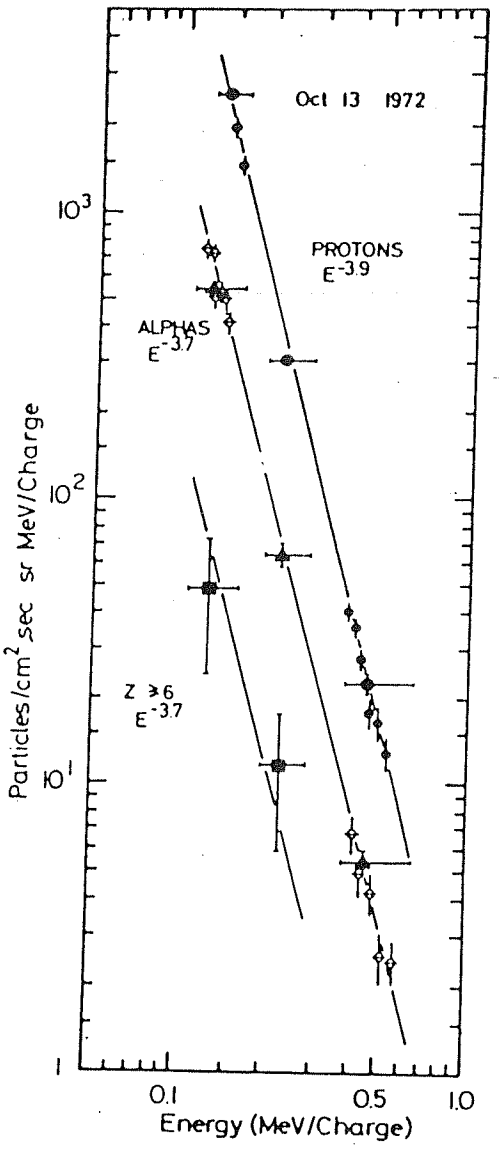

Fig.1-11 The differential energy spectra of H, He and heavy ions observed in the earth's magnetosheath and magnetotail by IMP-7 satellite. [Reproduced from Fan et al., 1975]

proportional to $E^{-3.9}$, for He^{+2} to $E^{-3.7}$ and for $Z \geq 6$ to $E^{-3.7}$. From these spectra and the instrumental response the relative abundance obtained in the energy-charge range 0.12-0.16 MeV/charge is H^{+1}: He^{+2}: (C^{+5}, C^{+6}): (O^{+7}, O^{+8}) = 1.0: 1.1 x 10^{-1}: 3.2 x 10^{-3}: 1.3 x 10^{-3}. Although the charge resolution of the instrument was not sufficient to resolve C^{+5} from C^{+6} and O^{+7} from O^{+8}; it is plausible that most of the particles are in fully ionized state.

1.2.3 Ionization States of Galactic Cosmic Rays

The only experiment aimed at estimating the ionization state of GCR was conducted by Kaplan *et al.* [1952] who considered the dependence of GCR flux on the geomagnetic latitude and measured them in two high altitude balloon flights at different latitudes. One flight was made at Minnesota (geomagnetic latitude $\lambda = 55^0$) and the other at White Sands ($\lambda = 41.7^0$). The residual atmospheric pressure in both the cases was ~15 millibar and the same apparatus was used in both the experiments. The flux of GCR was measured at $\lambda = 55^0$ and the expected number of particles at $\lambda = 41.7^0$ was calculated from the measured flux at $\lambda = 55^0$ by assuming that the GCR particles which enter the earth's magnetic field are either i) fully ionized, or ii) partially ionized and retain only their K-shell electrons, or iii) partially ionized and retain both K-shell and l-shell electrons. The cutoff energies for different nuclei at $\lambda = 41.7^0$ under these three different assumptions of ionization states are given in table-1.5. In table-1.6, the calculated number of particles are compared with the actual number observed.

Table-1.5 : Cut-off energy (BeV/n) for particles at geomagnetic latitude $\lambda = 41.7^0$.*

	Elements				
	Fe	Ca	Si	Mg	Ne
Completely Stripped	1.35	1.50	1.50	1.50	1.50
Retaining only K-shell electrons	1.21	1.29	1.21	1.16	1.09
Retaining both K and L shell electrons	0.655	0.525	0.20	0.07	0

* *From Kaplan et al.,1952*

Table-1.6 : GCR particles stopping in the stack at $\lambda = 41.7^0$.*

	Elements				
	Fe	Ca	Si	Mg	Total
No. observed	3	1	2	0	6
No. of particle which should be seen stooping if fully ionized	3.8	1.5	0.6	0	5.9
No. of particle which should be seen stopping if only K-shell electrons are present	5.4	2.8	4.4	2.3	14.9
No. of particle which should be seen stopping if both K and L shell electrons are present	17	13	53	65	148
No. observed below cut off of fully ionized particles	0	0	0	0	0

* *From Kaplan et al.,1952*

As can be seen from the table-1.6, energetic heavy nuclei enter the earth's magnetic field either completely stripped or retain at most one or two electrons. Thus the GCR particles are considered to be fully ionized. However, the results of direct measurement of the ionization state of individual ions in the low energy domain (20-125 MeV/n), presented in this thesis, clearly indicate the presence of partially ionized iron group particles in GCR. This is a significant new observation which is discussed in detail in chapter five.

1.2.4 Ionization States of the Anomalous Cosmic Rays

Several indirect methods have been adopted to measure the ionization states of the ACR particles. The hysteresis effect or the phase-lag effect that occurs between the low rigidity GCR and high rigidity ACR particles (if they are partially ionized), was used to infer the singly ionized state of the ACR helium [McKibben,1977]. However, Klecker *et al.* [1980], who have also used a similar approach, concluded that the most probable ionization state for the ACR oxygen is +2 with an upper limit of +4. Cummings *et al.*[1984] considered the dependence of the spectral shape of the ACR species on their ionization state and the rigidity dependent diffusion coefficient, assuming all the ACR species to have similar spectral shape outside the heliosphere, and concluded that ACR He, N, O and Ne are in singly ionized states. McDonald *et al.*[1988] compared the demodulated spectra for ACR He and O during the last solar minimum, assuming different ionization states, and inferred that they are predominantly in +1 state.

The approach of Mckibben and Klecker *et al.* are based on the model of O'Gallagher [1975] and O'Gallagher and Masylar [1976] in which the higher rigidity (energy) cosmic ray particles take less time to propagate from the heliospheric boundary to earth than time taken by lower rigidity (energy) particles. The intensities of the high energy particles at 1 AU, therefore, reflect a more recent sampling of the modulating conditions in the heliosphere than the low energy ones. Thus, to a first order approximation the low energy particles follow the time variations of the high energy particles (*i.e* those detected by neutron monitor data), but with a time lag. The time lag would be inversely proportional to the β.R (where, β = v/c and R is the magnetic rigidity (momentum per unit charge)). This effect was studied during the depression in the intensity of GCR particles at 1 AU for the period Jan,1974 to Dec,1975. The time lag between the Deep River neutron monitor data and the oxygen flux (E=7.6-24 MeV/n) obtained from IMP-8 are shown in fig.1-12. From the study of the time lag effect between the neutron monitor data and the low energy (<25 MeV/n) ACR He and O, compared to the high energy (~30-70 MeV/n) GCR proton and helium, it is concluded that ACR He and O ions are in +1 and +2 ionization states respectively.

Cummings *et al.* [1984] have derived the flux for the ACR He, N, O and Ne by subtracting the low energy solar/interplanetary and higher energy galactic cosmic ray component from the data obtained by the Voyager spacecrafts during 1977-78. They assumed that all the ACR species have similar spectral shape outside the heliospheric

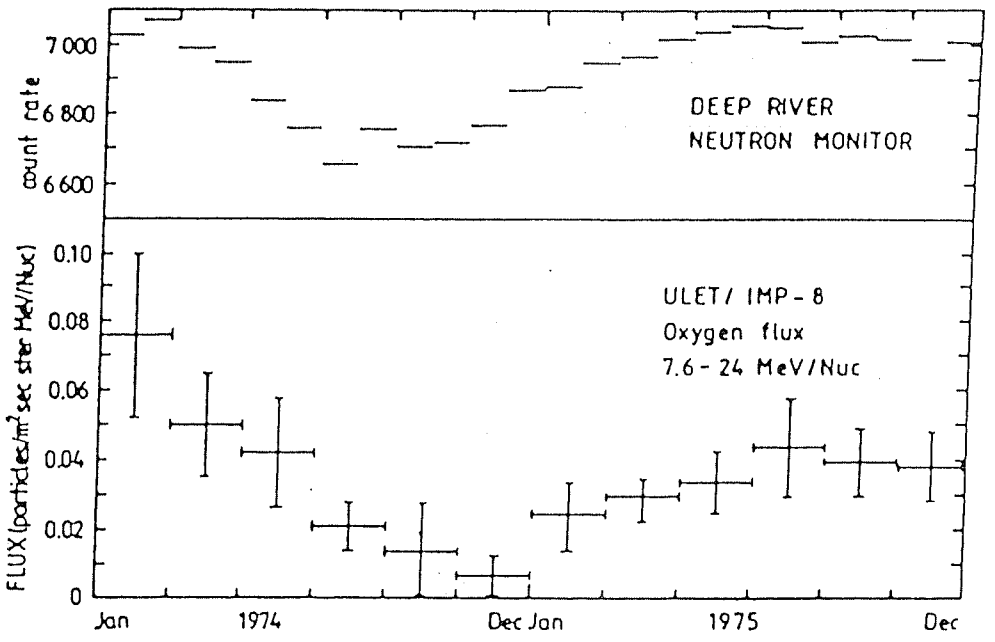

Fig.1-12 The Deep River neutron monitor counting rate (upper panel) and quiet time oxygen flux in the energy region 7.6-24 MeV/n (lower panel) measured by IMP-8 satellite for the time period January 1974 to December 1975. [Reproduced from Klecker et al., 1980]

boundary. Therefore, following the suggestion of Fisk [1983], they argued that the spectral peaks of these species should occur at those energies where their interplanetary diffusion coefficients are the same, and concluded that the observed ACR particle fluxes and their peaks are consistent with their being in singly ionized state.

McDonald *et al.*[1988] have measured the galactic and anomalous H, He and O flux for four different time periods [fig.1-13]. The modulation parameters were determined more accurately from the galactic He flux (E=150-450 MeV/n) measured at larger heliocentric distance (~38 AU). Same modulation parameters were used to demodulate three sets of data for anomalous He and O, obtained during 1978, 1986 and 1987, assuming different ionization states. The interstellar spectra derived for the three different periods are shown by three different symbols in fig.1-14. It is clear that all the data sets for oxygen fall on the same line when they are assumed to be in +1 ionization state. This is true even in the case of helium. The left hand side of the fig.1-14 show that the spectrum reproduced from three data sets do not match if the oxygen particles are assumed to be in +2 ionization state.

Thus there is a general consensus that the ACR particles are predominantly in singly ionized state. Since the ionization state of ACR is a crucial parameter for pinpointing their source and origin, a direct determination of the ionization states of individual ACR ions was needed to firmly establish the above inference. We have accomplished this task and have measured the ionization states of

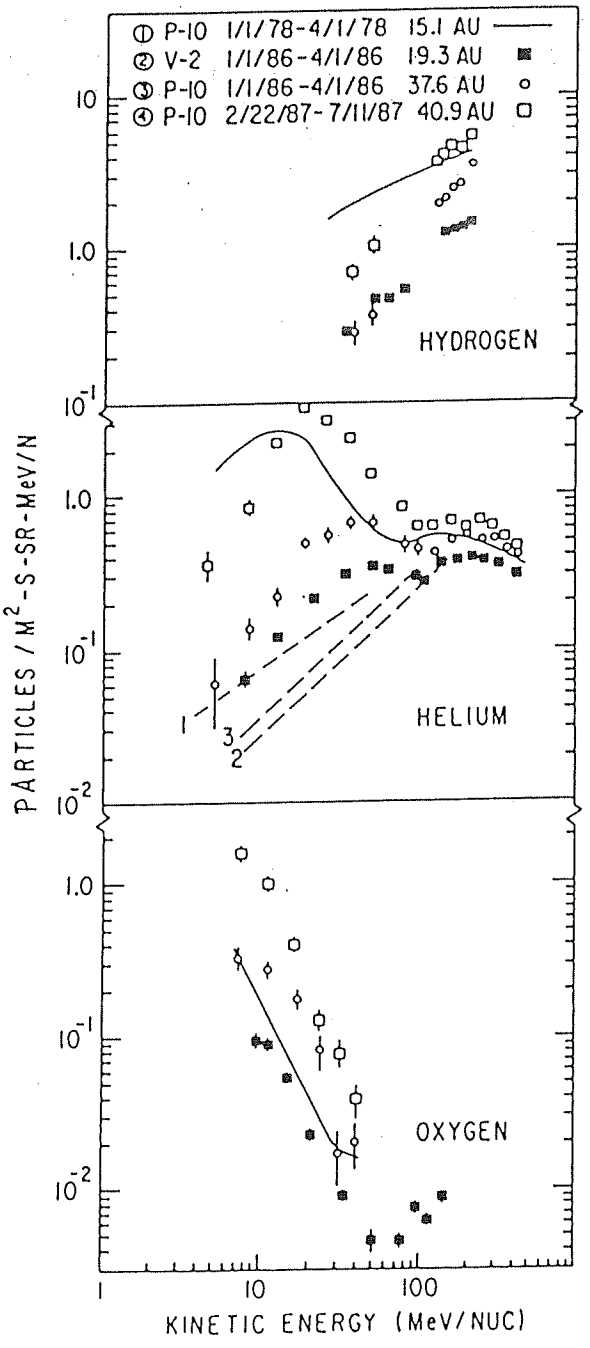

Fig.1-13 H, He and O energy spectra measured by Pioneer-10 and Voyager-2 spacecrafts for selected time periods. The dashed lines are estimates of the galactic He spectra in the anomalous region for the indicated time periods/ spacecrafts. [Reproduced from McDonald et al., 1988]

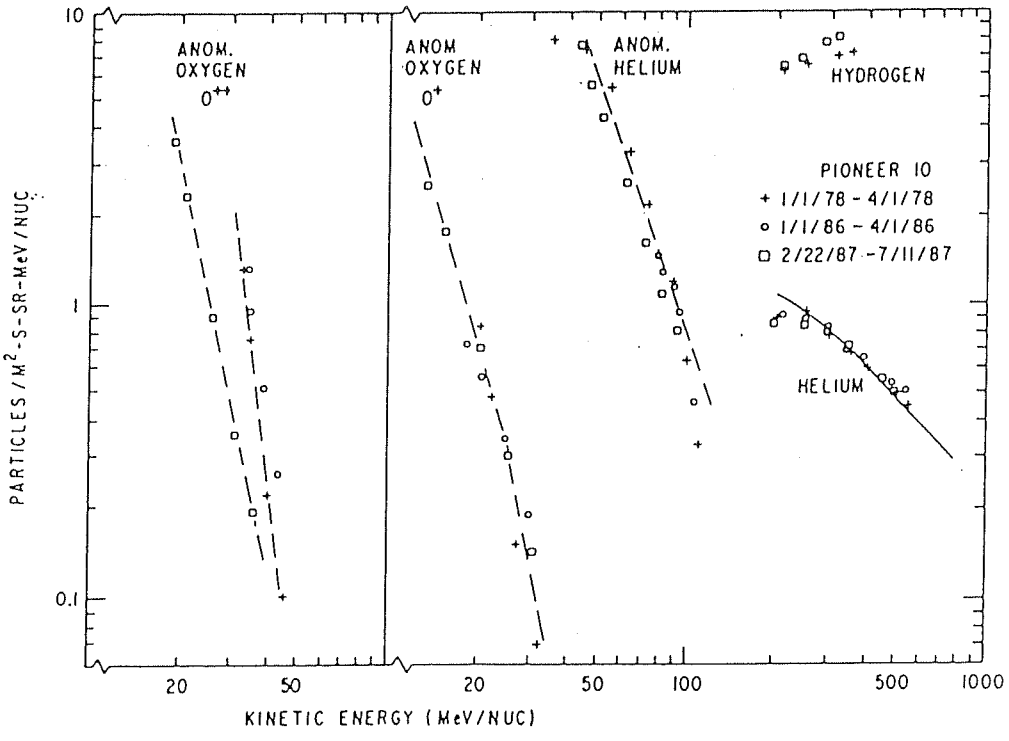

Fig.1-14 Demodulated local interstellar spectra for anomalous H, He and O using the modulation parameters derived from fitting the galactic He spectrum (150-450 MeV/n) to an assumed local interstellar spectrum (solid line). [Reproduced from McDonald et al., 1988]

individual ACR ions in an experiment conducted on board Space Shuttle Spacelab-3. The initial results from this experiment show them to be either in singly ionized state or consistent with their being in singly ionized state [Singh,1990]. We present in this thesis (Chapter-V) results from an expanded data base which confirm the earlier result.

1.3 The "Anuradha" Cosmic Ray Experiment

The work presented in this thesis is based on the cosmic ray experiment *Anuradha* conducted on board Space Shuttle Spacelab-3 Platform (orbital inclination (λ) = $\pm 57^0$, altitude = 365 km) during April-May, 1985. The experiment was jointly carried out by the Physical Research Laboratory, Ahmedabad and the Tata Institute of Fundamental Research, Bombay. The experiment payload contained solid state nuclear track detector (CR-39 plastics) which has been analyzed following space exposure to study the records of energetic charged particles. The main objective of this experiment was to determine the ionization state(s) of ACR particles using the geomagnetic field as a rigidity filter. The same approach was also used to determine the ionization states of low energy (20-150 MeV/n) GCR particles present in the near-earth space. The ionization states of low energy GCR particles were not measured earlier and such measurements may provide new information on the possible differences in the propagation history of the low and the high energy GCR particles. In addition to these objectives there are a number of other studies which were planned on the basis of this experiment.

These include studies of the low energy GCR oxygen spectrum near the period of last solar minimum (1985), studies of sub-iron to iron abundance ratio in low energy (50-400 MeV/n) GCR and search for the presence of elements like Mg, Si etc. that are normally absent in the ACR component. All these studies were feasible because of the large collecting power of about 1600cm^2.sr of the detector used in this experiment.

1.4 Scope of the Present Thesis

The details of the experimental arrangement, pre-flight checks, in-flight performances, post-flight analysis and the data handling procedure in the *Anuradha* experiment has been described in a thesis earlier [Singh,1990]. The results of the ionization states of the ACR particles obtained from the analysis of data from about a quarter of the detector area has also been reported in that thesis.

In the present thesis, results obtained from the analysis of data from about half of the detector area (400 cm^2) are presented. Following are the specific scientific aspects discussed in detail in the present thesis:

1) Results on the ionization state of ACR particles from the enlarged data set and their implications regarding the source of ACR.
2) New results on the ionization states of low energy (20-125 MeV/n) GCR particles and their implication.
3) Energy spectra of GCR oxygen particles in the energy range

50-250 MeV/n, during the last near solar minimum, and a check on the validity of the calculated geomagnetic transmission factor.

The plan of the thesis is as follows:

In chapter two we discuss the method followed in the present work to determine the ionization state(s) of low energy particles. We describe how the geomagnetic field can be used as a rigidity filter to infer the ionization state of energetic charged particles. We also describe the nuclear track technique, used to determine the atomic number, mass number and energy of the charged particles from the records they left behind in the plastic detector. The instrumentation part is described in brief as these are already discussed in detail earlier [Singh,1990]. In chapter three we present data on detector calibration and the method used to compute particle's range, energy etc.. The data acquisition procedures and the method used to determine the arrival position and arrival directions of the low energy charged particles in the Spacelab-3 orbit are also discussed in this chapter. Chapter four deals with the method of computing average geomagnetic cut off rigidity and the transmission factors for energetic charged particles at the Spacelab-3 orbit. The results obtained for the Spacelab-3 orbit-averaged flux of the low energy (50-250 MeV/n) GCR oxygen particles are also presented in this chapter. An inter-comparison of this flux with interplanetary flux during this epoch has been done to check the validity of the computed geomagnetic transmission factor. The method used to obtain threshold rigidity for individual

ions, based on their arrival position and direction is also discussed in this chapter. In chapter five we present the results obtained on the ionization states of low energy particles in two parts. In the first part the results on the ionization state of ACR particles are presented, followed by a discussion on their implications regarding the source and origin of the anomalous cosmic rays. The second part contains the new results on the ionization state of low energy iron-group particles and a discussion on the most probable source for the partially ionized iron group particles. As most of the evidences support them to be of GCR origin, a plausible model for the production of partially ionized iron group particles in the low energy GCR is also presented. The final chapter (Chapter six) contains a summary of the results presented in this thesis, their implications and the scope for further work in this area.

CHAPTER II

EXPERIMENTAL APPROACH AND INSTRUMENT DESCRIPTION

In this chapter we discuss the method used in the Spacelab-3 *Anuradha* experiment for the determination of the ionization states of low energy particles. In addition a discussion on the Nuclear Track method used for identification of the energetic charged particles, and a brief description of the experiment payload are also included.

2.1 Measurement of the Ionization States of Low Energy Charged Particles

Direct measurement of the ionization state of energetic charged particles, using conventional particle detector, is not possible because the particles attain their equilibrium charge states through interaction with the detector material itself, irrespective of their initial ionization states. The electrostatic charge analyzer, used for measuring the ionization states of low energy SW, SEP and trapped magnetosphere particles (Chapter-I; section-1.2), gives us only the average ionization state of these particles and cannot be used in the case of the higher energy ACR and GCR particles. In the *Anuradha* experiment, we have utilized the geomagnetic field as a rigidity filter for estimating the upper limit on the ionization state of individual ACR and GCR ions. In the next section we discuss in detail the method used by us.

2.2 Geomagnetic Field as a Rigidity Filter

The entry of energetic cosmic rays into the earth's magnetosphere is controlled by the geomagnetic field. For each point in the magnetosphere and for each direction of approach to that particular point , there exists a minimum value of magnetic rigidity (*i.e* momentum per unit charge), called geomagnetic cutoff rigidity. Particles possessing rigidity less than this value cannot reach that point from the specified direction *i.e* the particle does not possess enough energy to cross the magnetic field barrier. Hence, one can use the geomagnetic field as a rigidity filter to find the ionization state of an energetic charged particle that reaches a detector inside the magnetosphere, if the momentum of the charged particle is known accurately along with its arrival point and direction within the magnetosphere. This simply follows from the relation,

$$Z^{*} \leq \frac{p.c}{R_c} \qquad \ldots(2.1)$$

where, Z^{*} is the upper limit on the ionization state of the particle, p is its momentum, R_c is the geomagnetic cutoff rigidity and c is the speed of light.

An expression for the geomagnetic cutoff rigidity with a dipole approximation for the geomagnetic field was first given by Stormer [1930]:

$$R_c(r,\vartheta,\phi,\lambda) = \frac{M.\,Cos^4\,\lambda}{r^2\left[1+\left\{1-Sin\vartheta.\,Cos\phi.\,Cos^3\lambda\right\}^{1/2}\right]^2} \quad \ldots (2.2)$$

where, R_c is the minimum rigidity required by a particle to reach geomagnetic latitude λ at an angle ϑ from the local zenith and ϕ from the local east (see fig.2-1). M is the dipole magnetic moment and r is the distance from the center of the dipole to the arrival point of the particle.

Vallarta [1948] showed that there exists a range of allowed and forbidden bands in magnetic rigidities above the Stormer's cutoff value. This effect is caused by the earth which is an extended object and produces a "shadow effect" on the particle. The width of this shadow-zone varies between 10 to 100 percent of the value of R_c at the earth's surface for zenith angles $\leq 45^0$. Based on the above relation and including the shadow effect, one can predict the expected intensities of cosmic rays at different locations on earth within the frame work of a dipole field model. However, many a discrepancies were noticed between the expected and the measured cosmic ray intensities at various geographic locations [Rose *et al.*,1956; Kodama and Miyazaki,1957; Pfotzer,1957; Rothwell and Quenby,1957; Simpson,1957; Skorka,1958]. A disagreement between the observed and the predicted values of cutoff rigidities for α-particles was also found [Waddington,1956; McDonald,1957]. Quenby and Webber [1959] argued that a simple dipole representation of the earth's magnetic field may be the reason for the observed discrepancies and proposed that one must take into account the non-dipole nature of the geomagnetic field .

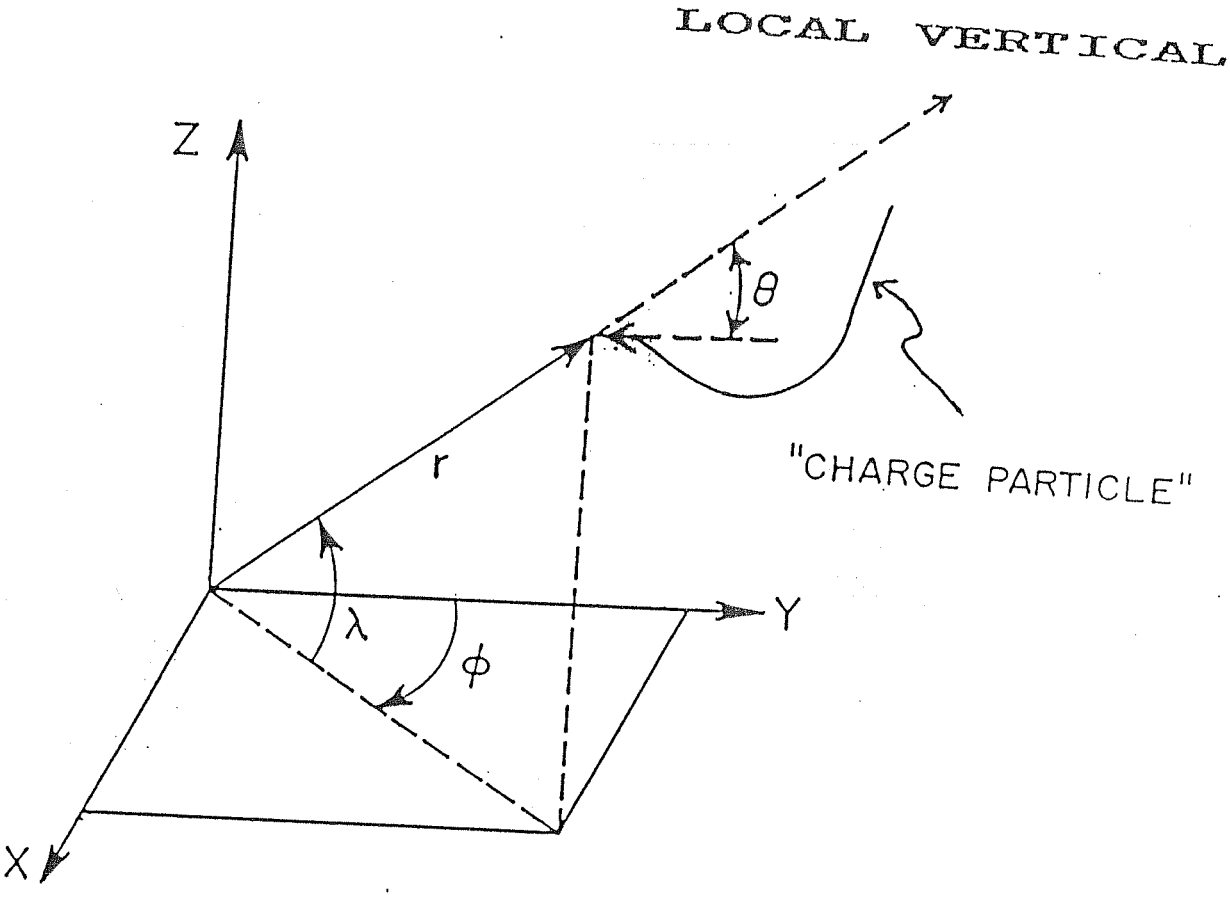

Fig.2-1 A schematic diagram showing the entry of a charge particle in earth's magnetosphere at a geomagnetic latitude λ. The azimuth angle is measured from local east and ϑ denotes the local zenith angle.

The geomagnetic field can be expressed mathematically as a negative gradient of a specific potential U, *i.e* $\mathbf{B} = -\nabla U$. The expansion of the potential in spherical harmonics was first used by Chapman and Bartels [1940] to describe the geomagnetic field. Following Chapman and Bartels, we can write the potential in spherical coordinate as follows:

$$U = R_E \sum_{n=0}^{max} \sum_{m=0}^{n} \left(g_n^m \, Cos(m\phi) + h_n^m \, Sin(m\phi) \right) P_n^m \, Cos(\vartheta) \left(\frac{R_E}{r} \right)^{n+1} \quad ..(2.3)$$

where, ϑ and ϕ are colatitude and east longitude respectively, P_n^m is the suitably normalized associated Legendre functions of order m and degree n, g_n^m and h_n^m are the gauss coefficients, r is the radial distance from the center of the earth to the location at which the magnetic field is evaluated, and R_E is the mean radius of the earth (6371.2 km).

The different magnetic field components are,

$$B_r = - \frac{\partial U}{\partial \vartheta}$$

$$B_\vartheta = - \frac{1}{r} \frac{\partial U}{\partial \vartheta} \qquad \ldots (2.4)$$

$$B_\phi = - \frac{1}{r \, Sin\vartheta} \frac{\partial U}{\partial \phi}$$

For such a field representation one can calculate the cutoff rigidity for a particular point and direction within the magnetosphere by what is known as the "trajectory-tracing" method. In this approach one considers the equation of motion of a charged

particle in the geomagnetic field:

$$\frac{d^2R}{dt^2} = \frac{q}{mc}\left(\frac{dR}{dt} \times B\right) \qquad \ldots (2.5)$$

and the trajectory of the individual charged particle is traced backwards by considering the particle charge to be negative and moving outward from the earth, anti-parallel to the direction of its approach. The cut-off rigidity is defined as the minimum value of rigidity for which the particle escapes from the magnetosphere into the interplanetary space.

Thus, one can calculate the cutoff rigidity by the trajectory-tracing method, if the arrival position and arrival direction of an energetic particle at a given point inside the magnetosphere are known. If the particle's momentum can also be obtained independently, the upper limit of its ionization state can be determined using relation 2.1. This has been accomplished in the Spacelab-3 *Anuradha* experiment and is the main subject matter of the present thesis.

2.3 The Nuclear Track Method

The passage of energetic charged particles in dielectric solids lead to ionization-induced damage in the structure of the solids along the paths of the charged particles. If the ionization loss rate exceeds a certain critical value, characteristics of each dielectric solid, the structural damage trails are stable under

normal environmental conditions, and can be seen directly by transmission electron microscopy or can be enlarged by suitable chemical etching and seen by conventional optical microscopes. The latent or chemically etched damage trails produced by the passage of energetic charged particles in solids are called nuclear tracks. The registration threshold for different dielectric solids differs widely; while a sensitive plastic like cellulose nitrate can record tracks produced by low energy α-particles, silicate minerals, like those found in terrestrial and extra-terrestrial samples, record tracks only of energetic particles with atomic number Z>20, *i.e*, primarily of the iron group and heavier ions. As the ionization loss rate of charged particles in any medium reaches a maximum near the end of their range, nuclear tracks are produced only near the stopping point of the ions irrespective of their initial energy. The track length is thus a function of the atomic number of the track producing particle.

2.3.1 Track Formation Mechanism

Fleischer *et al.* [1975] have reviewed several proposed track formation models. At present, the model based on the criterion of the Restricted Energy Loss (REL), introduced by Benton [1968], is widely accepted. Charged particle upon traversing matter, loses its energy predominantly through collision with atomic electrons. The rate of energy loss will depend on the atomic number z of the charged particle, its velocity v and nature of the stopping material. In the case of a low energy (few MeV/n) particle, energy is lost through many low energy collisions with atomic electrons and

the secondary ionization and excitation produced by the low energy recoil electrons will be confined to a small cylindrical volume; whereas, in the case of high energy (GeV/n) particles, many high energy (up to several MeV) recoil electrons (δ-rays) are produced. Because of their considerable range (up to few millimeters) these high energy electrons transfer or deposit their energy far from the particles path. Since the latent tracks have typical diameter of $\lesssim$ 100 Å in polymers [Fleischer *et al.*,1975], such high energy δ-rays will not contribute effectively to the track formation process. Therefore, it is convenient to separate the total energy loss term into two parts according to the energy ω imparted to the recoil electrons.

$$(dE/dX)_{Total} = (dE/dX)_{\omega \geq \omega_0} + (dE/dX)_{\omega < \omega_0} \quad \ldots (2.7)$$

where, the value of ω_0 is chosen in such a way that all the electrons having energy less than this value will contribute to the track formation process. One can therefore write the Bethe-Block formula for the total energy loss rate in two parts and the energy loss rate responsible for track formation, termed, the restricted energy loss rate, is expressed as,

$$\left(\frac{dE}{dX}\right)_{\omega<\omega_0} = \frac{2\,\pi\,n\,(z^*)\,r_0^2\,m_0c^2}{\beta^2}\left[\ln\left(\frac{2\,m_0c^2\,\beta^2\,\gamma^2\,\omega_0}{I_{adj}^2}\right) - \beta^2 - \frac{2C}{Z} - \delta\right] \quad ..(2.8)$$

where, $\gamma = (1-\beta^2)^{-1/2}$

n = density of electrons in the stopping material

z^* = effective charge state of the ionizing particle

$$= z\left[1-\exp\left(-125\beta/z^{2/3}\right)\right]$$

z = atomic number of the ionizing particle

$r_0 = e^2/m_0c^2$, the classical electron radius

I^2_{adj} = mean excitation potential of the material

$\frac{C}{Z}$ = tight binding shell correction

Z = mean atomic no. of the detector material.

δ = correction for the polarization effect.

The parameter ω_0 is the average recoil energy of an electron which delineates between the contributing and non-contributing electrons to the formation of the latent track region. ω_0 is an adjustable parameter and in case of CR-39 plastic detector, the best value that matches the experimental data is 350eV [Henke and Benton,1987].

2.3.2 Chemical Processing of Latent Tracks

Chemical processing of the latent tracks is needed to make them observable in a conventional optical microscope. The choice of the chemical for track etching depends upon the detector material used and should be such that the rate of dissolution of detector along the latent track (generally known as track etch rate, V_t) is much higher than the average dissolution rate of the detector material (generally known as bulk etch rate, V_g).

The formation of an etch cone around the path of an ion can be visualized from fig.2-2. At each position on the plastic surface, the bulk etch rate V_g acts in all directions. Hence, after a time t the material removed from the surface is given by an amount $V_g.t$. As $V_t > V_g$, the removing of material along the path of the particle will be much faster, and we get a conical shaped pit or a nuclear track.

For a charged particle with a given energy, the etching rates V_t and V_g depend on the nature of the detector material and the nature of the etchant and the etching temperature. It is necessary to optimize these parameters for a given experiment. In the Spacelab-3 *Anuradha* experiment we have used a specially prepared plastic detector (CR-39; DOP) which is extremely sensitive with the capability of registering tracks of charged particles with $Z/\beta \geq 8$. To achieve a good charge resolution and to be able to study both the light and heavy ions (Z = 6 to 26) at the same time, we have etched the CR-39 detectors, following their space exposure, in a 6.25N NaOH solution at $(70 \pm 0.2)^0$C for six hours. These conditions are based on studies of tracks in auxiliary CR-39 detector exposed to energetic beams of He, C, N, O, Ne, Al and Fe from the Berkeley Bevalac (USA), the Linear Accelerator at Dubna (Moscow) and the Variable Energy Cyclotron at Calcutta, (India) prior to etching of the Spacelab exposed detectors. The bulk etch rate V_g for the CR-39 detector was found to be ~1.3 micron per hour for the above etching condition.

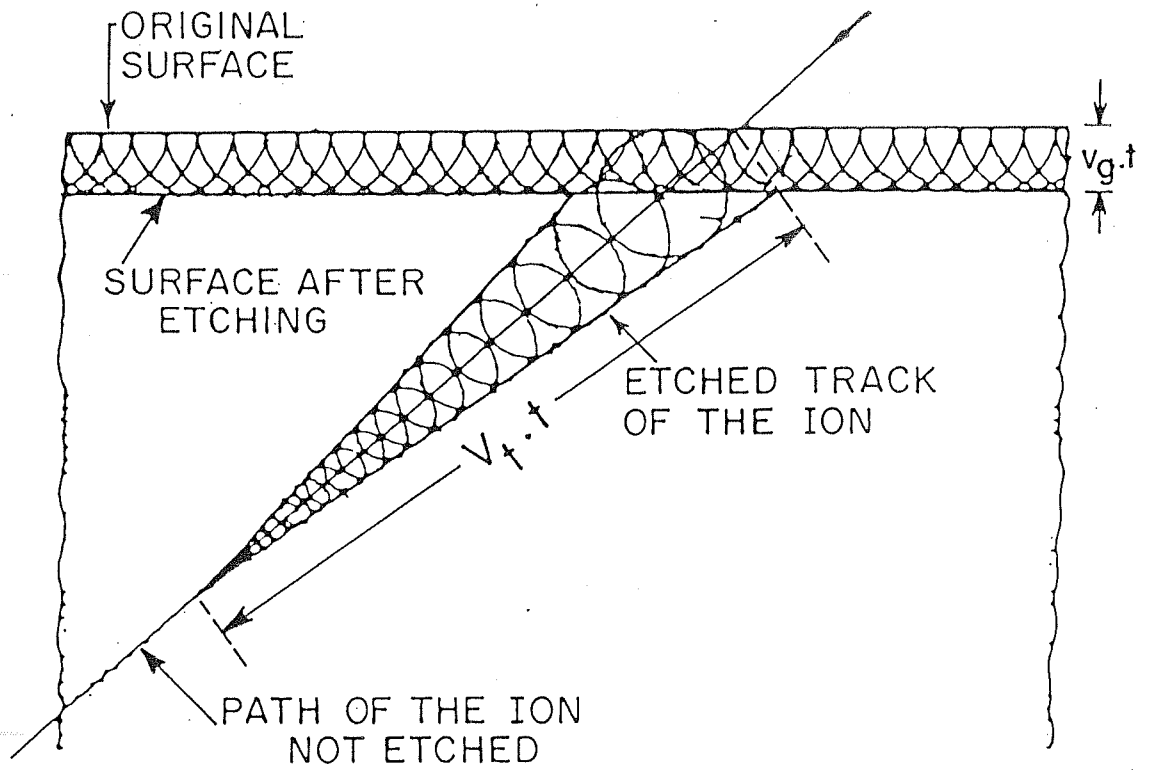

Fig.2-2 Side view of an etched track. The material removed from the surface is $V_g.t$ and the cone length is $V_t.t$. [From Enge, 1980]

2.3.3 Track Geometry

The geometry of a track depends on the angle of incidence and the energy loss rate of the charged particle and hence on the etching rate. A track can be approximated by a hollow etched pit. The opening of the track takes the shape of an ellipse unless the particle enters the detector vertically. From the projected view of an etched track on the detector surface, as seen under the microscope (see fig.2-3), the following quantities can be measured: i) projected length (s), ii) the semi-major axis (a), iii) the semi-minor axis (b), iv) the radius of the tip of the track (r) and v) the depth of the tip from the etched surface (z). The etched tracks can be classified into the following categories:

i) ST (sharp tip): The etching is stopped before the etchant could reach the stopping point of the particle (fig. 2-4(a)).

ii) RT (round tip): The etching progressed even after the solution reached the end point of the particle's range. The bulk etching around the end point will give rise to a RT track (fig.2-4(b)).

iii) DC (double cone): When the particle passes through in an etched plastic detector sheet, but the energy loss rate is high enough to produce tracks, two ST cones are formed at the entry and exit points of the particle on the two surfaces of the detector and we get a DC (fig.2-4(c)).

iv) JDC (joint double cone): If the energy loss rate is rather high in case of (iii), the higher etching rate will lead to merging of the tips of the double cone, and, we get a JDC (fig.2-4(d)).

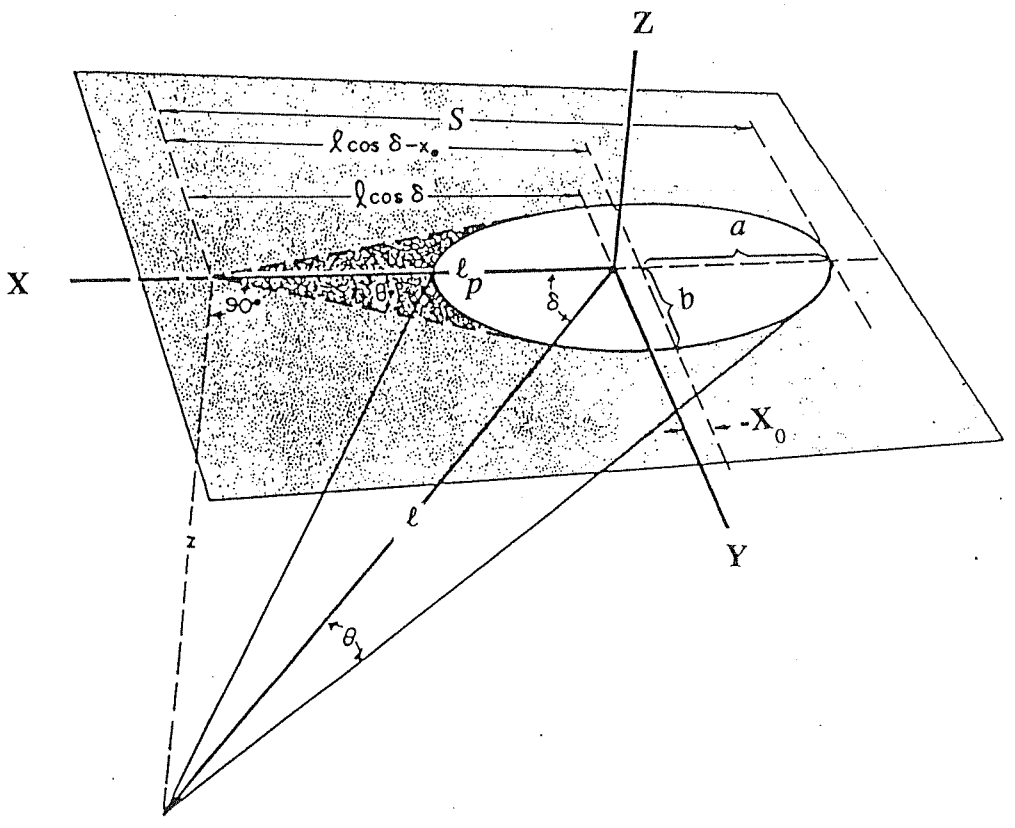

Fig.2-3 The general case of cone which intersects the XY plane at a dip angle δ. Here ℓ and ℓ_p represents the true and projected track length respectively. The semi-major and semi-minor axes of the elliptical opening are denoted by a and b respectively. [From Benton, 1968]

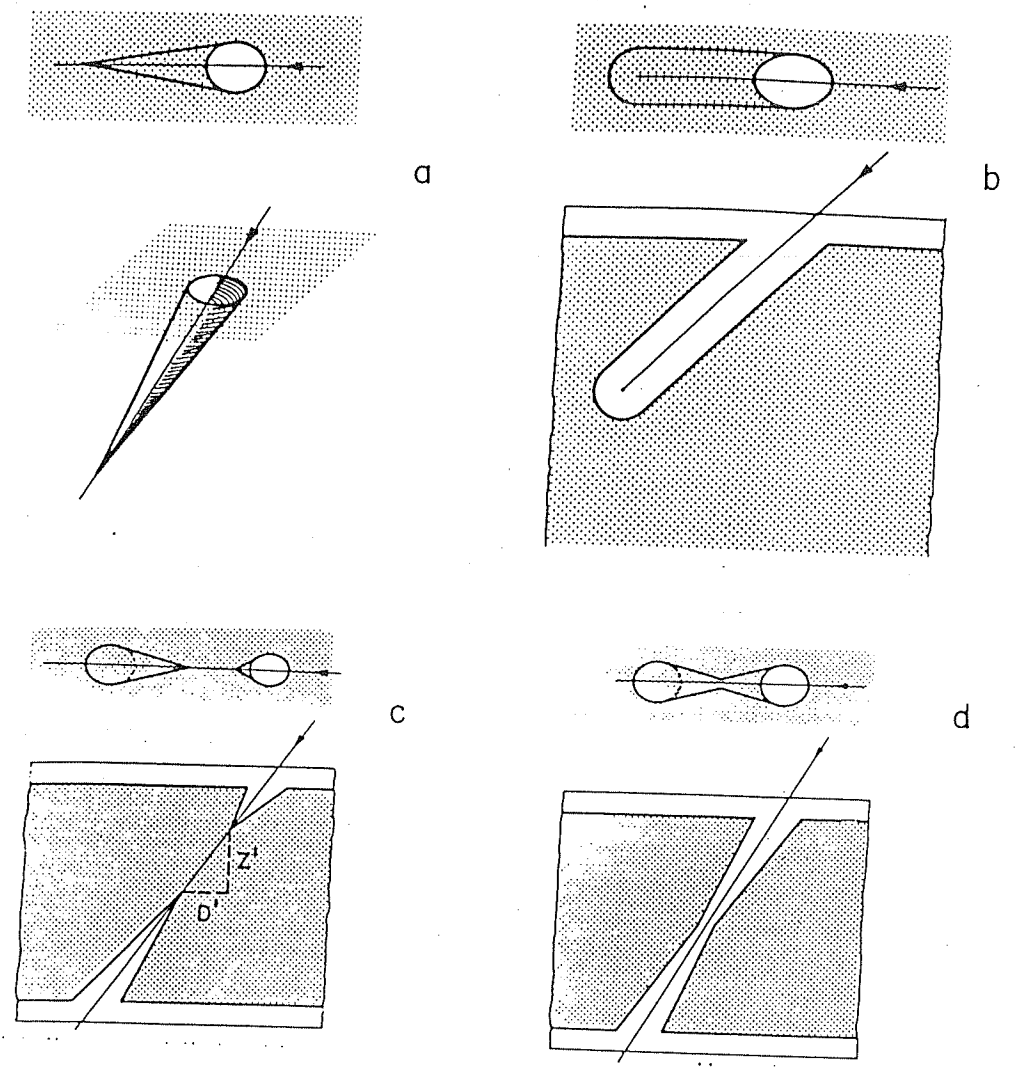

Fig.2-4 (a) Two views of a Sharp Tip track. (b) Round Tip track (top and side views). (c) Double Cone (top and side views). (d) Joint Double Cone (top and side views). [From Enge, 1980]

For simplicity we will assume V_t as a constant over the etched track length and express all the track parameters in terms of the measurable quantities following the approach of Henke and Benton [1971]. Let us consider a ST track (fig.2-3). Here, a, b, s, r and z are already defined. δ and ϑ denote the incident or the dip angle and the cone angle respectively. From the measurable parameters one can find the relevant quantities like the true track length L_r, the dip angle δ, the bulk etch rate V_g and the etch rate ratio V_t/V_g in two ways:

I. From the measured values of s, z, b and r:

$$\text{Sin}(\delta-\vartheta) = \frac{r(s-r) + z\,[\,s^2 - 2sr + z^2\,]^{1/2}}{(s-r)^2 + z^2}$$
$$= z\,(\,s^2 + z^2\,)^{-1/2} \qquad [\text{for ST; } r=0\,] \qquad ...(2.9)$$

$$\frac{\text{Sin}(\vartheta)}{\text{Sin}(\delta)} = \frac{b\,[z^2 + b^2 - r^2]^{1/2} - zr}{z^2 + b^2}$$
$$= b\,[\,z^2 + b^2\,]^{-1/2} \qquad [\text{for ST; } r=0\,] \qquad ...(2.10)$$

From equation (2.9) and (2.10) one can calculate the values of δ and ϑ. Remaining quantities can be calculated as follows,

$$\left.\begin{aligned} V_t/V_g &= 1/\text{Sin}(\vartheta) \\ L &= (z+r) \,/\, \{\text{Sin}(\delta)-\text{Sin}(\vartheta)\} \\ \text{and,}\quad V_g &= (\,L_r\,\text{Sin}(\vartheta) + r\,)\,/t \end{aligned}\right\} \qquad ...(2.11)$$

where, t is the etching time.

II. From the measured values of s, a, b and r :

$$\tan(\vartheta) = \left[\frac{(a^2 - b^2)^{1/2}}{a}\right] \times \frac{[\, b^2(s-r-a)^2 - (a^2-b^2)\,(b^2-r^2)]^{1/2} - r(s-r-a)}{(s-r-a)^2 - (a^2 - b^2)}$$

$$= \left[\frac{b(a^2 - b^2)^{1/2}}{a}\right] \times [\, (s-a)^2 - (a^2-b^2)\,]^{-1/2} \quad \text{[for ST; r=0]}$$

...(2.12)

$$V_t/V_g = 1/\mathrm{Sin}(\vartheta)$$

$$\left.\begin{aligned} \mathrm{Sin}(\delta) &= [a^2\, \mathrm{Sin}^2(\vartheta) + b^2\, \mathrm{Cos}^2(\vartheta)\,]^{1/2} \;/a \\ L_r &= \left[s-r-a + (a^2 - b^2)^{1/2}\right] / \mathrm{Cos}(\delta) \\ \text{and,}\quad V_g &= (\, L_r\, \mathrm{Sin}(\vartheta) + r\,)\,/t \end{aligned}\right\} \quad ...(2.13)$$

The value of the dip angle δ, can be obtained most precisely from measurement of the tip to tip distance,D', and tip to tip depth, Z', of a double cone (see fig.2-4(c)). The value of δ can then be used as an additional parameter to calculate the values of L_r, V_t/V_g etc. These measured parameters are then used for identification of the atomic number of the track forming particles. The stopping point of a track provides the particles range in the detector and hence its energy and momentum can be estimated using range-energy relation appropriate for the detector material.

2.3.4 Particle Identification

Identification of the atomic number and the mass of a track producing charged particle can be done by using the conventional

E–dE/dX method, where E is the energy of the incident particle at a given point and dE/dX is the energy loss rate at that point. As discussed earlier, it is the restricted energy loss rate (REL), $(dE/dX)_{\omega \leq \omega_0}$, and not the total energy loss rate that contribute to the track formation, and in the following dE/dX will refer to REL unless otherwise stated. The track length (L) or the track etch rate (V_t) of a track producing particle at a given point in its path is a function of its energy loss rate (dE/dX) at that point, and the residual range (R) is related to the energy of the particle at that point. So, we need to have a calibration curve (L, V_t vs R) for different charged particles for their identification from the track data. To construct the V_t vs R plot for different ions in a given detector one has to first calibrate the detector by exposing it to particle beams of known energy. This will be clear from fig.2-5. In this figure a schematic of tracks formed by an energetic heavy ion in successive sheets of plastic detector is shown. The length of the track increases as the energy (residual range) of the particle decreases. This is expected because restricted energy loss rate (dE/dX) increases with decreasing energy (fig.2-6). Therefore, the dE/dX–E curve can be converted to a (L, V_t–R) curve. In practice, one more often uses the parameter V_t/V_g instead of V_t, where V_g is the bulk etch rate. Such a representation takes care of small spatial non-uniformity in the bulk etch rate of the detector. Once the V_t/V_g–R plot is obtained for one or more energetic ion species with given atomic number(s) from calibration experiments, one can generate a relation between track etch rate and dE/dX, which is true for all charged particles. The V_t/V_g–R plots for ions with different atomic numbers can be obtained from the above relation considering

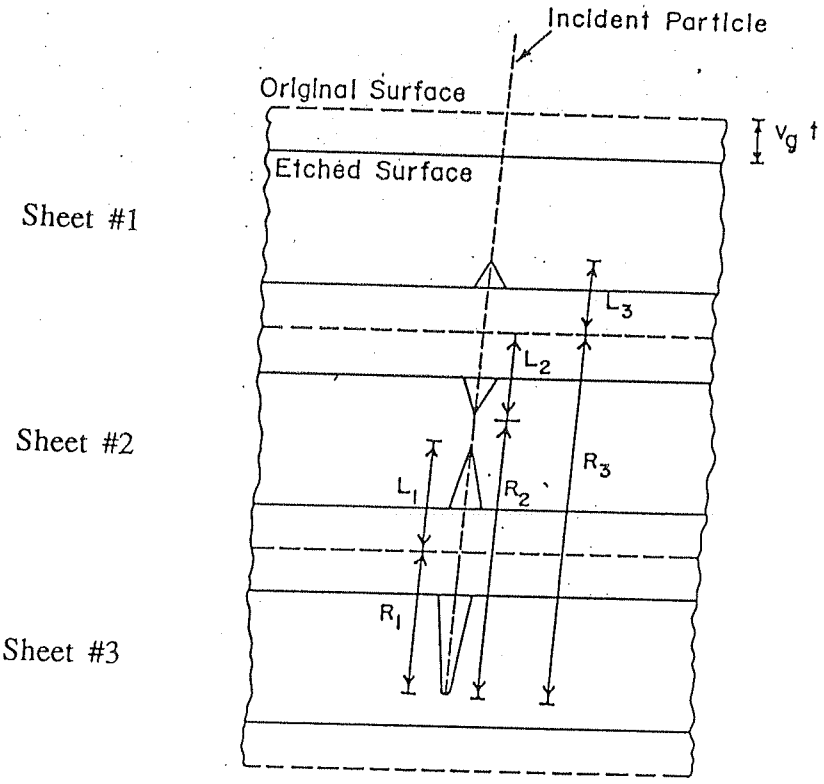

Fig.2-5 Tracks formed by an energetic charged particle in successive sheets of plastic detector. Particles are identified by measuring the track lengths L_i at residual ranges R_i. [From Fleischer et al.,1975]

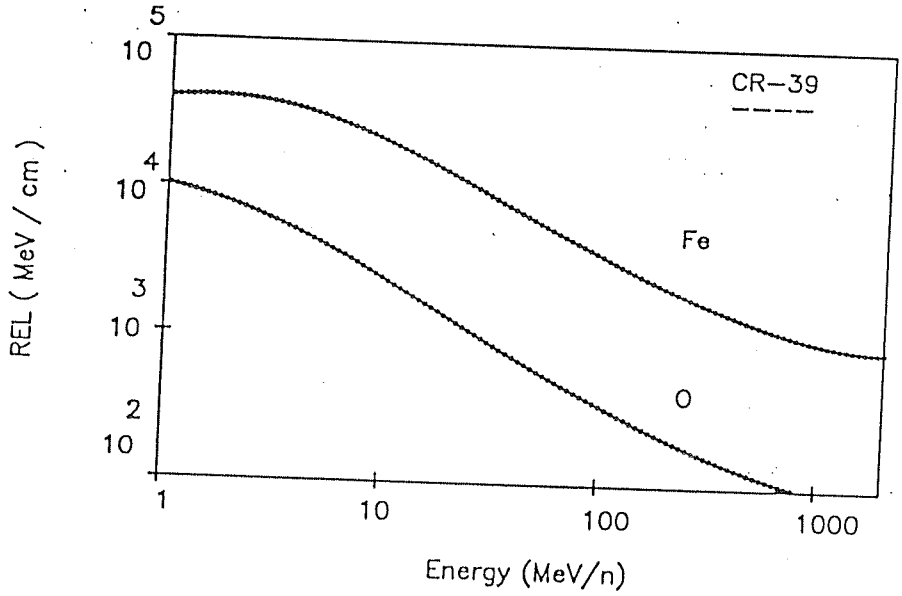

Fig.2-6 Energy vs. Restricted Energy Loss rate (REL) of oxygen and iron particles in CR-39 detector.

the appropriate energy loss rate and range- energy relations for different ions in the detector material. The identification of the atomic number and mass of the track producing charged particles is done by matching the measured values of V_t/V_g and R for each track with the calibration curves for different charged particles. The calibration of the detector used in the present experiment will be discussed in chapter-III. An example of a heavy ion track detected in the present experiment is shown in fig.2-7. This photomicrograph represents an iron ion which has produced a double cone in the first detector sheet followed by a joint double cone in the next before coming to a stop in the third detector sheet where we see a round tip track.

2.4 The Spacelab-3 Anuradha Experiment

The Spacelab-3 *Anuradha* experiment (IONS), was especially designed to determine the ionization states of the low energy cosmic rays using the geomagnetic field as a rigidity filter. A photograph of the *Anuradha* instrument is shown in fig.2-8. This experiment was carried out on board space shuttle Challenger (Spacelab-3) during the last near solar minimum. The shuttle was launched into space on 29th April 1985 and it landed back on earth on 6th May 1985. The orbit of the space shuttle had an altitude of about 365 km with an inclination of 57^0 to the equator. The space exposure of the *Anuradha* instrument started as soon as the shuttle cargo-bay doors were opened, following the placement of the shuttle in its orbit. For most part of the mission the shuttle was placed in a gravity gradient mode, in which the nose cone of the shuttle was always

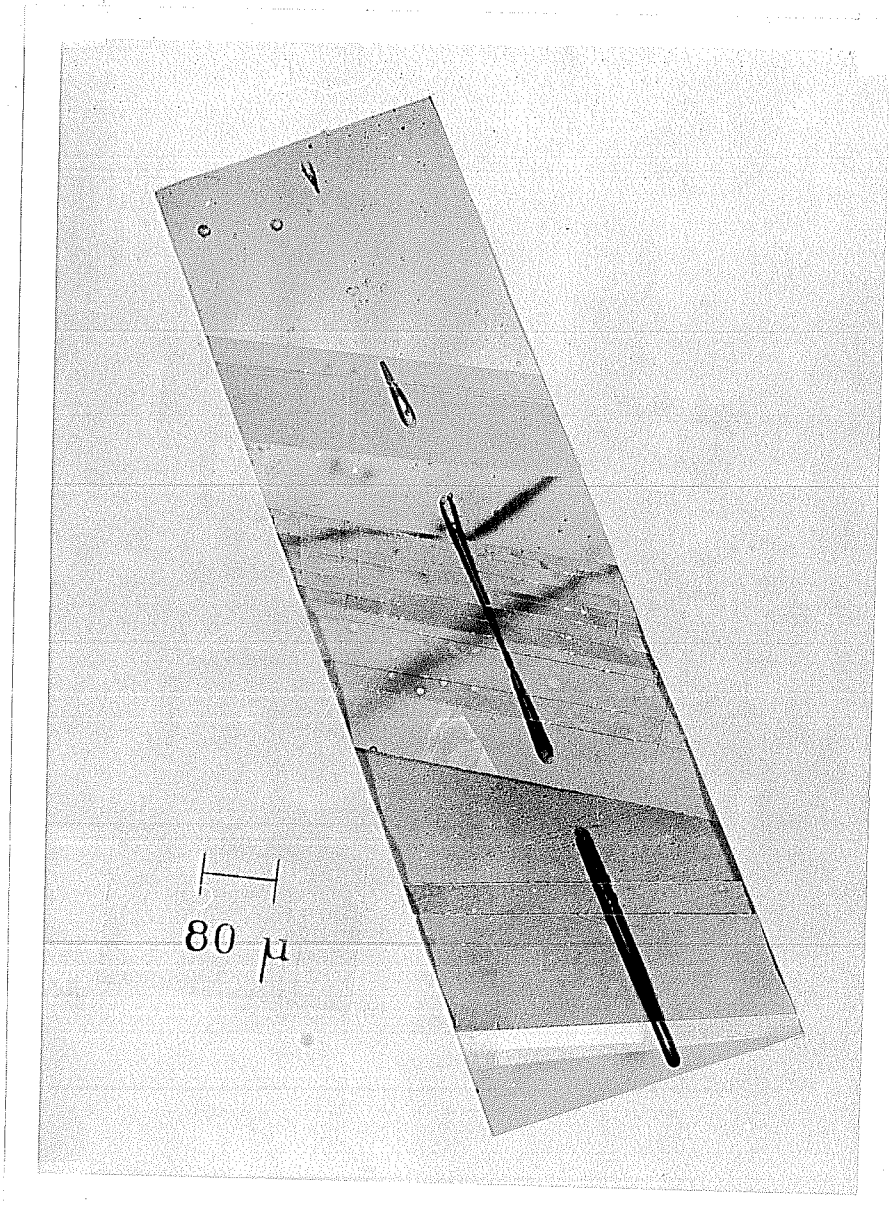

Fig.2-7 A photomicrograph of tracks formed by an iron ion in CR-39 plastic detector, as seen in the present experiment.

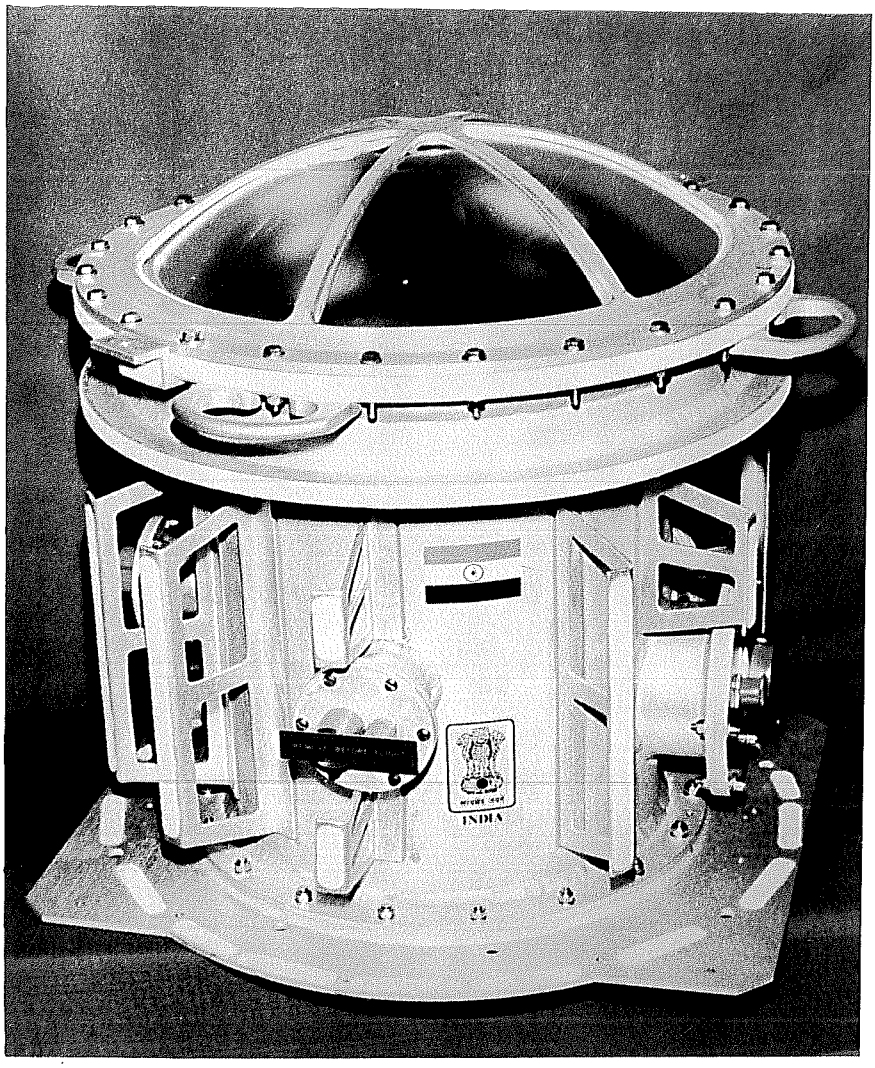

Fig.2-8 The Spacelab-3 Anuradha cosmic ray instrument.

pointing radially outwards. Such a configuration is most suitable for determining the arrival direction of the energetic charged particles incident on the instrument detector, one of the important parameter in this experiment. However, for the last 13 hours of the exposure period, the shuttle was placed in an inertial frame of reference, in which the nose cone of the shuttle was always pointing towards a fixed direction in the sky. Fig.2-9 shows the viewing cone of the *Anuradha* (IONS) in Spacelab-3 experiment. The Z-axis of the instrument was tilted by 25.15^0 towards the spacelab module to reduce the earth's shadow on the viewing cone of the instrument, in the 'gravity gradient' stabilized mode of the spacecraft. The total collecting power of the detector was ~1600 cm^2.sr.

2.5 Experimental Approach

We have already discussed (section-2.2) that the use of the geomagnetic field as a rigidity filter for the determination of the ionization state of an energetic charged particle require the determination of the momentum and the arrival location and direction of the particle, which has to be supplemented by the estimation of appropriate value of the geomagnetic cutoff rigidity (R_c). To achieve these objectives the detector module used in the *Anuradha* experiment was made of two co-axial circular passive plastic detector stacks. The first or the top stack was a single circular sheet of CR-39, and was kept fixed during the exposure period. The second or the bottom stack consisted of circular sheets of CR-39 and lexan polycarbonate, and was made to rotate by step movement during a part of the exposure period. A small gap was maintained between

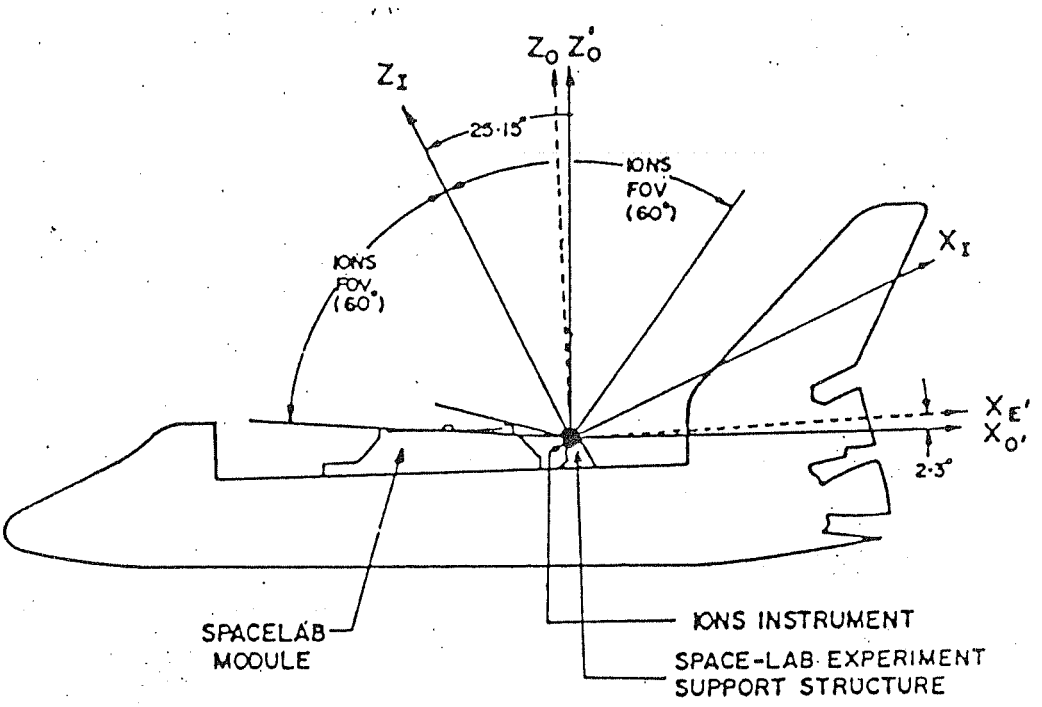

Fig.2-9 Field of view of Anuradha (IONS) in Spacelab-3 experiment support structure. The Z-axis of the instrument was tilted by 25^0 towards the Spacelab-3 module to reduce the earth's shadow on the viewing cone of the instrument in the 'gravity gradient' mode of the Spacecraft.

these two stacks.

An energetic charged particle incident on the detector stack and coming to rest in the bottom stack can produce nuclear tracks in both top and bottom detector stacks. If the particle was incident when the rotation of the bottom stack was active, the track segments corresponding to a particular charge particle in the top and the bottom stacks will not coincide when the rotation is stopped. If at the end of the rotation the angular shift between the track segments in the top and the bottom stacks is denoted by ϑ and the angular speed of rotation of the bottom stack be ω, then,

$$\vartheta = \omega\ t \qquad \ldots(2.14)$$

where, t is the time interval between the arrival time of the particle and the time when bottom stack rotation was stopped. This is shown schematically in fig.2-10 with reference to the '0' lines in the top and bottom stacks, which were coincident before the start of the bottom stack rotation. The angles between these reference lines were ϑ_1 and ϑ_2 at the time of arrival of the particle and at the end of rotation of the bottom stack respectively. The exact procedure of track matching will be discussed in the next chapter. The arrival position (latitude, longitude and altitude) of the particle is obtained from the knowledge of the arrival time of the particle, as these parameters for the Space Shuttle were continuously monitored by NASA and were made available to us. The arrival direction of the particle in geocentric or local coordinate system is obtained by combining the following information:

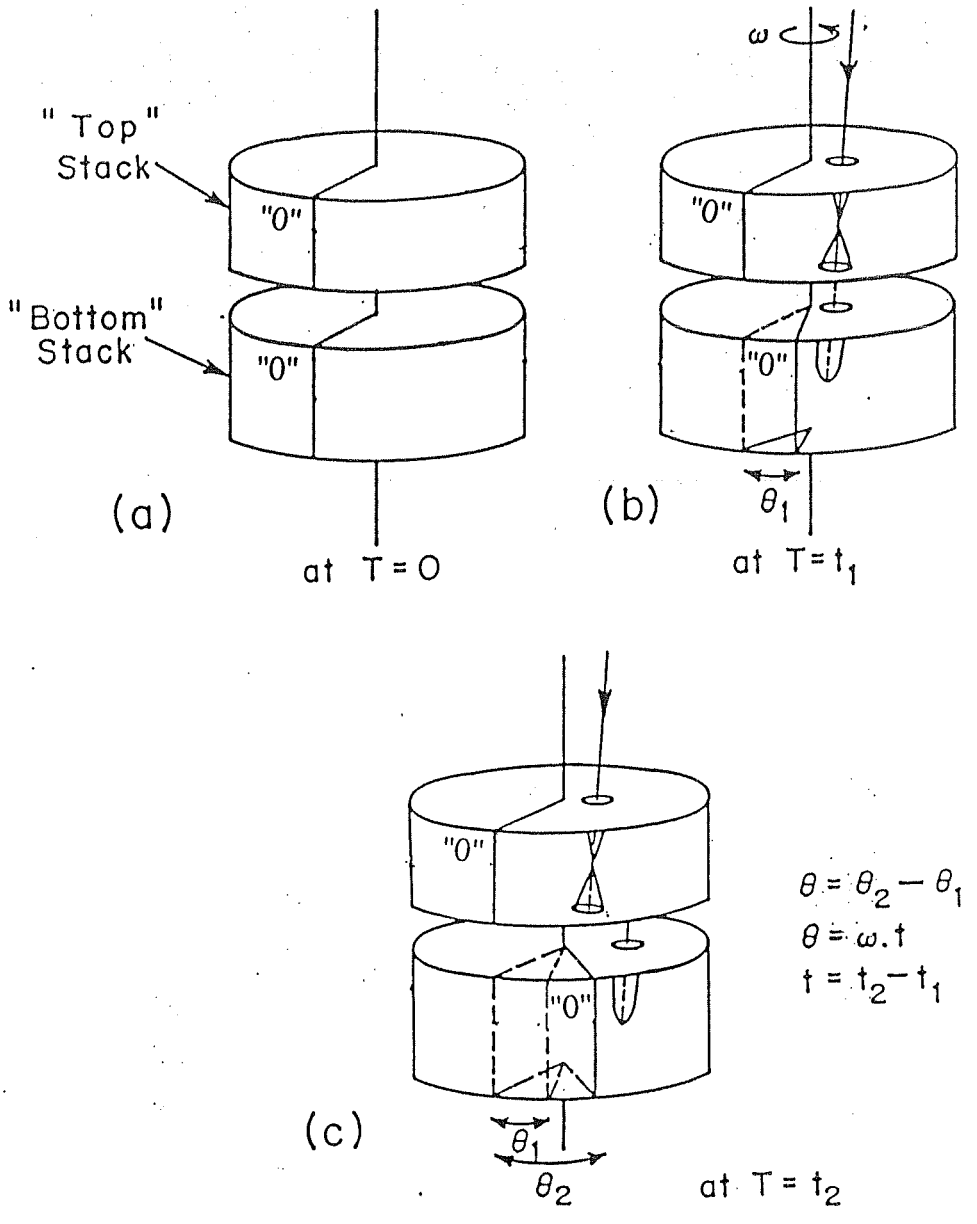

Fig.2-10 A schematic diagram for the procedure used to determining the arrival time of a particle incident on the Anuradha detector. a) The '0' lines on the top and the bottom stacks were coincident before the start of the bottom stack rotation (at T=0). b) At $T=t_1$, when the particle arrived the bottom stack has rotated by an angle ϑ_1. c) At $T=t_2$, the experiment was stopped and the angular difference between the '0' lines in two detector stacks was ϑ_2. The angular difference ϑ (= ϑ_2-ϑ_1) gives the time of arrival of the particle prior to stop of the bottom stack rotation.

i) arrival direction of the particle in the detector (*i.e* dip angle, azimuth angle), ii) relative orientation between the detector coordinate system and the Space shuttle coordinate system, and iii) the orientation of the Space Shuttle in geocentric and local coordinate systems. Coupling the information on the arrival position and arrival direction with the geomagnetic field model, the cutoff rigidity (R_c) for the particular arrival location and direction of each particle is determined by the trajectory-tracing method. The information on the atomic number, mass, energy and momentum of the charged particle incident on the *Anuradha* detector module was obtained independently by using the nuclear track method discussed earlier. Combining these two data set we could determine the ionization states of the charged particles incident on the detector of the *Anuradha* experiment.

2.6 Instrumentation

A schematic diagram of the different components in the *Anuradha* payload is shown in fig.2-11. The cylindrical instrument had a diameter of 48 cm and a height of 56 cm with a weight of ~50 kg. The top enclosure of the instrument was a thin shell of aluminum about 75 μm thick which was covered with a 12μm thin thermal tape. The total thickness of the top shielding was small enough to allow low energy (≥10 MeV/n) CNO group particles to reach the top detector sheet placed below the top shell. A five element rib structure of aluminum provided support to the top enclosure. The top detector stack consisting of a single CR-39 sheet of diameter 40 cm and thickness of ~337 μm was mounted on the top stack ring, which was

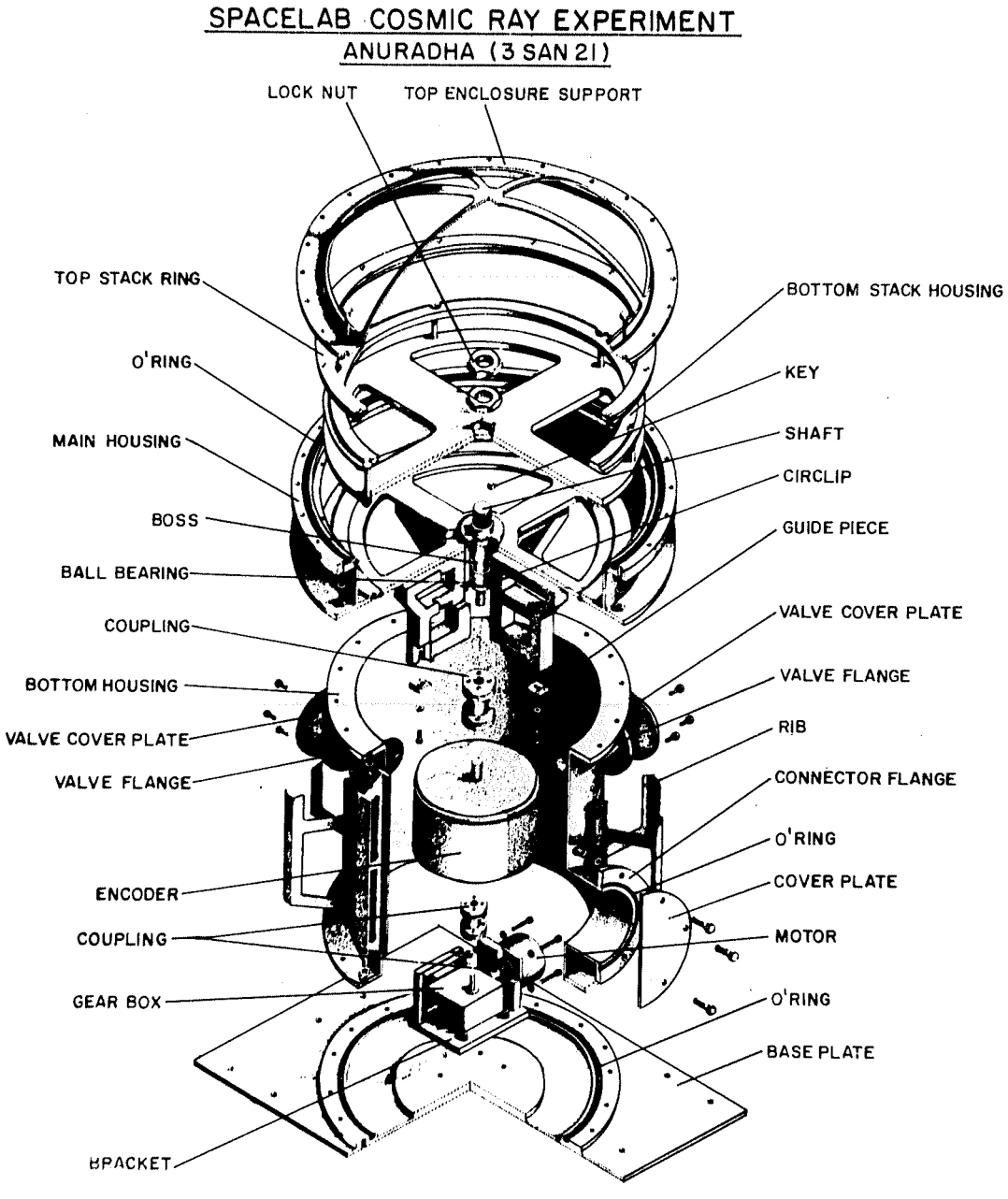

Fig.2-11 A three dimensional schematic view of different parts in the Anuradha instrument.

fixed to the main housing of the instrument. The second or the bottom stack consists of 149 circular sheets of CR-39 and lexan polycarbonate, each with nominal thickness of about 250μm and diameter 38cm. The bottom stack was mounted on a vertical shaft coupled to a 15-bit absolute shaft encoder and a stepper motor-gear-box assembly. A separation of 500 μm was maintained between the top and the bottom detector stacks. Suitable pulsing of the stepper motor enabled the rotation of the bottom stack in small steps of about 40 arc sec at suitably chosen time intervals. In the present experiment, the time interval chosen was 10 sec and under these conditions it took nearly 90 hours for one complete rotation of the bottom stack. A temperature sensor was placed close to the detector module to monitor the temperature inside the enclosure. The instrument was pressure sealed and was maintained at 0.1 atm during the flight by a pair of venting valves. The instrument electronics were housed in a specially designed box at the base of the instrument and were also fixed to the support structure above the encoder box. The base plate of the instrument was mounted on a cold plate. The instrument was wrapped with a multi-layer thermal blanket. The stack movement and the temperature were monitored during the experiment from the telemetered data of the encoder and the sensor output. The temperature inside the detector module was maintained within 25 to 40^0C. The instrument activation and operation were performed through either crew-interface or Spacelab-3 on board computer via ground command. A detail description of these procedures are given in earlier work (Biswas *et al.*, 1986; Singh, 1990).

2.7 Flight Performances

The space shuttle Challenger was launched from Marshall Space Flight Center on 29th April, 1985, at Greenwich Mean Time (GMT) 119:16:02:18. Mission elapsed time (MET) was set to 000:00:00:00 at the time of launch. The spacelab was first set in the gravity gradient stabilized orbit and then activated at MET 000:02:07:35. A power-on command was issued to *Anuradha* at MET 002:13:30:00 to activate bottom stack rotation, but the instrument did not respond. The fault was traced to a NASA interface between the instrument and the on board computer and an alternate arrangement was made by the crew members. The instrument was finally put "ON" and the rotation of the bottom stack was activated at MET 003:20:30:00. It was shut off at MET 06:13:00:00, giving a total of about 64 hr and 30 min of activation time during which the bottom stack was rotation was active and thus the arrival information of cosmic ray particles incident on the detector could be obtained. The encoder readings before the start and following the stop of rotation were noted as 13 and 23456 respectively.

2.8 Post-flight Analysis Procedure

After the payload was brought back to the laboratory, it was activated with the ground support equipments and the bottom stack was rotated back to the starting position by matching the encoder reading to its initial value before the start of rotation of the bottom stack. The two detector stacks were then locked by a specially designed clamp and the entire assembly of the top and the

bottom detector system was taken to the Variable Energy Cyclotron Center (VECC) at Calcutta. The detectors were exposed to collimated beam of 50 MeV alpha particles of ~2-3 mm diameter in six positions near the periphery and these were used for later alignment of top and bottom stack. These alpha particles beam could penetrate only the top four sheets of the detector module. The rest of the bottom stack sheets were exposed to 1 GeV/n gold beam at 8 spots for alignment and to 140.2 MeV/n iron beam at six spots for charge calibration at the Berkeley Bevalac. The fluence of the gold beam was so high that after the chemical processing circular holes are formed at the beam spots, which served as good markers to align and hence to follow tracks of particles in successive detector sheets in the bottom stack. After the chemical processing with 6.25N NaOH at 70 ± 0.2^{0}C for six hours, the single sheet top stack and the topmost sheet of the bottom detector stack were mounted together on a specially designed microscopic stage, that allow us to scan annular strips of these two sheets together. The rest of the detector sheets in the bottom stack were cut into four equal quadrants after chemical processing, and scanned under four different optical microscopes. The detail of the scanning and calibration procedures will be discussed in the next chapter.

Chapter-III

DATA ACQUISITION AND ANALYSIS PROCEDURES

In this chapter we discuss the procedures adopted for data acquisition and analysis in the *Anuradha* experiment. In particular, we discuss the procedures for scanning the CR-39 plastic detectors for identifying the individual events, as well as determining the arrival time and arrival location and direction of each event. The experimental and systematic uncertainties in obtaining these information are also discussed. Most of these aspects are discussed briefly as they have been considered in detail by Singh [1990] while presenting the initial results from this experiment.

3.1 Detection and Scanning Procedures

The scanning of the detector sheets were carried out in two parts. The two top detector sheets, *i.e* the single circular sheet of the stationary top detector stack labelled 1-0 and the topmost sheet of the rotating bottom detector stack labelled 1-1, which provided the information on the arrival time of the particles, were scanned together. The bottom detector sheets which provided information needed for identifying each event, as well as for estimating their energies and momentum, were cut into four quadrants and were scanned separately using optical microscopes. The bottom detector stack also provided data on the medium energy (50-250 MeV/n) GCR oxygen ion flux discussed in the next chapter.

3.1.1 Scanning of the "Top" detector sheets

One of the most important parameter needed for determining the ionization states of low energy cosmic ray particles in the present experiment is their arrival time. The arrival location and direction of a particle can then be obtained by combining the knowledge of its arrival time with Spacecraft-orbit data. As already noted the two topmost detector sheets (1-0) and (1-1) provide the required information on arrival time. This is done by matching the track segments, produced by individual events in these two detector sheets, and the relative angular displacement of the matched pair of track segments can then be used for obtaining the information on the arrival time. To simplify the matching of track segments in these two detector sheets, we have scanned annular strips of the top two detector sheets (1-0 and 1-1) placed together with their center aligned. For this purpose, a microscope stage was specially designed by combining two separate arrangements. First, a spare model of *Anuradha* payload with all the associated electronics was utilized and the stage in this payload used to hold the "bottom" detector stack, was used as the stage for the microscope. Both the detector sheets (1-0 and 1-1) were mounted together on the stage. The center of both the sheets were made to coincide with the center of rotation of the stage which can be activated as in flight using a ground-support computer system. In the second arrangement a Zeiss optical microscope was used which could move only in Y-direction in

a X-Y plane. This two arrangements referred as R-ϑ microscope stage, were made in such a way that the microscope objective could move only towards or away from the center of the rotating stage. Therefore, we could scan the detector, first over a small radial distance by moving the microscope objective and then going to a new position by rotating the stage in suitable angular steps. Repeating this procedure an annular strip of the detector sheets could be scanned. The microscope objective movement was controlled by coupling it to a linear encoder that provides step-size of 1μm, and the angular steps were provided by the same experimental electronics as in the flight payload and was monitored by a 15-bit absolute shaft encoder as in the case of actual experiment. In the initial phase of data analysis, a 2cm wide annular strip from the periphery of the detector, equivalent to a detector area of ~200 cm^2 was scanned. All the four surfaces (upper and lower surfaces of 1-0 and 1-1 sheets) are scanned simultaneously. These data were reported by Singh [1990]. In the next phase, we have now scanned a 3cm wide strip inwards, equivalent to a detector area of another 200 cm^2. All the events found during the scanning are assigned an unique event number. The data obtained from this scanning are reported in this thesis.

3.1.2 Scanning of the lower sheets in the bottom stack

If an energetic charged particle, incident on the instrument, can produce tracks in both 1-0 and 1-1 detector sheets and still has enough energy left, it is expected to stop somewhere in the bottom

detector stack. To identify the track forming particle, in terms of its mass and atomic number as well as to find its range, energy, momentum etc. one needs to know the stopping point of the particle. For this purpose, the CR-39 detector sheets in the bottom stack (starting from 1-2 onwards) were chemically etched under similar conditions. All the particles (up to iron group), which could produce tracks in detector sheets 1-0 and 1-1, have stopped within the 15th detector sheet (1-15) in the bottom stack. To make the scanning procedure faster, we have cut each of these lower sheets into four pieces along four quadrants and scanned them under four different optical microscopes.

The bottom stack detector sheets also provided data for the orbit-averaged GCR oxygen ion flux at energies (50-250 MeV/n), which are discussed in this thesis (chapter-IV). The main objective here was to check the validity of the geomagnetic transmission factors used in this study. To calculate the orbit-averaged flux of GCR oxygen ions at different energies, we have chosen different sets of detector sheets positioned at different points in the bottom stack. The selection of the detector sheets are done, first by calculating the ranges for oxygen ions in the CR-39 detectors with energies of 50, 125 and 250 MeV/n and from these ranges the position of the sheets to be analyzed are determined by assuming them to have uniform thickness (250μm) and for an average incidence angle of 45^0. The different detector sheets we have scanned for this purpose are 1-7 and 1-8, 1-41 to 1-46 and 1-59 to 1-66, and 1-129 to 1-130. The corresponding energy bands, for acceptance angles between 30^0 and

70^0 of incident particles, are 50±10; 125±40 and 250±70 MeV/n respectively.

The identification of the events during the scanning of the 1-0 and 1-1 sheets was done at low magnification (typically 100X) whereas the measurement of the track parameters were carried out at much higher magnification (530X). For the determination of the oxygen flux at higher energies the scanning was carried out at 200X to ensure hundred percent detection efficiency because of the extremely small number of expected GCR oxygen events, and the measurement was done at a magnification of 1200X.

3.2 Calibration of the CR-39 Detector

The CR-39 (DOP) detector stacks used in the present experiment were specially prepared for us by Pershore Moulding (UK). The response of the detector was studied, prior to the experiment, by exposing it to the low energy C, N, O and Ne particle beams at the accelerator facility at Dubna, Moscow. Following the successful space exposure of the instrument, the bottom stack (except the top four sheets) was exposed to 140.2 MeV/n iron beams from the Berkeley Bevalac, at six positions, for calibration purposes. As discussed in chapter-II (section-2.3.4) the identification of the atomic number and mass of the track forming charged particles is possible if we have a well established relation between track etch rate (V_t/V_g) and restricted energy loss rate (REL) for the detector under consideration and for the given etching conditions. The accelerator

iron-ion tracks, revealed along with the cosmic ray tracks during the etching treatment, were used to obtain this relationship. As the ambient pressure and temperature during the space exposure of the detector was somewhat different than those for the laboratory exposure (0.1 atm. vs. 1 atm; 25^0-40^0C vs. 22^0C), we have also identified a few cosmic ray iron events in the detector, and used them for the calibration purposes. The final plot of REL vs. V_t/V_g obtained from inflight and accelerated beam calibration is shown in fig.3-1. The relation obtained between REL and V_t/V_g can be written as,

$$V_t/V_g = 1 + 1.625*10^{-4}.\ (REL) + 5.835*10^{-15}.\ (REL)^{3.93318}$$

In practice, we measure the residual range and corresponding V_t/V_g values from tracks formed by the charged particles. We have used the appropriate E vs. $(dE/dX)_{REL}$ and Energy(E) vs. Range(R) relations to generate the R – V_t/V_g plots for all ions from carbon to iron. This is shown in fig.3-2 and was used in this work for the identification of the track forming ions.

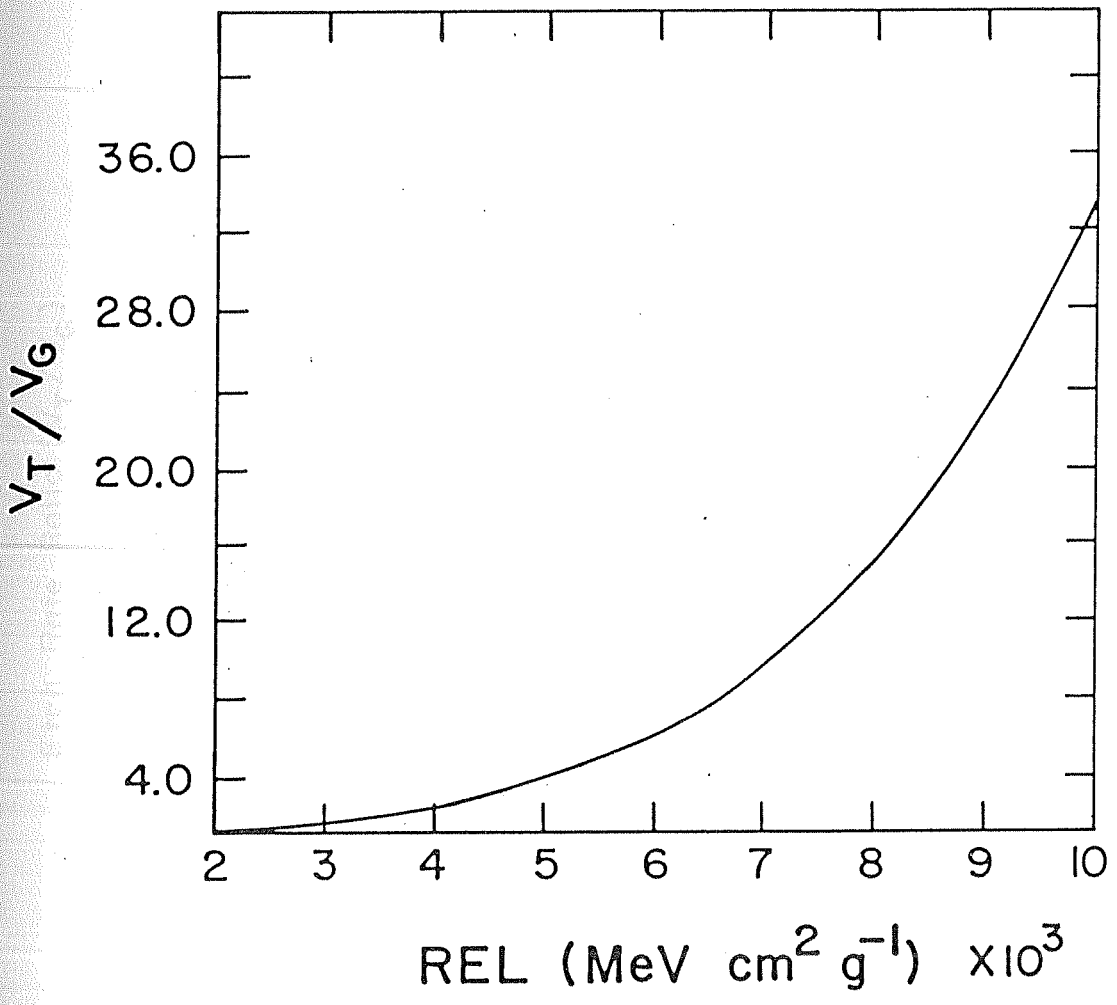

Fig.3-1 The calibration curve of Restricted Energy Loss (REL) vs. V_T/V_G (track etch rate/ bulk etch rate).

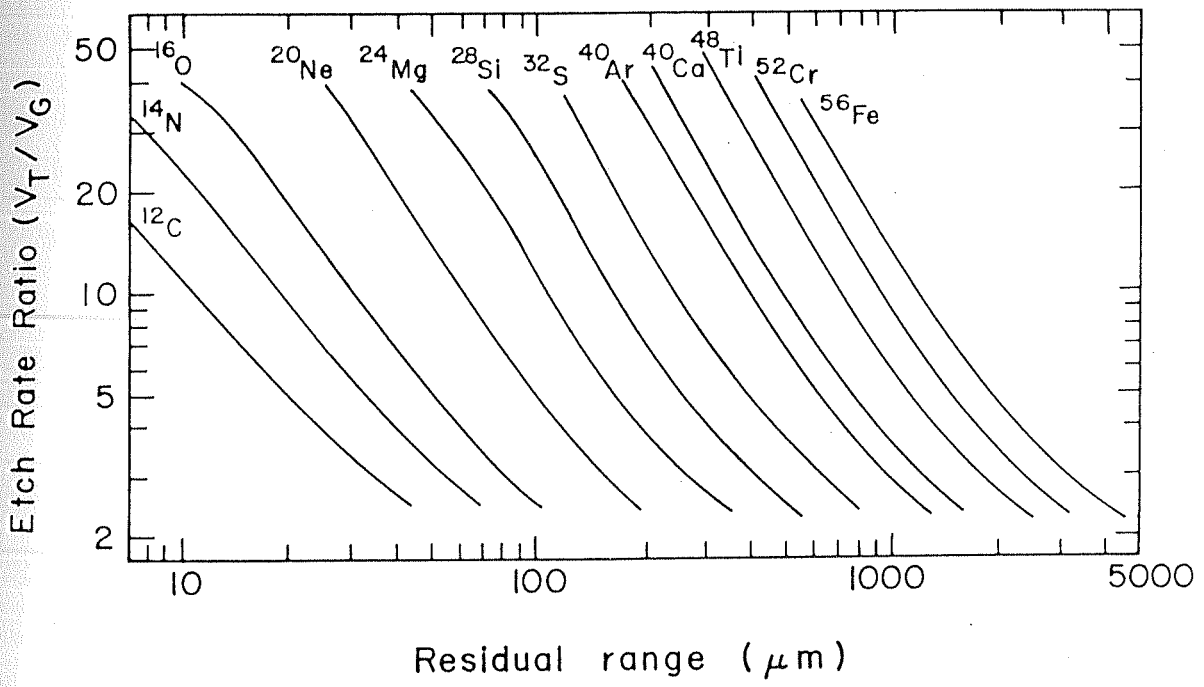

Fig.3-2 Calibration curves for the detector used in the Anuradha experiment showing Residual Range vs. V_T/V_G for ^{12}C to ^{56}Fe.

3.3 Determination of the Arrival Time of Individual Events

On Spacelab-3, the total exposure time of the *Anuradha* experiment was 154 hr. Out of this duration, for ~64 hr towards the later part of the flight, the bottom stack was set into rotation. Therefore, one could determine the arrival time of those particle events which were recorded in the detector during this period. These particle events are referred to as the Rotating State Events (RSE) or time annotated events, and the rest of the events which were recorded when the bottom stack was stationary are referred to as the Stationary State Events (SSE).

3.3.1 Scanning of Tracks in the Detector Sheets 1-0 and 1-1

The two cylindrical stacks of plastic sheets (the top and the bottom detector stacks) in the *Anuradha* experimental module, were mounted in such a way that the axis of symmetry (which was also the axis of rotation) passed through the centers of the stacks. During the exposure, the gap between the stacks was kept at about 500 μm and the bottom stack was rotated in steps of about 40 arc sec per 10 seconds in the counterclockwise direction. Angular position of the bottom stack was measured by a 15-bit absolute shaft encoder. As depicted in fig.2-10, the arrival time for a given particle event recorded in the detector is thus encoded in terms of the angle by which the bottom stack rotated by the time the particle arrived. Therefore, determination of the arrival time of an event is reduced to the following steps : (a) finding the track segments in the two

sheets (1-0 and 1-1) produced by the same particle, (b) measurements of their angular displacements, and (c) use of telemetered data on the angular rotation vs GMT, recorded every two seconds during the experiment, to finally obtain the arrival time of the particle.

Since the information about the arrival time of a particle is fully contained in the top two circular sheets only these two detector sheets were mounted on the R-ϑ microscope after chemical processing. Care has been taken to see that the centers of these circular detector sheets coincide with the axis of rotation of the stage, as in the case of actual flight payload. The positioning of the detector sheets 1-0 and 1-1 on the stage of the R-ϑ microscope could be done in a precise manner by taking help of two fiducial marks (termed 'zero'; see fig.2-10) made on the top and bottom stack detectors, prior to the flight , which correspond to zero encoder reading. Following the relative angular positions of the two sheets were also made the same as in the experiment proper prior to the activation of rotation of the bottom stack. In this arrangement, tracks segments produced on the two detector sheets could be observed under the microscope in each field of view and a 3cm wide annular strip equivalent to a detector area of ~200cm^2 was scanned and reasonably large etched tracks (> 22 μm) from both the plates were measured. The physically relevant quantities such as the track length, ratio of track etch rate to bulk etch rate (V_t/V_g), azimuth and dip angles of incidence were computed from the measured values of the track parameters like the projected track length, major and minor axes of the elliptical opening of the track on etched surface, diameter of the track tip and depth of the track, following standard

procedure [Henke and Benton, 1971]. The positions of each track in the detector sheets were determined in the R-ϑ coordinate system.

3.4 Matching of Tracks

In order to match the track segments produced by the same event in the detector sheets 1-0 and 1-1, it is necessary to identify the parameters which could impose constraints on the candidate events from these two detector sheets. The assumption made here is that values of no parameter can change arbitrarily across the detector sheets *i.e* there must be proper correspondence for all measured parameters across the two nearest surfaces; the lower surface of the detector 1-0 and the upper surface of the detector 1-1, if the track segments are produced by the same event. Several such parameters, related either to the position and orientation of each track or to the measured track parameters were chosen for this purpose. These are:

i) Radial position: Radial position of the two candidate track segments on the detector sheets 1-0 and 1-1 should be same (after allowing for the 500μm gap between the sheets).

ii) Angle of incidence: Azimuth and dip angles of the track segments should also be the same.

iii) Difference in the angular position: The difference in the angular position of the two candidate events should be less than the maximum angle of rotation of the bottom stack during the experiment. This puts a limit on the maximum allowed difference in the encoder value of 23469 which was the encoder readout

when the experiment was deactivated and bottom stack rotation was stopped.

iv) Track length and etch rate ratios: The track length (L), and, the ratio of the track etch rate to the bulk etch rate (V_t/V_g) should change only by a small amount over the two nearest surfaces of the measurement (lower surface of 1-0 and upper surface of 1-1) in majority of the cases. These two parameters are however related and hence not independent.

v) Minor axis: The minor axis of the elliptical opening of the tracks on the two nearest surfaces provide a very good constraint on the matching of the candidate cones as they are expected to remain nearly constant. This is because of the fact that the distance travelled by the particle between the two points of measurement of minor axis is only the etched out thickness from the respective two surfaces, which is about 15 μm.

3.5 Tolerance Limits on the Parameters used for Identifying Matched Pairs of Track Segments

We have first completed measurements of track parameters for all the stationary state events (SSE), before we attempted to match the rotating state events. The stationary state events were very easy to identify during scanning, since the detector sheets 1-0 and 1-1 were placed on the microscope stage in the same configuration as in the experiment, prior to the activation of rotation of the bottom stack. Thus the matched pair of the track segments for the SSE can

be seen in the same field of view and identified easily. The distributions of the differences in the values of various parameters for the SSE across the two detector surfaces of 1-0 and 1-1 were then considered as the basis of setting the tolerance limits on the corresponding parameters for the matching of time annotated or the rotating state events (RSE). The only exception to the previous statement is the distribution of the difference in encoder position of the SSE, because for SSE it is expected to be zero, after giving due allowance to the angle of incidence and the 500μm gap between the top and bottom stacks, whereas for RSE, the difference in encoder value provides the arrival time.

A total of 96 SSE events were matched successfully in the 3cm annular strip scan from which data are presented in this thesis. Out of these, 77 events had double cone (DC) in 1-0 and 1-1, for which the dip angle values could be measured more accurately. In fig-3.3 the distributions in the difference in azimuth and dip angles, radial positions, and minor axis for stationary state events are shown. From the standard deviations of these distributions we have chosen a tolerance limit of three standard deviations (3σ) in trying to match candidates cases for the rotating state events. These tolerance limits for matching the RSE events are $\pm 9^0$, $\pm 13^0$, $\pm 1300\mu m$ and $\pm 1.6\mu m$ respectively for the parameters azimuth, dip, radius and the minor axis. In case of the parameters cone length (L) and V_t/V_g the deviations are 5.0μm and 0.8. If the particle stops in the detector sheet 1-1 then no constraint was imposed on these two parameters. The matching was done by a simple computer code which

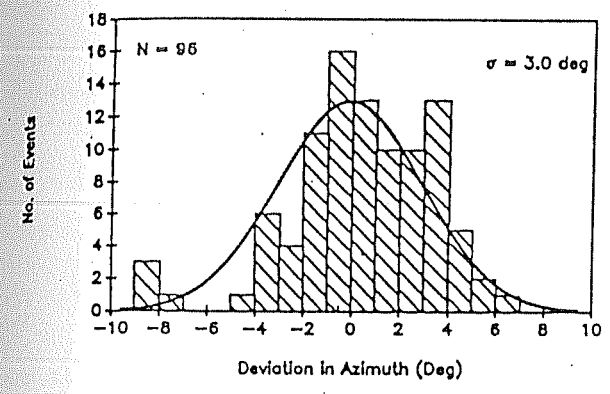

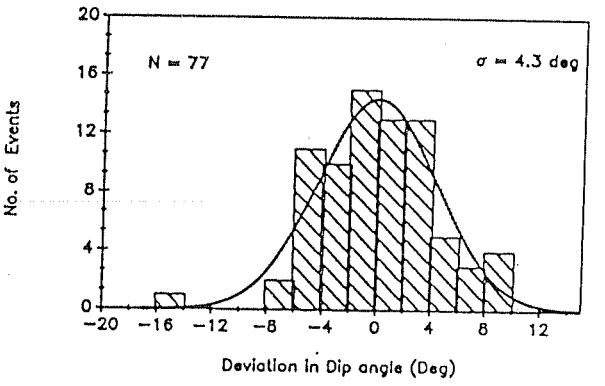

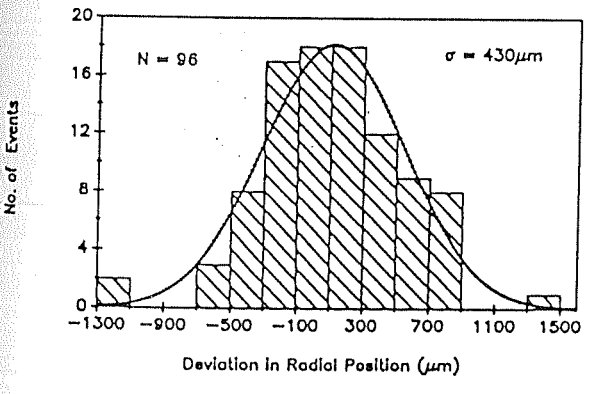

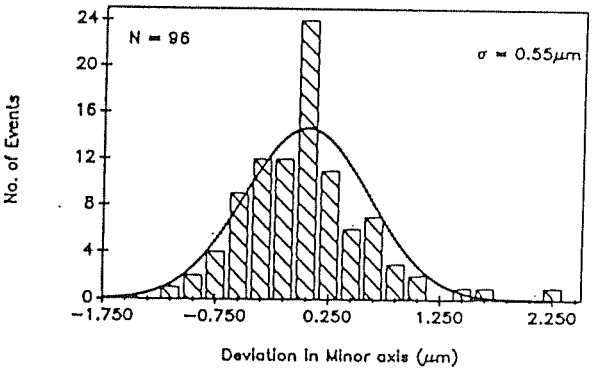

Fig.3-3 The distribution of the differences in measured a) Azimuth, b) Dip, c) Radial position and d) Minor axis of the matched pair of stationary state events. (All data are from 3cm scan).

lists the probable candidate events that may match each event, for which a search of matched pair is made, and the list is further analyzed for identifying the actual matched pair. In general for each event we get 1 or maximum 2 probable events because of the very small number of events involved. In all we have been able to unambiguously identify 45 matched pair of events in the 3cm scan. The analysis of these events and results obtained are presented in chapter-V. We have also considered the random probability of matching events in the present analysis. This can be calculated on the basis of the distributions in the differences in the various parameters across the detector sheets for all the SSE. The random matching probability associated to ith parameter P_r^i is equivalent to the ratio of the width of the tolerance limit to the entire possible range, if the distribution of values is uniform. If for a parameter the distribution is not uniform, the ratio of the averages for the candidate events to that for all matched cones is considered as the random matching probability associated with that parameter. The random matching probability (R) is then given by,

$$R = \text{Total number of candidates for matching} * \Pi_i P_r^i$$

The value of R is extremely small because of the small number of events involved. For example, if we consider just the tolerances in azimuth angle, dip angle, radius and encoder difference, the value of R is ~1/4000. In no case more than two parameters were allowed to have extreme limits of their tolerance in choosing the matched pair of events. Therefore, the above value gives a fairly good estimate

on the random matching probability.

3.6 Arrival Direction and Location of Events Recorded

For the data analysis purpose, we need to know the arrival time of the event, as well as the arrival direction in the local and geocentric coordinate systems. As already discussed, the encoder reading difference between the matched pair of tracks provides information on the arrival time of each events. This also provides information on the arrival location, as the spacecraft's position was known at all instant of time. To obtain the information on arrival direction in local and geocentric coordinate systems, we use the azimuth and dip angles of the track in the detector frame of reference as input parameters and make appropriate transformation as outlined below. During the whole period of the flight, the encoded angular position of the bottom stack, the time, and the position and orientation at the spacecraft with respect to earth was recorded by NASA for us at two seconds interval and data were provided to us after the flight. Therefore, once the angular position of the bottom stack is obtained at the time of arrival of a given event, which is simply the differences in the encoder reading for the matched pair of events, the position and orientation of the spacecraft at that instant can easily be determined. The position of the spacecraft was recorded in terms of latitude, longitude, and altitude in the geocentric coordinate system. The orientation of the spacecraft was recorded in terms of three Euler angles about roll (X), pitch (Y) and yaw (Z) axes of the craft, which provided three rotation angles

about their respective axes in the same order to transform a vector from spacecraft's body coordinate system to geocentric coordinate system. The measurement of the azimuth and dip angles of incidence for each event in the coordinate system of the detector was made from the data on etched tracks in the top stack which was kept fixed during the entire exposure duration. A transformation of the arrival direction from the detector coordinate system to the coordinate system of the spacecraft is achieved by a rotation in counterclockwise direction through an angle, $(180^0 - 25^0\ 15')$, *i.e*, $154^0\ 45'$,(where $25^0\ 15'$ is the angle between the zenith of the instrument and the z-axis of the craft) about the common y-axis of the detector and the craft; this is evident from the fig.2-9. The resultant vector was then transformed similarly to the geocentric coordinate systems using the three angles mentioned above. Again a new rotation of the transformed vector in the geocentric coordinate system was made, depending on the latitude and longitude of craft at that time, to finally obtain the arrival direction in the local coordinate system.

The error limits in the arrival position of a given event is estimated from the uncertainty in the determination of the arrival time due to the uncertainty in the inferred encoder value at the time of the particle arrival. The probable error associated with the differences in encoder values for matched pair of tracks was estimated by measuring the encoder readings for the matched pair of tracks belonging to the stationary state events. For all such events the expected differences in their encoder values are calculated by

first predicting the encoder value in 1-1 for each event according to the position and orientation of the event in 1-0 and the total error associated in the encoder value was obtained by subtracting it from the measured value for each event. We then subtract the systematic errors due to the misalignment of the circular sheets, while placing them on the microscope stage for scanning, and found that the standard deviation of the distribution for the encoder reading difference for matched pairs of SSE events is 4.5, which is equivalent to ±45 seconds of uncertainty in arrival time. In the analysis of data, the uncertainty in the arrival position of each event was estimated by considering a worst case uncertainty of ±90 sec in arrival time. The uncertainty in the arrival direction is calculated from the errors in the determination of the azimuth and dip angles of the particle incidence. In order to determine the errors in the arrival direction in local earth coordinate system, the transformations were also applied on the error limits of the angle of incidence on the detector. The magnitude of the errors in arrival direction in geocentric and the local earth coordinate systems, therefore, are the same as measured for the angle of incidence in the detector coordinate system.

Chapter IV

GEOMAGNETIC CUTOFF AND TRANSMISSION FACTOR

In this chapter we present the result on the calculated values of the orbit-averaged geomagnetic cutoff rigidity obtained by trajectory-tracing method and hence the transmission factors at the Spacelab-3 orbit as a function of the rigidity of the charged particles. Results obtained on the Spacelab-3 orbit-averaged flux of the low energy (50-250 MeV/n) GCR oxygen are also presented alongwith a discussion on the validity of the calculated geomagnetic transmission factors. Finally, we outline the method used to obtain the geomagnetic cutoff rigidity of individual ions.

4.1 Geomagnetic Transmission Factor

The calculation of the orbit-averaged geomagnetic transmission factor for the Spacelab-3 orbit, as a function of particle momentum (rigidity), was done by determining the weighted average cutoff rigidity (R_c) for 5^0 latitude x 5^0 longitude bins and combining this data set with the fractional time spent by Spacelab-3 in these bins during its space flight. To calculate the weighted geomagnetic cutoff rigidity for the 5^0 X 5^0 bins, the vertical cutoff rigidity for the center point of each of these bins have been computed by the "trajectory-tracing" method using the International Geomagnetic Reference Field for the 1985 epoch. The trajectory-tracing is performed by back-tracing the path of the energetic charged particle

in the earth's magnetosphere and the minimum rigidity required by the particle to arrive at the particular bin of interest from vertical direction (zenith=0, azimuth=0) is considered as the vertical cutoff rigidity for that bin. A detail discussion on the trajectory-tracing method is given in the last section of this chapter. However, the cutoff rigidity in directions other than the vertical direction will depend on the zenith angle (ϑ) and the azimuth angle (ϕ) of incidence. To calculate the weighted geomagnetic cutoff for each of these bins for the period of our experiment, we first consider the vertical cutoff rigidity obtained by trajectory-tracing method [Shea and Smart,1988] for each of these bins. We then determine the cutoff rigidity values for other angle of incidence using the relation between the Stormer's cutoff R_c, as defined by the equation (2.2) and the vertical cutoff R_v :

$$R_c = \frac{4R_v}{[1+\{1-\mathrm{Sin}(\vartheta)\,.\,\mathrm{Cos}(\phi).\mathrm{Cos}^3(\lambda)\}^{1/2}]^2} \qquad ...(4.1)$$

Since the viewing cone of the detector always includes the local vertical in the gravity gradient stabilized mode of the space shuttle, we subdivide the viewing cone in steps of 5^0 for the zenith angles and 10^0 for the azimuth angles. The cutoff rigidity for each of the 5^0zenith x 10^0 azimuth grids within the allowed viewing cone for all the 5^0latitude x 5^0longitude bins are calculated by using relation 4.1. The weighted rigidity for a particular latitude-longitude bin is obtained by summing up rigidities over all the zenith-azimuth grids and dividing by the total number of grids.

The average value of the cutoff which includes all the viewing directions of the detector in a particular latitude by longitude bin is accepted as the weighted geomagnetic cutoff rigidity for that bin. The relation (4.1) which was used for simplicity in obtaining the average values of cutoff rigidity over the 5^0 X 5^0 bins may introduce some uncertainties in the calculated values of geomagnetic cutoff rigidities. We have checked the magnitude of the possible deviation by comparing the cutoff rigidities for specific angle of incidence obtained by the above approach and the trajectory-tracing method. The deviation is mostly within ±10% with occasional excursions of up to 25%.

Once the weighted average cutoff rigidities for different bins are known, we can obtain the geomagnetic transmission factor for the energetic charged particles from outside the earth's magnetosphere to reach the Spacelab-3 orbit as a function of their momentum (rigidity). It is more convenient to express the geomagnetic transmission factor in terms of fractional exposure time. The fractional exposure time for a charged particle possessing a certain rigidity can be obtained by summing up the time periods spent by Spacelab-3 at those 5^0latitudes X 5^0longitude bins for which the cutoff rigidity is lower than the specified rigidity. The time spent by the Space Shuttle at different latitudes is shown in fig.4-1. The orbital period of the Space Shuttle was 92 minutes and it repeats an orbit after every 31st orbit. The total number of orbits made by Spacelab-3 during the exposure period of the detector was 116. As depicted in fig.4-2, if we consider the ith orbit of the Space

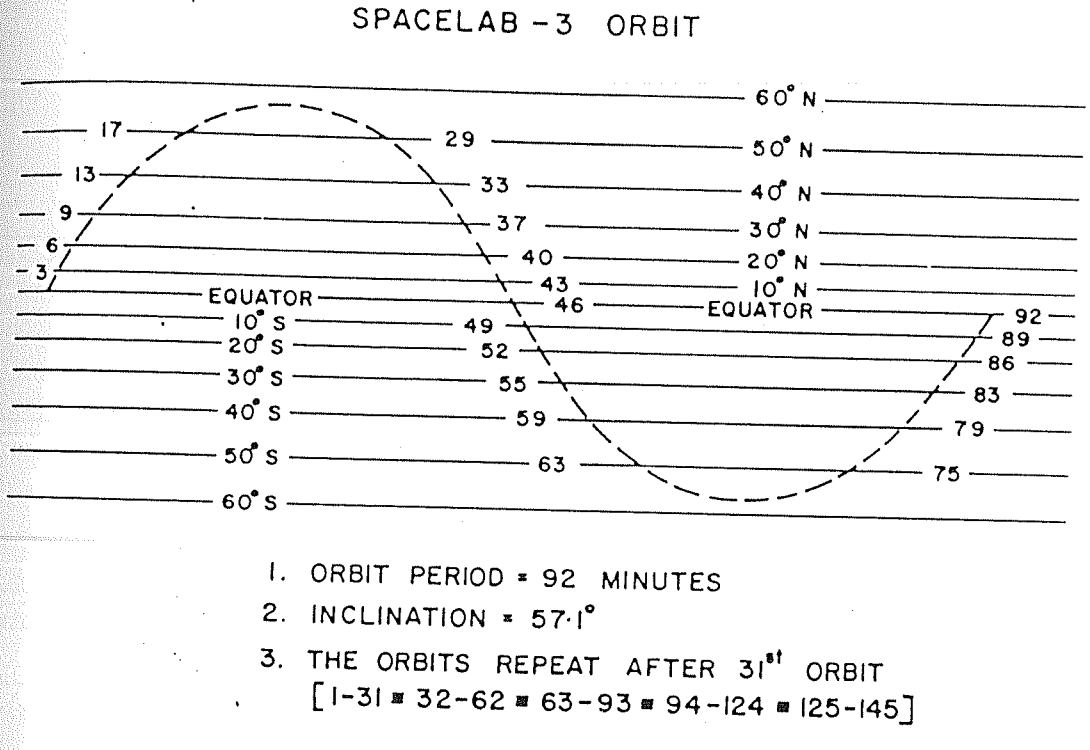

Fig.4-1 The Spacelab-3 orbit showing time spent by the spacecraft at different latitudes during its orbital period of 92 minutes.

Shuttle, particle with rigidity R can arrive only between the regions a_1^i to a_2^i and b_1^i to b_2^i where the cutoff rigidities are <R. Therefore, the geomagnetic transmission factor or the fractional exposure time for the particles with rigidity R can be written as,

Geomagnetic Transmission Factor for the particles with Rigidity, R

$$= \sum_{i=1}^{116} \Big[\textit{Orbital time spent between the segments } a_1^i \textit{ to } a_2^i \textit{ and } b_1^i \textit{ to } b_2^i \textit{ for the ith orbit} \Big] \; X \; \Big(\textit{Total orbital time} \Big)^{-1}$$

The geomagnetic transmission factor calculated for particles with different rigidities for the Spacelab-3 orbit is shown in fig.4-3. As expected the geomagnetic transmission factor increases with the increasing rigidity of the particle and reaches a value of unity for R ≥ 25 GV.

4.2 Determination of Low Energy (50-250 MeV/n) GCR Oxygen Flux and Test of the Geomagnetic Transmission Factor.

A special effort was made in the present study to check the validity of the orbit-averaged geomagnetic transmission factors and hence of the trajectory-tracing method for determining cutoff rigidities. We consider this to be important as the trajectory-tracing method is used for the first time to determine the ionization states of individual cosmic ray particle in this

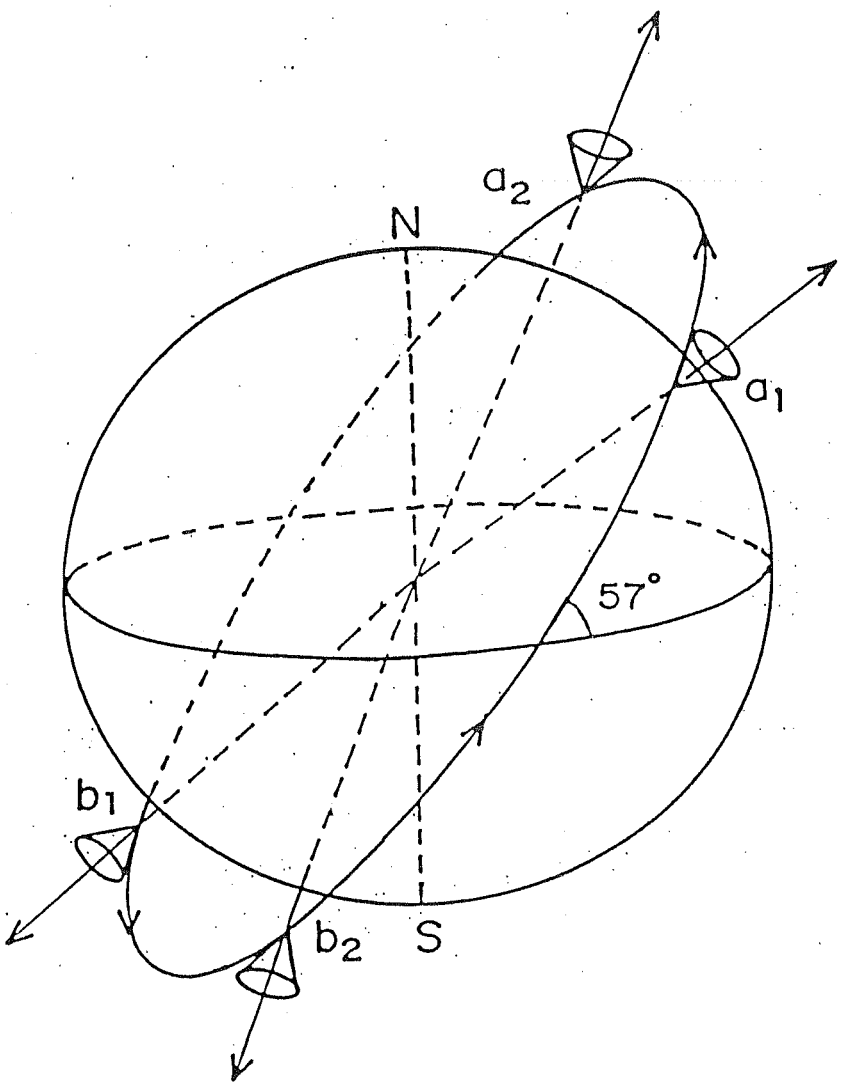

Fig.4-2 A sketch showing a typical Spacelab-3 orbit and effective exposure factor. Energetic particles with rigidity >R are recorded when the Spacelab traverses from locations a_1 to a_2 and b_1 to b_2 where the cutoff rigidity is ≤R.

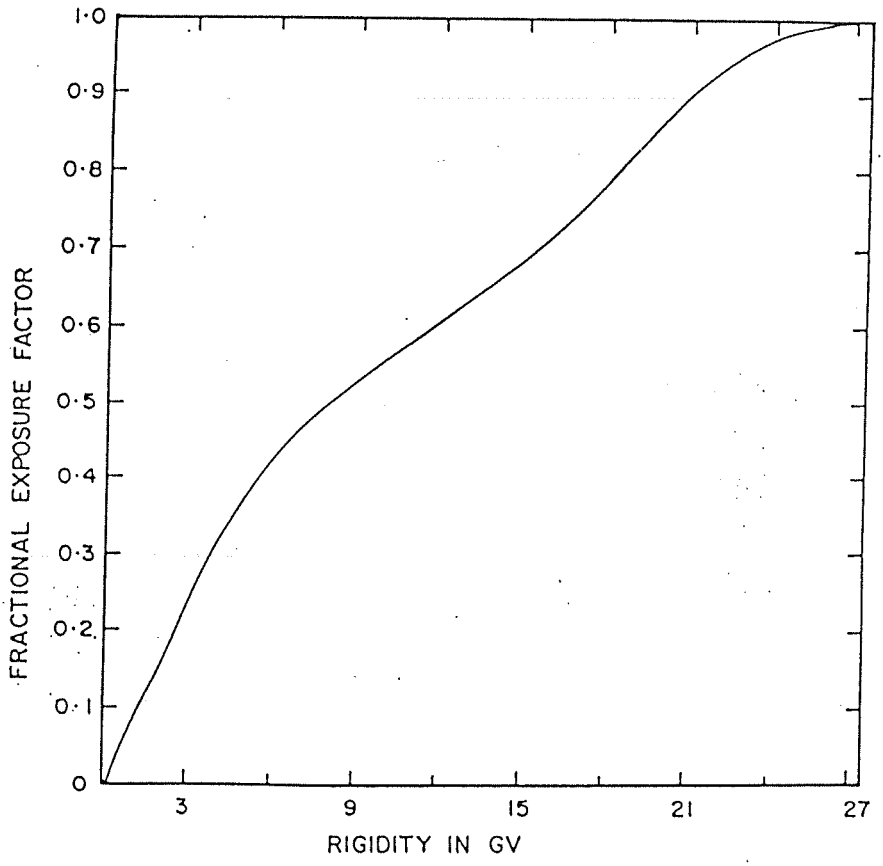

Fig.4-3 Fractional exposure time plotted as a function of effective cutoff rigidity for the Spacelab-3 orbit.

experiment. The basic approach used was to compare the Spacelab-3 orbit averaged cosmic ray fluxes at different energies, corrected appropriately for geomagnetic transmission factors, with those measured directly outside the magnetosphere. An good agreement between these two sets of values was considered as a measure of validity of the computational method used.

To obtain the galactic oxygen ion fluxes in the energy interval of 50-250 MeV/n, we have selected different sets of CR-39 detector sheets positioned at different shielding depths within the bottom detector stack. The different set of detector sheets analyzed, area scanned and the corresponding average energies of oxygen particles are given in table-4.1.

The orbit-averaged oxygen ion fluxes are calculated using the following expression,

$$F = \frac{N}{A.T.dE\,.\,d\Omega.\xi} \qquad ...(4.2)$$

where, N denotes the number of oxygen particles detected in a particular set of detectors, A is the area scanned. T is the total exposure time (5.57×10^5 secs), dE and $d\Omega$ are the effective energy interval and solid angle of acceptance respectively and ξ is the detection efficiency. The solid angle of acceptance in these measurements was restricted to dip angles (δ) between 30^0 and 70^0 and the product of dE and $d\Omega$ for a given energy range was obtained using the expression:

$$dE.d\Omega = \sum_{\substack{\delta=30^0 \\ \text{step, } i=5^0}}^{70^0} \left\{ (E_{max}-E_{min})*(\phi_2-\phi_1)*\left(\text{Cos}^2(\delta_1)-\text{Cos}^2(\delta_2)\right) \right\}_i \quad ..(4.3)$$

where $(\phi_2-\phi_1)$ is the allowed azimuth angle, which is 2π for an unobstructed view of the detector. The product of $(\phi_2-\phi_1)$ and $\left(\text{Cos}^2(\delta_1)-\text{Cos}^2(\delta_2)\right)$ gives the effective solid angle for a particular bin, and $E_{max}-E_{min}$ is the corresponding energy interval calculated at dip angle steps of 5^0. The results are summed up numerically to obtain the effective value of $dE.d\Omega$. The calculation of the effective solid angle for the detector, which takes account of various factors like obstructions due to Earth, Spacelab-3 module and rib structure on the top of the instrument are discussed in detail by Singh [1990].

The value of the detection efficiency ξ depends on the recordable track length of the oxygen ions in the detector under the given etching condition and the thickness of individual detector sheets. The recordable track length of oxygen ions in the etched CR-39 sheets was found to be ~90 microns for the etching conditions used by us. Depending on the variation in the thickness of the detector sheets, the value of ξ varies between 0.25 to 0.4.

Table-4.1 Spacelab-3 orbit-averaged oxygen ion fluxes.

Detector sheet analyzed*	Area Scanned (cm^2)	Energy (MeV/N)	Flux ($p/(m^2.sr.sec.MeV/n)$)
1-7,1-8	125	35-55	$(7.3\pm4.2)\times10^{-5}$
1-41 to 1-47 & 1-59 to 1-66	66	85-133 101-159	$(2.25\pm1.0)\times10^{-4}$
1-127 to 1-129	66	162-307	$(5.31\pm3.7)\times10^{-4}$

* The detector sheets were sequentially numbered. 1-1 refers to the topmost detector sheet of the bottom stack.

The orbit-averaged differential fluxes obtained for the three different energy ranges are given in the table-4.1 along with the relevant data. An increase in the differential flux with increasing energy was expected both due to the lower transmissibility of low energy particles compared to high energy particles, and also due to the solar modulation of galactic cosmic rays in this energy range, which suppresses the flux of low energy particles.

To obtain the fluxes of oxygen particles outside the magnetosphere from the Spacelab-3 orbit-averaged flux (inside the magnetosphere), it is necessary to use the appropriate orbit-averaged geomagnetic transmission factor or the fractional

exposure time for the corresponding energies. This was done by using following relation:

Flux outside the magnetosphere in the energy interval E_1 *to* E_2 = *[(Orbit average flux in the energy interval* E_1 *to* E_2 *inside the magnetosphere) / (Fractional exposure time for the rigidity interval* R_1 *to* R_2*).]*

where, R_1 *and* R_2 *are the rigidities corresponding to the energies* E_1 *and* E_2 *for a fully ionized oxygen particle.*

The results thus obtained are shown in fig.4-4. They should represent the interplanetary GCR oxygen fluxes at 1 AU for the 1985 epoch. As no published data for interplanetary oxygen flux for this epoch were available , we have derived the expected values from the measured flux of interplanetary helium by ISSE-3 during Oct.-Dec.,1985 [McDonald and Lal, 1986], assuming a GCR α/O ratio of (40.2± 5.8) in this low energy range [Cartwright *et al.*, 1971]. These values are also shown in fig.4-4.

The agreement between the expected interplanetary GCR oxygen ion flux and those derived from our experimental data is quite good, even though the error bars in the derived flux is somewhat large due to the small number of observed events. This agreement gives us good confidence in the validity of the trajectory-tracing method, which was principally used to find the orbit-averaged geomagnetic transmission factors.

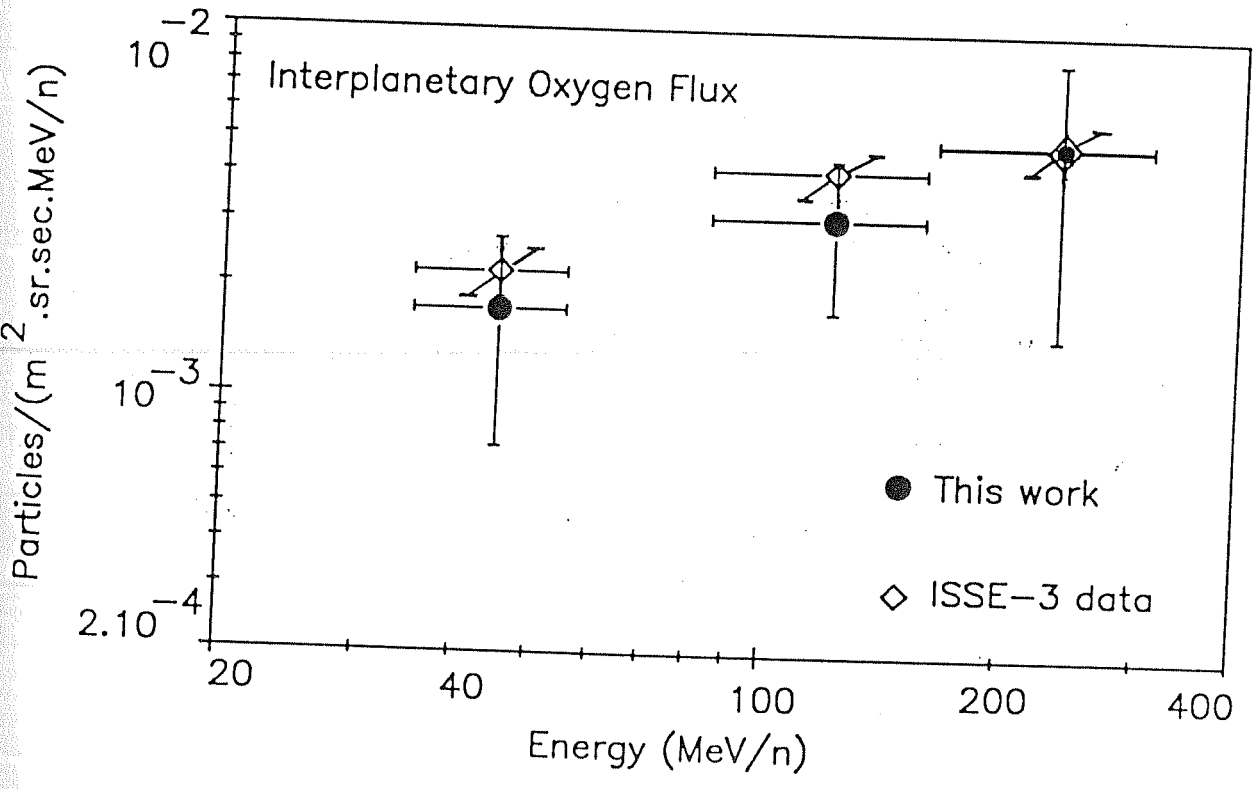

Fig.4-4 The interplanetary GCR oxygen ion fluxes for the epoch 1985 as obtained by Anuradha experiment. The open diamonds represent the oxygen fluxes inferred from interplanetary helium fluxes as measured by ISSE-3 for the same epoch.

In addition to the above, we have also made a comparative study of the modulation parameter ϕ obtained from the estimated interplanetary oxygen flux from our experiment with those obtained from direct measurement of proton and α particles fluxes at 1 AU. The modulation parameter was obtained using the expression suggested by Gleeson and Axford [1968] =:

$$\frac{J_i(E+\phi)}{J_1(E)} = \frac{(E+\phi)^2 - E_0^2}{E^2 - E_0^2} \qquad ...(4.4)$$

where, ϕ represents the energy loss per nucleon in travelling from the heliospheric boundary to 1 AU. $J_1(E)$ is the flux of the particle with total energy E $(=E_0+E_k)$ at 1 AU and $J_i(E+\phi)$ is the corresponding interstellar flux at energy $E+\phi$. E_0 and E_k are the rest mass energy and the kinetic energy per nucleon respectively. To obtain the appropriate value of ϕ, we use the flux at 1 AU for a particular energy E, and consider different values of ϕ to evaluate the interstellar flux for the energy $E+\phi$. The ϕ value that yields appropriate interstellar flux is then considered as the proper value of modulation parameter for that energy. The calculation is repeated for all the three energy ranges for which we have measured the fluxes and a mean value of ϕ is obtained. The interstellar oxygen flux was taken for Webber [1983] and the proton and alpha spectra were from Simpson [1983b].

In fig.4-5 we show our data alongwith the interstellar oxygen

spectrum. The value of ϕ for the last near solar minimum (1985) that best fit our data (the solid line) is 320±30 MeV/n . The modulation parameter for the same epoch (1985-86) from the data on proton and helium ions [McDonald and Lal,1986] are also determined. As the modulation parameter ϕ depends on the mass to charge ratio of a particle, we have taken the normalized modulation parameter Φ ($=\frac{A}{Z} * \phi$) for comparing the proton, helium and oxygen data. The Φ values of 650±20 MV and 670±40 MV for proton and helium respectively, compare favorably with 640±60 MV obtained for oxygen in the present work.

A more rigorous treatment of our data for evaluating the modulation parameter would require consideration of the time dependence in the cosmic ray transport equation, to make it most appropriate for the minimum solar modulation period (1985 epoch). Further, there could also be some uncertainty in the assumed interstellar spectrum in the energy region <500 MeV/n. Even then, the overall agreement, both in flux and in modulation parameter provide proof for the validity of the trajectory-tracing method. In the next section we discuss the approach used for determining the geomagnetic cutoff rigidities for individual particles.

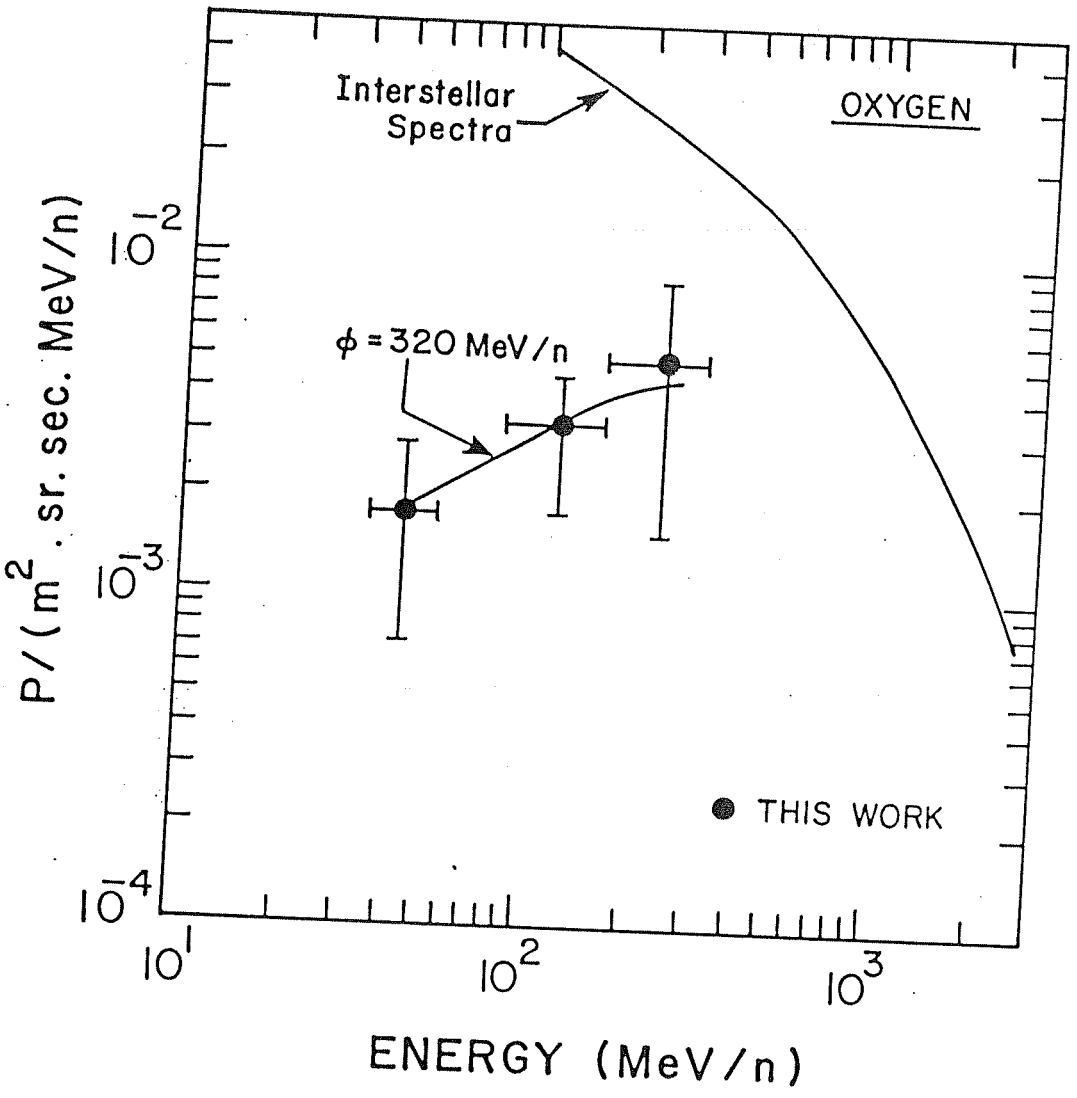

Fig.4-5 Oxygen ion fluxes in interplanetary space at 1 AU as obtained by the Anuradha experiment are shown alongwith the interstellar spectrum. The solid line through our data is for a modulation parameter, ϕ = 320 MeV/n.

4.3 Geomagnetic Cutoff Rigidities for Individual Particles

The cutoff rigidity of a charged particle is defined as the lowest rigidity it can possess and still arrive at a specific point inside the earth's magnetosphere. For any geographical location, the cutoff rigidity is a function of both the zenith and azimuth angles of arrival. Therefore, once the arrival location and direction of the charged particle are known, the trajectory of the particle can be traced back by solving the equation of motion of the charged particle in earth's magnetic field.

The equation of motion can be written as :

$$\frac{d^2R}{dt^2} = \frac{q}{mc}\left(\frac{dR}{dt} \times B\right) \qquad ...4.5$$

The method of trajectory-tracing is reproduced here from the reports of AFCRL [Shea *et al.*,1968; Shea *et al.*,1975]. This is the modified version of the original trajectory program by McCracken *et al.*[1962], where the modifications have been made to increase the efficiency of the program. Referring to the equation 4.5 we note that if the sign of charge q and the direction of motion is reversed, the equation remains unaltered; that is, the trajectory of a negatively charged particle leaving the earth is same as that of a positively charged particle approaching the earth.

To integrate equation 4.5 numerically the components of the magnetic induction in spherical coordinates B_r, B_ϑ and B_ϕ should be

known as explicit functions of r,ϑ and ϕ . We have discussed in the second chapter how this can be done by expressing the earth's internal magnetic field in terms of a potential expanded in spherical harmonics. Spherical harmonics of degree and order 10 is found to be sufficient to represent the geomagnetic field properly [Langel *et al.*, 1982]. The gauss coefficient g_n^m and h_n^m defined in the equation 2.3 are quoted in units of nanotesla for the epoch 1985 [IGRF revision 1985]. Thus, **B** is known at all the points for the time period of our experiment (April-May,1985), and, it is possible to determine the trajectory of the particle by numerical integration of equation 4.5. In practice a fourth order Runge-Kutta method was applied to solve the above equation. The problem is divided into two distinct stages:

(1) Determination of the initial point and velocity of the particle on the trajectory *i.e* $(r,\vartheta,\phi)_{initial}$ and $(v)_{initial}$, which provide the initial conditions for the integration.

(2) Tracing back of the trajectory of the particle into interplanetary space *i.e* outside the magnetosphere, to make sure that it is a true cosmic ray particle.

All calculations are carried out for a single nucleon, but the results are immediately applicable to other particles since the trajectories of two particles with equal momentum to charge ratios (rigidities) are identical.

The FORTRAN computer program for the trajectory calculation has been provided by Shea and Smart. We have made required modifications

as needed to suit our requirement. The gauss coefficients used were as quoted for the epoch 1985. As the experiment was carried out in April-May, 1985, we have not introduced any secular variation terms.

The initial position and the initial velocity of the particle provided the initial conditions for the integration and the trajectory is calculated in small steps of time. Since the earth's magnetic field is not uniform, the gyration time is divided into small step. In our case the step size was one hundredth of the gyration time calculated for the uniform field in the initial position. This is chosen to compromise between the computation time and the errors due to change in the magnetic field. After every step the position and velocity of the particle and the magnetic field at that position are recalculated. If the current value of velocity differs from the initial velocity by more than 10^{-5}, the integration is declared unacceptable and the trajectory is recomputed with previous step size divided in half. The gyration time computed for the new position is again divided into 100 small steps. The computation is continued unless one of the following conditions are met.

(1) If the particle's trajectory goes beyond 25 earth radii then it is considered as a true cosmic ray particle coming from interplanetary space, and the trajectory is considered as allowed.

(2) If the distance of the charged particle becomes less than the actual earth's radius, that is, the trajectory has intersected

the earth, the trajectory is considered as forbidden.

(3) If even after 40,000 steps none of the above conditions are satisfied then the trajectory is considered as forbidden.

For each location, calculations were initiated with a rigidity high above the highest possible cutoff and the cosmic ray trajectories are calculated at discrete intervals of $\Delta R = 0.01$ GV in decreasing rigidities until we are satisfied that cutoff value has been reached. As the calculation progresses through the rigidity spectrum the result changes from easily allowed trajectory to the complex structure of allowed and forbidden (called penumbra) zones of rigidity and finally to a set of all forbidden trajectories. As a result of these types of trajectories, three distinct kind of cutoffs are defined. The main cutoff R(M), above which all rigidities are allowed, the Stormer's cutoff R(S) below which all rigidities are forbidden and an effective cutoff R(C) defined as

$$R_C = R_M - \int_{R_S}^{R_M} R_{allowed}$$

The second term in the above relation allows for the opacity in the penumbra. We therefore consider R_C as the actual cutoff for the specific location and direction. The one dimensional plot in fig.4-6 is a typical example for the penumbra structure and three kind of cutoffs. The results obtained on the ionization states of low energy cosmic ray particles using the above procedure for estimating their cutoff rigidities are discussed in the next chapter.

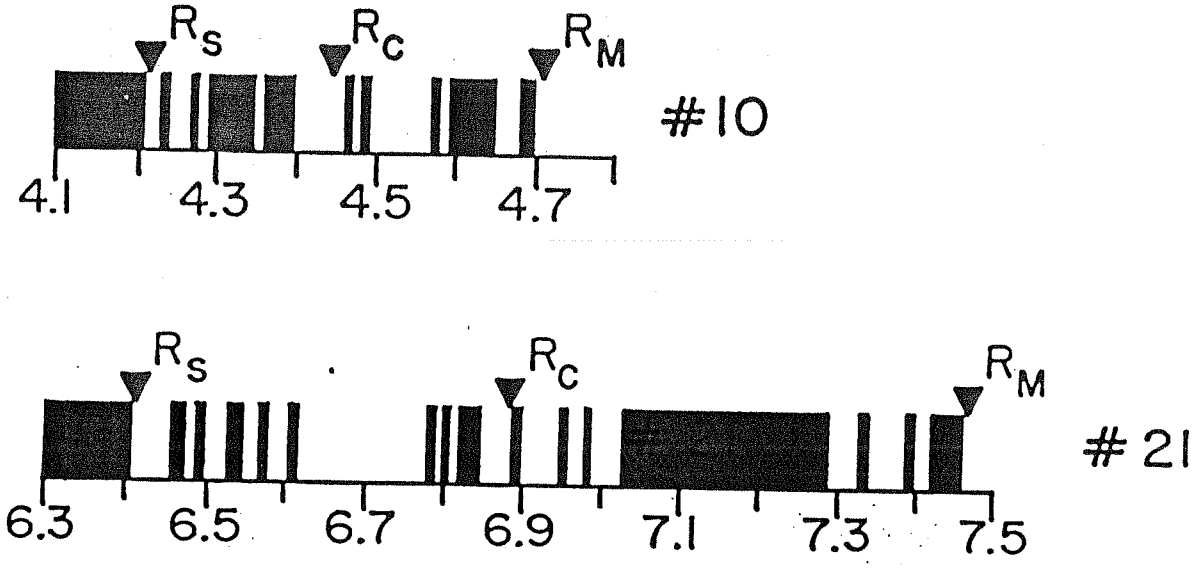

Fig.4-6 Typical penumbra structure for two events detected in the present experiment are shown. The allowed and forbidden zones for different rigidity (in GV) of the particle are indicated by white and black bands respectively. The numbers shown refer to two specific events (see Table-5.4).

Chapter V

RESULTS AND DISCUSSIONS

The results obtained on the ionization states of low energy cosmic rays in the Spacelab-3 *Anuradha* experiment and their implications are presented in this chapter in two parts. The first part contains the results on the ionization states of anomalous cosmic rays and a discussion of their implications towards understanding the source of ACR. In the second part the results on the ionization states of the low energy (20-125 MeV/n) heavy nuclei are presented which clearly establish the presence of partially ionized GCR heavy ions in the near-earth space. A plausible model to explain this new observation is also included.

Part-I : Anomalous Cosmic Rays

5.1 Ionization States of the Anomalous Cosmic Rays

The main objective of the direct determination of the ionization state of individual anomalous cosmic ray ions in the present experiment was to unequivocally establish the source and origin of these particles. The first results on the ionization state of ACR based on the results from this experiment has been presented in a recent thesis by Singh [1990]. In the present work the main emphasis was to expand the data base from further analysis and consolidate the results.

We have now unambiguously determined the ionization states of thirteen ACR particles out of 18 time annotated ACR events in the expanded data base. The details of these events are given in table – 5.1. The identification of the events is based on the track data using procedure described in chapter II and III. The encoder position refers to the difference between the encoder reading of the matched pair of tracks from the same event as measured during the actual scanning. This provides information on the arrival time and location, which are also given in the table. The dip and the azimuth angles refer to the direction of the entry of the particle in the detector frame of reference, which are then converted into arrival direction in geocentric and local coordinate systems using appropriate coordinate transformations. These values for each of the events are also given in the table. In table – 5.2, we show the arrival time of each particle, their energies and momenta and the cutoff rigidities calculated from the information on their arrival locations and directions using the trajectory-tracing method. Combining the data on the particle momenta and calculated cutoff rigidities we show the results on the upper limits on the ionization state of each particle in the last column of the table. Events reported earlier in the thesis of Singh [1990] are also indicated. These results show that 9 events (1 nitrogen, 5 oxygen and 3 neon) have ionization state of 1^+. The upper limits on the ionization state of 4 other ACR events are 2^+, $2^+$and 5^+ (oxygen) and 3^+ (nitrogen). The present data therefore substantiate the claim of Singh [1990] for a singly ionized state for the anomalous cosmic rays.

Table-5.1 : List of all time annotated ACR events and their arrival location and direction.

Serial No	Identification	Encoder position	Dip† (deg)	Azi† (deg)	Arrival Position Long (deg)	Lat (deg)	Alt (km)	GmLat (deg)	Arrival Direction Geocentric Zen (deg)	Geocentric Azi	Local Zen (deg)	Local Azi
1	O	20581	57.0	279.1	97.2	-50.1	364.1	-57.9	144.1	-80.3	75.7	181.5
2	O	21072	38.3	123.4	2.7	-51.5	367.4	-50.6	156.8	111.8	50.3	151.0
3	O	19937	57.8	104.2	39.2	-47.0	366.2	-51.0	159.6	-135.8	63.3	181.9
4*	N	21390	56.8	122.9	212.4	56.9	365.7	59.7	111.7	235.2	80.8	291.4
5*	N	17696	61.0	215.2	135.1	-48.7	366.6	-54.1	141.2	62.0	45.3	212.3
6*	O	7330	59.9	342.9	67.1	57.1	365.7	49.9	128.6	55.0	96.2	260.5
7*	O	11240	40.9	10.0	231.0	52.2	363.2	57.3	142.3	290.7	116	305.9
8*	O	13240	71.1	343.5	1.0	-57.1	367.5	-55.7	127.5	188.7	85.3	263.8
9*	O	21365	63.9	149.2	189.3	56.1	364.6	55.8	115.7	220.1	85.7	297.5
10*	O	1748	72.6	184.2	332.6	51.5	365.2	54.9	84.7	309.2	50.5	239.0
11*	Ne	4515	81.2	57.5	175.1	56.9	365.3	54.7	104.6	188.8	72.3	284.0
12*	Ne	14611	57.6	246.8	92.5	52.5	363.2	44.5	96.1	85.3	58.8	261.6
13*	Ne	327	28.2	201.7	40.5	52.2	365.5	47.0	39.8	7.9	20.4	171.9
14	N	9387	63.1	77.4	231.5	-27.0	355.7	-21.1	105.7	-47.3	75.2*	100.3

Serial No	Identification	Encoder position	Dip†	Azi†	Arrival Long	Position Lat	Alt	GmLat	Arrival Direction Geocentric Zen	Geocentric Azi	Local Zen	Local Azi
			(deg)		(deg)	(deg)	(km)	(deg)	(deg)		(deg)	
15	O	20932	65.4	318.9	303.1	15.7	358.4	22.5	106.6	-138.1	86.3	251.6
16	O	22833	50	298.7	15.1	-44.4	361.6	-45.3	136	-173.9	89.2	173.7
17*a	O	17758	49.3	332.4	199.4	-54.7	365.9	-51.8	111.4	17.2	104	272.1
18*a	Ne	11500	50.5	232.6	21.9	43.6	364.8	-45.3	120.9	320.6	49.3	186.8

* These events were analyzed during the first phase of scanning and were reported by Singh [1990]

a) These events have ST tracks at the stopping sheet. As their stopping point is not accurately known there could be large error in residual range calculation and hence in identification.

† The systematic error in dip and azimuth angle measurements as evaluated from data on SSE, are ± 4.0 deg & ±3.0 deg respectively (fig.3-3).

Table-5.2 : List of all time annotated ACR events and their ionization states.

Serial No.	Identification	Arrival Time (GMT) Day	Hr	Min	Sec	Energy[a] (MeV/n)	Total[a] Mom. (GeV/c)	Cut off Rigidity (GV)	Vertical Cutoff Rigidity (GV)	Upper limit ionization state (Z^*)
1	O	125	21	13	25	16.4	2.8	$0.57^{0.42}_{0.82}$	0.62	5 (7, 3)
2	O	125	22	33	35	17.9	2.9	$2.17^{2.72}_{1.87}$	2.47	1 (1, 2)
3	O	125	19	28	23	17.5	2.9	$1.87^{2.37}_{1.22}$	2.18	2 (1, 2)
4*	N	125	23	25	45	14.8	2.3	$1.30^{1.40}_{1.10}$	1.38	1 (1, 2)
5*	N	125	13	22	45	14.6	2.3	$0.67^{1.10}_{0.55}$	0.76	3 (2, 4)
6*	O	124	9	15	45	16.1	2.8	$1.82^{2.00}_{1.82}$	2.25	1 (1, 1)
7*	O	124	19	51	25	18.0	2.9	$1.35^{2.25}_{1.10}$	2.79	2 (1, 2)
8*	O	125	1	17	5	15.1	2.7	1.88	1.93	1 ‡
9*	O	125	23	22	25	15.5	2.7	$2.25^{3.60}_{1.75}$	2.31	1 (-, 1)†
10*	O	123	18	5	35	19.3	3.0	$1.57^{2.35}_{1.05}$	1.95	1 (1, 3)
11*	Ne	124	1	36	55	17.3	3.6	$2.34^{2.75}_{1.95}$	2.58	1 (1, 1)
12*	Ne	125	5	0	55	17.9	3.7	$3.10^{3.95}_{2.10}$	3.59	1 (-, 1)†
13*	Ne	123	13	30	35	24.3	4.3	$2.73^{3.55}_{2.15}$	3.30	1 (1, 2)
14	N	124	14	50	45	14.1	2.3	$30.32^{23.37}_{32.52}$	12.13	- (-, -)†

Serial No.	Identification	Arrival Time (GMT) Day	Hr	Min	Sec	Energy[a] (MeV/n)	Total[a] Mom. (GeV/c)	Cut off Rigidity (GV)	Vertical Cutoff Rigidity (GV)	Upper limit ionization state (Z^*)
15	O	125	22	11	13	16.1	2.8	$5.92^{5.12}_{8.32}$	11.13	- (-, -)†
16	O	126	3	22	7	17.5	2.9	f	2.96	1
17*	O	125	13	32	55	17.4	2.9	f	1.61	2
18*	Ne	124	20	33	35	20.7	3.9	$2.39^{2.80}_{1.95}$	2.95	1 (1, 2)

Note: The values of ionization states given within the parenthesis are obtained for an uncertainty in arrival time of ±90 sec. The corresponding calculated cutoff rigidities are shown as super- and sub-scripted values.

* These events were analyzed during the first phase of scanning and were reported by Singh [1990].

a) The errors in energy are mostly within 2%., as estimated from uncertainty in measurement of ranges of the particle due to the uncertainty in the measured dip angles. The errors in momentum are nearly half of that in energies.

† Missing entry (-) indicates that the calculated ionization state is less than one.

‡ Limits on cutoff rigidity are not available because the trajectory tracing yield allowed trajectory for only one extreme value of arrival time.

f Trajectory-tracing did not yield allowed trajectory hence vertical cutoff rigidity is used to calculate the value of Z^*.

5.2 Spatial and Temporal Distribution of the ACR Events

We have considered the distribution in the arrival location and time of the individual ACR ions to see if there are any specific trends. The local arrival time of all the 13 ACR events are shown in fig.5-1. Events are seen to be evenly distributed with no particular preference in arrival time. The arrival point of these events span the geomagnetic latitude 40^0 to 60^0 (fig.5-2). Also the geographic arrival locations of these events do not show any clustering in any specific location, for example, over South Atlantic anomaly. The suggestion of Chan and Price [1975], that the geomagnetically forbidden high flux of low energy CNO particles observed during the earlier Skylab experiment, and suggested to be a part of ACR by Biswas *et al.*[1975], are in fact particles from the inner radiation belt that are registered in the Skylab detector when it crossed over the South Atlantic anomaly, is therefore not correct.

5.3 Possible Uncertainties in the Estimated Ionization States

It is obvious from table – 5.2 that ACR particles particles are either in 1^+ state or are consistent with their being in 1^+ state. Before discussing the implications of these results we would like to consider the possible uncertainties in the estimation of the ionization states of these particles. Since the ionization state obtained by us depends on the calculated geomagnetic cutoff rigidity using the trajectory-tracing method, we first consider the possible uncertainties in the two main input parameters for these

calculation:

i) Geomagnetic field values

ii) Arrival time information

The use of IGRF for the 1985 epoch makes the trajectory tracing calculation most appropriate as the experiment was conducted in 1985. However, as the IGRF represents only the internal field we must make sure that there was no external perturbation affecting the geomagnetic field as there could be considerable changes in the geomagnetic cutoff at lower latitudes during severe magnetic storms [Fluckiger, 1982] and also during flare time. The available data show that the experiment duration and particularly the period when the time annotated events were registered (3 - 6 May, 1985), was completely free from any magnetic storms as well as solar particle event. The absence of geomagnetic disturbances during this period is evident from the three hourly k_p indices shown in fig.5-3. Energetic particle flux from a small solar flare event, which occurred on April 24 , a few days prior to the mission , completely dropped down to the background level by April 28, and, we do not anticipate any contamination in our sampling from this event. We shall discuss this further in the next part of this chapter while discussing the results on the ionization states of low energy heavy ions. Finally the possibility of a day night variation in the geomagnetic cutoff, as shown by Smart *et al.* [1969], Smart and Shea [1972] and Fanselow and Stone [1972], is true only at geomagnetic latitude $>65^0$, whereas in our case all the events are registered at geomagnetic latitude $\leq 60^0$. So, as far as the effect of geomagnetic field is concerned, our results stand unaffected.

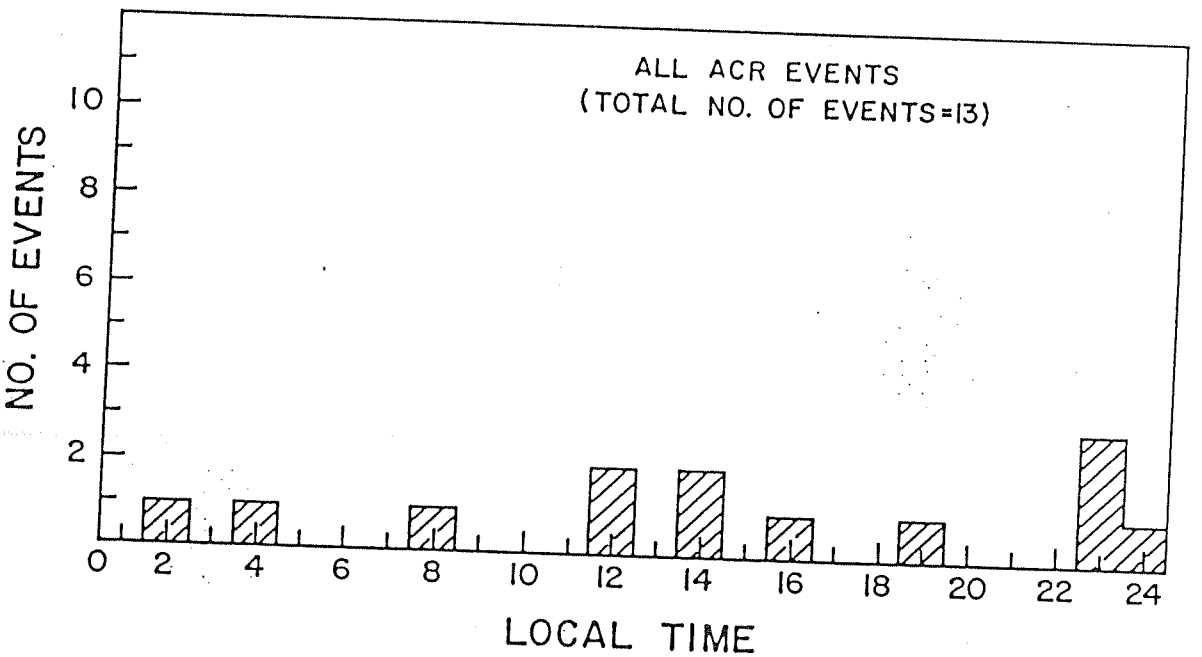

Fig.5-1 The distribution of local arrival time for the anomalous cosmic ray events detected in the "Anuradha" experiment.

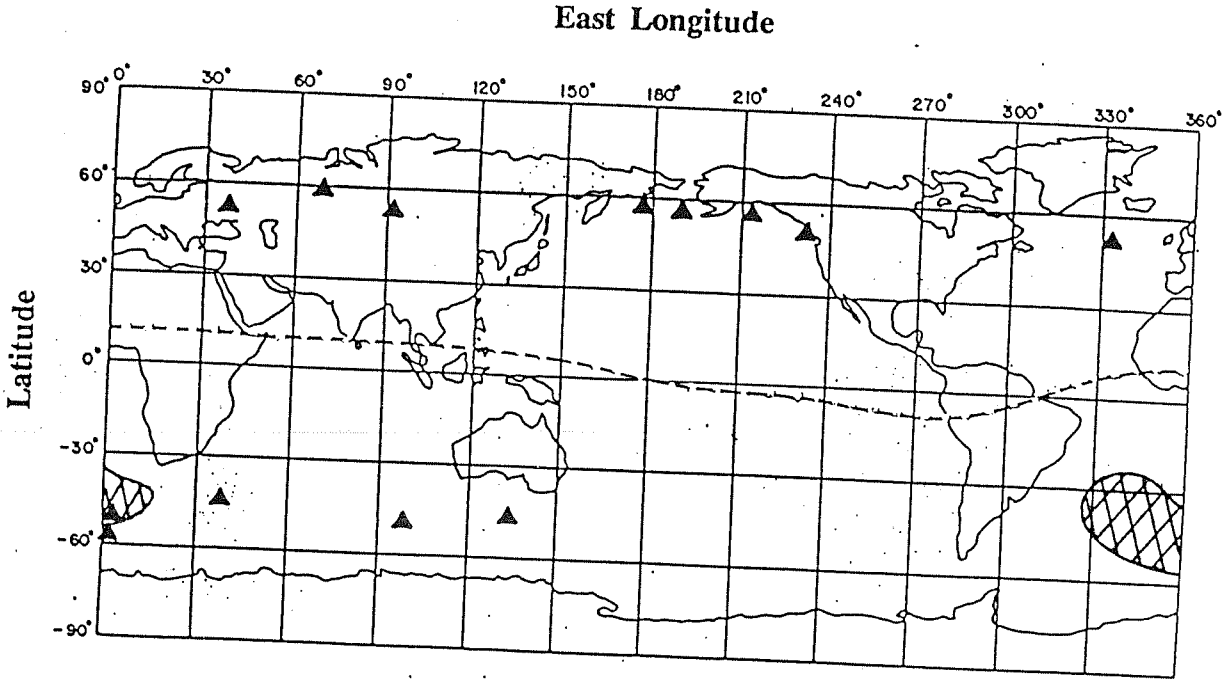

Fig.5-2 The geographical arrival locations of the anomalous cosmic ray events detected in the Anuradha experiment. The dashed line across, near the geographic equator, represents the geomagnetic equator. The South Atlantic anomaly is shown by the hatched region.

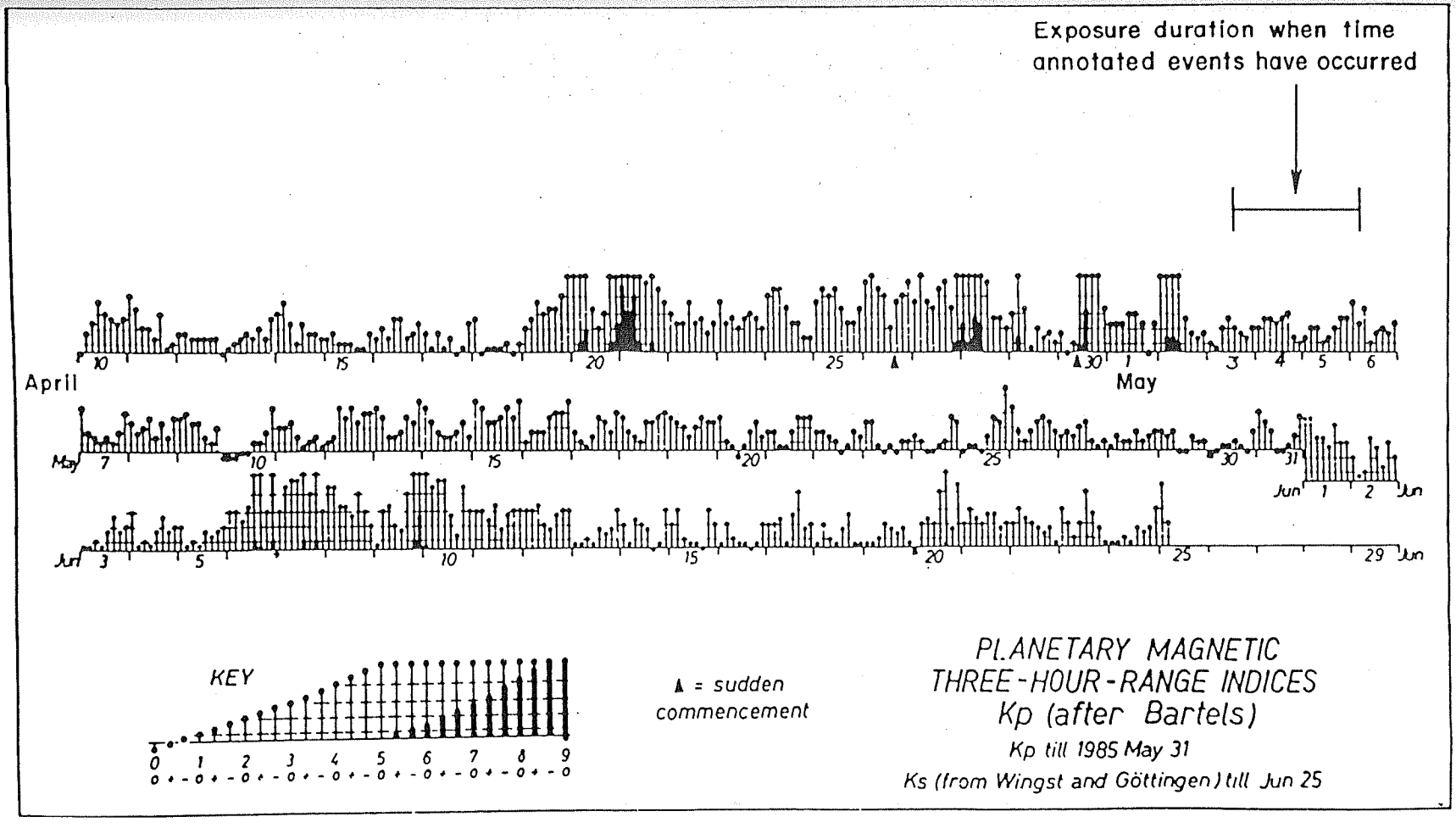

Fig.5-3 The three hourly k_p indices, for the period 10 April - 29 June. The absence of geomagnetic disturbances during 3-6 May, 1985, when the time annotated events were recorded, is clearly evident. [From Solar Geophysical Data, 1985]

The uncertainty in the estimation of arrival time of the particle, however, could be an important parameter that can alter our results on the deduced ionization states of the particles. Such an error can significantly change the arrival location (latitude and longitude) of the particle and hence the calculated cutoff rigidity. While the encoder reading difference for the matched pair of tracks provide information on the arrival time of an event nominally within ± 10 sec, a detailed analysis of the differences in the encoder readings for matched pairs of tracks for the stationary state events, where this difference should have been zero, showed that the deduced arrival time may have uncertainties upto 45 sec (± 1σ). We have therefore estimated the cutoff rigidities and the ionization states of all the events allowing for a worst case uncertainty in the arrival time of 90 sec (± 2σ) in each case. These results are shown in Table– 5.2 as super/sub-scripted values for R_c and Z^* (within parenthesis). The ionization state values thus obtained do not differ by more than one unit of charge in most of the cases. Thus, our conclusion that the ionization states of ACR are consistent with their being in singly ionized state remains unaltered.

The only previous attempt to determine the ionization states of individual ACR ions was that of Oschiles *et al.* [1989] who conducted a similar experiment on Spacelab-1 during November 28– December 8, 1983. The flux of ACR during this period was unfortunately extremely low , being much below the detection level for the IMP-8 and ISSE

satellite monitoring this component at 1 AU. Only a few ACR events could be detected in this experiment even after scanning a large area (about 600 cm^2) of the detector. In addition, the time resolution achievable in this experiment was rather poor, with a best value of about 2 minutes. Because of this limitation, the data from this experiment were analyzed by grouping the events into several zones, each of which were characterized by different ranges of cutoff rigidities. These authors finally claimed observation of four low energy ACR events (three oxygen and one neon) that arrived in a particular zone (zone #2) which would require these particles to be in 1^+ or 2^+ state. The results from the *Anuradha* experiment, with its superior time resolution and larger number of events, provide conclusive evidence for the singly ionized state of the anomalous cosmic rays.

5.4 Source and Origin of Anomalous Cosmic Rays

There are several hypotheses proposed for the source and origin of ACR. These can be classified into two broad groups according to the proposed sources: i) local galactic or solar system source; and ii) neutral particles in nearby interstellar space. While the second model predicts the ionization states of the ACR particles to be uniquely singly ionized, the first group of models in general predict a mixed ionization states for the ACR particles.

Considering the first group of models, McDonald *et al.*[1974; 1977] proposed a nearby unusual galactic object enriched in He, N

and O as the source of ACR. The acceleration of the particles to the observed energies took place either in the source itself or in the interstellar medium.

Local galactic objects like novae and O-type stars are also proposed as the source for ACR [Durgaprasad and Biswas, 1977; Biswas *et al.*,1981]. In these models the authors proposed that particles are emitted from the sources with energies of the order of 10 to 100 KeV/n either during novae outburst or as stellar winds. At these energies the equilibrium charge states of ions between carbon to iron can be in the range of +1 to +3. It is proposed that a fraction of these particles will be accelerated through interaction with supernova remnant shock fronts in the interstellar medium to energies of ~1 to 50 MeV/n. The ACR particles are therefore expected to be in a mixed ionization states. Fowler *et al.*[1979] proposed a cometary origin for the ACR particles where one expects presence of molecules like CO^+, OH^+.

The local interstellar neutrals as the source of ACR was proposed by Fisk *et al.*[1974], who noted that the elements enriched in the low energy ACR *i.e* He and O are expected to be neutral in the local interstellar medium. They proposed that neutrals from local interstellar medium enter into the solar system and become singly ionized either by photoionization or by charge exchange with the solar wind. Once ionized they are picked up by the solar wind and carried upto the heliospheric boundary where they get accelerated upto few tens of MeV/n through interaction with the solar wind

termination shock, before they diffuse back into the solar system and are observed as ACR. This model thus predicts the ionization state of ACR to be uniquely 1^+ and that elements with higher first ionization potentials (like H, Ne and Ar ions) should also be present in ACR.

The singly ionized state of the ACR ions determined in our experiment supports the model by Fisk *et al.* [1974]. The presence of H, Ne and Ar in ACR in addition to He, N and O has also been confirmed (see chapter I). The question of the source of the ACR ions can therefore be considered as resolved from the results obtained from the present experiment and also the results obtained from earlier attempts using direct [Oschiles *et al.*, 1989] and indirect approaches [Mckibben,1977; Klecker *et al.*,1980; Cummings *et al.*, 1984; McDonald *et al.*, 1988]. However, many aspects related to the acceleration and heliospheric propagation of the ACR component are yet to be understood in their totality.

Part-II : Low Energy (20-125 MeV/n) Galactic Cosmic Rays

5.5 Ionization States of Galactic Cosmic Rays

The experimental setup and the analytical procedure that were used in the *Anuradha* experiment to determine the ionization states of the anomalous cosmic rays can in principle be used to determine the ionization states of low energy particles of solar and galactic

origin as well. We have therefore utilized the same approach to determine the ionization states of low energy (≤ 125 MeV/n) galactic cosmic rays, incident on the *Anuradha* detector module. The initial aim of this work was to see whether the GCR particles are in fully ionized state as expected (Chapter-I; Section-1.2.3), which will then validate the approach itself. The initial results obtained [Biswas *et al.*, 1990; Singh, 1990] were completely unexpected as we found three low energy iron group ions, in a sample of 16 events, to be in partially ionized states. A thorough investigation of this new observation has been taken up in this thesis and constitute the subject matter of the remaining part of this chapter. A total of 60 heavy ion events (Z >10), whose arrival time could be obtained accurately from track matching procedure, were detected during the scanning of ~ 400 cm^2 of detector area. Out of these, ionization states of 46 events could be determined without ambiguity. In the remaining cases there are uncertainties in the identification of the particle (4 events) or the trajectory-tracing resulted in forbidden trajectories (10 events). In table - 5.3 the relevant parameters needed for determining the ionization states of these particles are given. These include the identification of the particles, the differences in the encoder readings for the matched pairs of tracks in top and bottom detector stacks and the arrival location and direction of each particle. As already discussed in the first part of this chapter, the difference in the encoder reading between the matched pair of tracks from a given event provides the information on the arrival time which can have a worst case uncertainty of ~90 sec. The dip and the azimuth angles of incidence of the particle are

measured in the detector frame of reference. The angle of incidence (dip and azimuth) in the detector coordinate system and the arrival location of the particle (latitude, longitude and altitude) are used to calculate zenith and azimuth angles in geocentric and local coordinate systems. In table - 5.4 the arrival time, energy, momentum, cutoff rigidity and the upper limits on the ionization states of the particles are given. The energy is calculated from the measured range of the particle in the detector by using appropriate range – energy relation. The super- and sub-scripted values for the cutoff rigidity show the values one gets by considering the worst case uncertainties in the arrival time (±90 sec), and, the ionization states obtained for these values are shown within parenthesis in the last column.

A total of 26 events out of the 46 events for which the ionization states could be determined are found to be in fully ionized state. An additional 4 events are most probably fully ionized, if we consider the error limits on their arrival times. The remaining 16 events are found to be in partially ionized state even after considering all the experimental and analytical uncertainties. These include one Titanium (6^+), two Vanadium (10^+, 16^+), two Chromium (5^+, 8^+), one Manganese (4^+), eight Iron (3^+, 3^+, 10^+, 11^+, 14^+, 14^+, 20^+, 20^+) and two Nickel (8^+, 14^+) ions. It can be noted that the events which are in partially ionized state all belong to the Iron group. The distribution of both fully and partially ionized events are shown in Table - 5.5.

Table-5.3 : List of all time annotated GCR events from 3cm scan and their arrival locations and directions.

Serial No.	Identification	Encoder position	Dip[a]	Azi[a]	Arrival Position				Arrival Direction			
					Long	Lat	Alt	GmLat	Geocentric		Local	
			(deg)		(deg)	(deg)	(km)	(deg)	Zen (deg)	Azi	Zen (deg)	Azi
1	Si	17713	72.6	13.1	148.6	-53.5	367.6	-57.5	129.6	-4.8	84.1	200.2
2	Ca	10434	57.0	273.2	124.4	-56.8	367.0	-63.2	135.7	-17.4	72.6	198.9
3	Ti	9547	45.4	251.8	297.1	50.7	362.6	57.8	99.0	-79.2	61.4	198.4
4	V	9539	52.3	223.3	290.7	47.8	361.5	55.2	86.3	-69.9	44.1	180.9
5	V	3730	70.2	263.3	84.2	-45.0	361.7	-52.7	133.4	168.0	57.1	120.7
6	Cr	9815	43.5	307.2	96.3	-46.3	365.7	-54.1	95.2	-10.8	97.8	253.8
7	Cr	20215	59.7	326.3	204.4	45.2	360.5	47.3	133.0	-122.7	92.9	156.6
8	Cr	577	45.9	272.8	175.1	-56.9	367.2	-57.4	127.7	47.2	75.6	220.1
9	Cr	1723	83.6	260.6	310.1	56.3	365.9	62.3	98.4	-67.0	66.2	198.5
10	Mn	20621	32.6	75.7	122.1	-32.5	357.1	-39.3	78.3	156.8	89.0	75.3
11	Mn	11277	74.3	81.6	269.6	56.8	366.0	64.5	103.1	-82.0	70.2	171.3
12	Mn	20243	44.9	47.0	230.3	54.9	364.5	60.1	120.0	-68.0	99.8	129.2
13	Mn	2540	56.2	231.2	64.7	-55.4	367.2	-61.9	143.1	-27.7	49.9	231.6
14	Fe	3411	44.7	103.3	237.1	56.6	366.0	62.5	91.4	-86.8	64.9	139.4
15	Fe	9841	48.0	92.8	117.8	-54.4	367.4	-61.4	139.8	-98.5	71.4	156.2

Serial No.	Identification	Encoder position	Dip[a]	Azi[a]	Arrival Position				Arrival Direction			
					Long	Lat	Alt	GmLat	Geocentric		Local	
			(deg)		(deg)	(deg)	(km)	(deg)	Zen (deg)	Azi	Zen (deg)	Azi
16	Fe	10952	41.1	133.3	60.2	-51.9	366.7	-57.4	164.1	156.3	42.9	156.5
17	Fe	19816	50.0	8.2	349.4	15.9	358.4	17.7	132.0	-109.0	106.8	230.1
18	Fe	20611	55.1	174.1	117.2	-37.4	358.5	-44.5	140.2	159.5	32.5	126.8
19	Fe	9241	43.8	53.6	112.6	-41.8	364.6	-49.2	130.5	-57.7	97.2	181.4
20	Fe	8718	67.1	40.6	164.1	-54.4	367.3	-56.4	130.2	-7.4	85.1	186.4
21	Fe	23434	63.5	146.7	8.5	-29.6	355.8	-29.8	122.9	63.1	46.2	108.8
22	Fe	9573	68.3	114.7	323.3	56.5	365.3	61.1	88.8	-8.6	59.7	147.0
23	Fe	19411	64.9	39.6	87.1	-55.3	367.8	-63.0	127.5	-90.6	87.1	181.7
24	Fe	2269	62.0	161.5	268.3	56.7	365.5	64.5	72.9	-77.3	41.1	158.8
25	Fe	10174	34.3	286.8	342.7	51.8	365.4	54.0	95.6	-100.2	90.0	260.9
26	Fe	20861	43.9	345.4	264.1	50.7	365.3	58.3	136.3	-160.6	111.9	222.4
27	Fe	3702	34.7	298.9	60.7	-54.4	365.7	-60.6	113.7	-91.5	98.3	205.4
28	Fe	2267	59.9	254.7	268.1	56.7	365.4	64.5	93.4	-113.8	62.7	204.7
29	Ni	2538	45.6	266.7	64.5	-55.3	367.2	-61.9	119.3	-35.8	71.6	244.6
30	Ni	10686	55.1	223.0	261.9	54.2	364.2	61.8	80.5	-106.3	45.2	191.4

Serial No.	Identification	Encoder position	Dip[a]	Azi[a]	Arrival Position				Arrival Direction			
					Long	Lat	Alt	GmLat	Geocentric		Local	
			(deg)		(deg)	(deg)	(km)	(deg)	Zen (deg)	Azi	Zen (deg)	Azi
31	Ni	9908	50.4	262.3	183.8	-47.7	363.0	-47.2	153.8	18.3	67.8	186.8
32	Ni	22535	24.3	306.9	191.8	51.6	365.4	52.0	111.9	96.6	110.1	259.9
33[b]	Fe	11838	68.0	39.0	248.2	56.6	366.1	63.4	118.0	-106.4	84.7	175.3
34[b]	Fe	1612	54.0	334.9	108.5	-54.9	367.2	-62.4	108.6	-35.9	100.5	214.1
35[c]	Fe	10681	42.2	260.5	255.2	52.3	363.4	59.6	102.6	-128.0	68.0	204.6
36	Mn	9923	46.0	6.7	193.8	-41.5	360.4	-39.7	102.7	-33.1	110.8	131.4
37	Mg	11073	57.6	258.1	158.7	-30.7	356.3	-33.8	165.5	-93.6	64.5	164.6
38	Mg	10598	59.1	304.9	213.2	18.1	352.2	21.7	143.1	-89.9	86.4	149.8
39	Cr	12700	48.1	48.5	50.4	-54.0	365.6	-59.2	104.9	175.6	96.8	127.4

21 events analyzed during the first phase of scanning which led to the observation of 3 partially ionized low energy iron group particles [Biswas *et al.*, 1990; Singh, 1990] are not included in this table.

a) The systematic error in dip and azimuth angle measurements as evaluated from data on SSE are ± 4.0 deg & ±3.0 deg respectively (fig.3-3).

b) These events are identified on the basis of JDC in 1-0 and RT in 1-1 sheets, there can uncertainty in identification.

c) For this event the stopping cone is ST. Therefore, there can be large uncertainty in identification.

Table-5.4 : List of all time annotated GCR events from 3cm scan and their ionization states.*

Serial No.	Identification	Arrival Time (GMT) Day	Hr	Min	Sec	Energy[a] (MeV/n)	Total[a] Mom. (GeV/c)	Cut off[b] Rigidity (GV)	Vertical Cutoff Rigidity (GV)	Upper limit ionization state* (Z*)
1	Si	125	13	25	23	20.6	5.5	$0.42^{0.52}_{0.37}$	0.49	13 (11,14)
2	Ca	124	17	40	15	111.5	18.8	$0.12^{0.12}_{0.22}$	0.16	20 (20,20)
3	Ti	124	15	16	13	41.3	13.5	$0.77^{0.92}_{0.62}$	0.84	17 (15,22)
4	V	124	15	14	53	43.6	14.7	$0.93^{1.27}_{0.72}$	1.05	16 (12,20)
5	V	123	23	28	53	32.5	12.7	$1.31^{0.97}_{2.02}$	1.36	10 (13,6)
6	Cr	124	16	0	3	60.3	17.7	$0.86^{1.32}_{0.52}$	1.02	20 (13,24)
7	Cr	125	20	13	23	109.6	24.2	$4.43^{6.62}_{2.92}$	4.36	5 (4,8)
8	Cr	123	14	11	7	49.8	16.1	$0.57^{0.42}_{0.82}$	0.64	24 (24,20)
9	Cr	123	18	1	53	39.8	14.3	$0.52^{0.32}_{0.92}$	0.59	24 (24,16)
10	Mn	125	21	20	7	65.3	19.5	$4.44^{3.02}_{6.67}$	4.23	4 (6,3)
11	Mn	124	19	57	33	45.1	16.1	$0.27^{0.32}_{0.27}$	0.29	25 (25,25)
12	Mn	125	20	18	25	56.0	18.1	$1.03^{38.3}_{0.57}$	1.06	18 (-, 25)[d]
13	Mn	123	20	14	45	115.6	26.4	$0.62^{0.87}_{0.47}$	0.71	25 (25,25)
14	Fe	123	22	36	3	89.6	23.5	$0.67^{0.82}_{0.52}$	0.72	26 (26,26)
15	Fe	124	16	4	13	109.9	26.1	$0.22^{0.37}_{0.17}$	0.24	26 (26,26)

Serial No.	Identification	Arrival Time (GMT) Day	Hr	Min	Sec	Energy[a] (MeV/n)	Total[a] Mom. (GeV/c)	Cut off[b] Rigidity (GV)	Vertical Cutoff Rigidity (GV)	Upper limit ionization state (Z^*)
16	Fe	124	19	5	23	22.7	11.6	$1.01^{1.67}_{0.67}$	1.11	11 (7,17)
17	Fe	125	9	8	3	126.9	28.2	$8.64^{8.32}_{9.17}$	14.2	3 (3,3)
18	Fe	125	21	18	27	112.9	26.5	$2.58^{1.57}_{3.82}$	2.71	10 (17,7)
19	Fe	124	14	26	43	64.4	19.7	$1.40^{8.67}_{0.95}$	1.69	14 (2,21)
20	Fe	124	13	1	5	64.1	19.7	$0.57^{0.62}_{0.62}$	0.64	26 (26,26)
21	Fe	126	4	58	53	69.0	20.5	$6.88^{5.37}_{13.35}$	6.01	3 (4,2)
22	Fe	124	15	20	33	95.9	24.3	$0.77^{0.67}_{0.97}$	0.85	26 (26,25)
23	Fe	125	18	1	25	92.2	23.8	$0.32^{0.47}_{0.17}$	0.37	26 (26,26)
24	Fe	123	19	30	45	123.3	27.8	$0.32^{0.37}_{0.27}$	0.30	26 (26,26)
25	Fe	124	16	58	43	86.3	23.0	$1.69^{1.22}_{2.37}$	2.35	14 (19,10)
26	Fe	125	21	58	53	83.5	22.6	$0.72^{0.57}_{1.12}$	0.76	26 (26,20)
27	Fe	123	23	24	13	36.6	14.8	$0.72^{0.75}_{0.76}$	0.86	20 (20,19)
28	Fe	123	19	30	43	86.1	23.0	$0.27^{0.42}_{0.22}$	0.30	26 (26,26)
29	Ni	123	20	14	43	119.4	28.8	$0.57^{0.92}_{0.42}$	0.72	28 (28,28)
30	Ni	124	18	21	23	143.2	31.7	$0.47^{0.77}_{0.32}$	0.49	28 (28,28)

Serial No.	Identification	Arrival Time (GMT) Day	Hr	Min	Sec	Energy[a] (MeV/n)	Total[a] Mom. (GeV/c)	Cut off[b] Rigidity (GV)	Vertical Cutoff Rigidity (GV)	Upper limit ionization state (Z*)
31	Ni	124	16	14	53	116.3	28.4	$2.00^{1.22}_{2.97}$	2.28	14 (23,10)
32	Ni	126	2	33	3	58.1	19.7	$2.35^{2.22}_{2.62}$	3.24	8 (9,8)
33	Fe	124	21	29	23	30.1	13.4	$0.46_{0.39}$	0.51	26 (21,26)
34	Fe	123	17	11	13	32.8	14.0	$0.22^{0.35}_{0.17}$	0.23	26 (26,26)
35	Fe	124	18	20	13	71.5	20.9	$0.67^{1.02}_{0.32}$	0.74	26 (20,26)
36	Mn	124	16	17	23	74.2	20.5	f	4.35	5
37	Mg	124	19	24	13	24.7	5.2	$5.77^{3.72}_{9.47}$	5.98	- (1,-)[d]
38	Mg	124	18	7	45	32.7	6.0	$29.22^{33.5}_{22.95}$	13.04	- (-,-)[d]
39	Cr	124	23	49	23	54.1	16.8	f	1.09	15

• 21 events analyzed during the first phase of scanning which led to the observation of 3 partially ionized low energy iron group particles [Biswas *et al.*, 1990; Singh, 1990] are not included in this table.

a The errors in energy are mostly within 2%., as estimated from uncertainty in measurement of ranges of the particle due to the uncertainty in the measured dip angles. The errors in momentum are nearly half of that in energies.

b The super- and sub-scripted values for cutoff rigidities are calculated for a ±90 sec of uncertainty in arrival time for each event.

c The values shown within parenthesis represent the calculated ionization states for ±90 sec uncertainty in arrival time.

d Missing entry (-) indicates that the calculated ionization state is less than one.

f Trajectory-tracing did not yield any allowed trajectory, hence the vertical cutoff rigidity was used to calculate the ionization states.

Table-5.5 Distribution of partially and fully ionized heavy ion events detected in *Anuradha* experiment.

Element	*Total No.of Events*	*Partially ionized events*	*Fully ionized events*
		Ionization state	*No. of events*
C	1	-	1
Si	1	13*	-
Ca	1	-	1
Ti	3	+6, +17*	1
V	2	+10, +16	-
Cr	7	+5, +8, +20*	4
Mn	4	+4, +18*	2
Fe	22	+3, +3, +10, +11 +14, +14, +20, +20	14
Ni	5	+8, +14,	3

* *These events could belong to the fully-ionized group, if we consider uncertainties on their arrival time.*

5.6 Spatial and Temporal Distributions of the Partially Ionized Events

The distribution of geographic arrival locations for all the heavy ion events show some trend (fig.5-4). Most of the events have come between 55^0 to 180^0 east longitude in the southern hemisphere and between 230^0 to 345^0 east longitude in the northern hemisphere. Since the orbital inclination of the space shuttle was $\pm 57^0$, such an effect could be expected because of the lower geomagnetic cutoff in these zones as is clear from the position of geomagnetic equator shown in the same figure.

The local arrival time of all the events as well as the partially ionized events are shown in fig.5-5(a) and fig.5-5(b) respectively. These events are seen to be evenly distributed with no particular preference in arrival time. The changes in geomagnetic cutoff due to day night variation, which are significant only at geomagnetic latitudes $>65^0$ [Smart *et al.*,1969; Smart and Shea,1972; Fanselow and Stone, 1972], can not be of much importance in the present case as all the partially ionized events are detected within geomagnetic latitude of 60^0 [fig.5-6]. We have already discussed in section-5.3 that the reference geomagnetic field model used for the trajectory-tracing to obtain the cutoff rigidity values was for the epoch 1985, during which our experiment was conducted. Moreover, the data on k_p indices during the experiment period (fig.5-3) clearly indicate the absence of any geomagnetic disturbances and the estimated cutoff rigidities can not have much uncertainties.

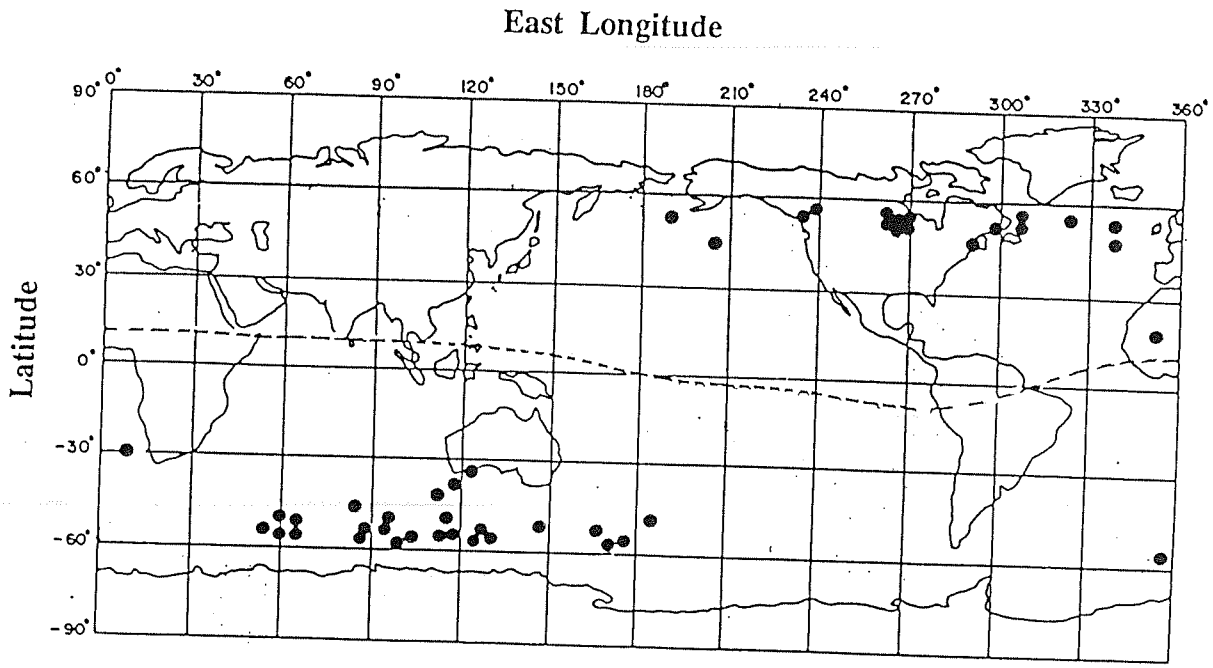

Fig.5-4 The geographic arrival locations of all 46 heavy ions (Z >10), analyzed from an detector area of 400 cm^2. The dashed line indicate the geomagnetic equator.

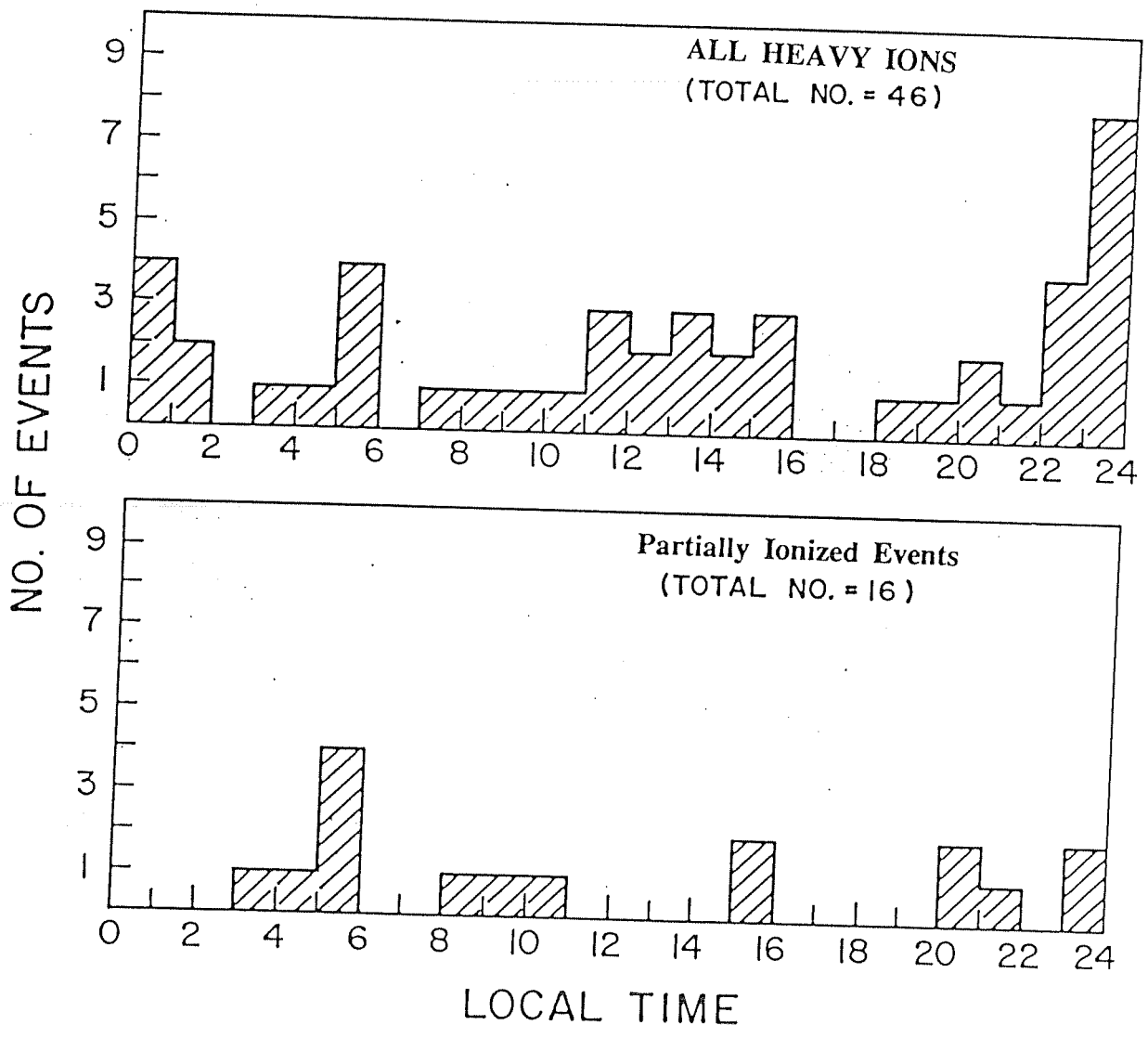

Fig.5-5 The distribution of local arrival time, a) for all heavy ions (Z >10), and, b) only for the partially ionized events.

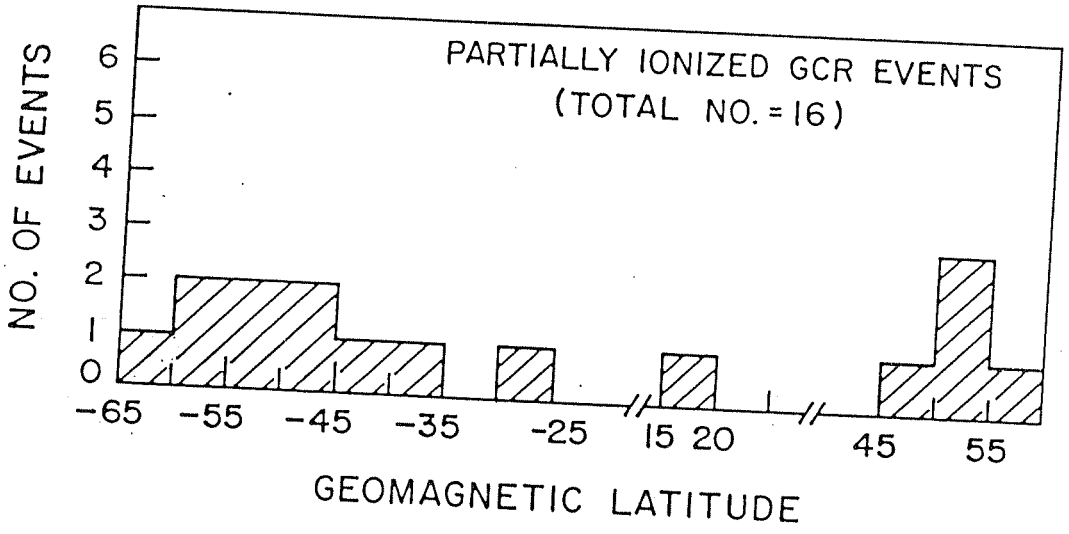

Fig.5-6 The distribution of arrival locations in geomagnetic latitude for all partially ionized events.

5.7 Possible Uncertainties in the Estimated Ionization States

We have critically evaluated the possible systematic errors in measurements and computations that may affect the deduced values of the ionization states of the low energy heavy ions. In fig.5-7 we show the calculated values for the cutoff rigidities including the penumbra zone for all the partially ionized events. The uncertainty in the effective threshold rigidity (R_c) due to the spread of the penumbra region is $\leq$ 10 % in most cases. It may be noted that we have to lower the cutoff rigidities by a factor of 3.7 (for Titanium), 1.4 and 2.3 (for Vanadium), 3.0 and 4.8 (for Chromium), 6.3 (for Manganese), 1.3, 1.3, 1.9, 1.9, 2.4, 2.6 and 8.7 (for Iron) and 2.0 and 3.5 (for Nickel) respectively, if these are fully ionized particles. Such a reduction is completely outside the range of the estimated uncertainty in the cutoff rigidity values. As discussed in the case of ACR, we have also performed a worst case analysis of the data by allowing the error in arrival time estimate to be $\pm$90 sec for each event, which is almost twice the systematic error in this parameter as evaluated from the encoder readings for the "stationary state events". The effect on the ionization states allowing for such an uncertainty is shown in the last column in Table-5.4. These values do not alter our conclusion for the presence of partially ionized low energy iron group particles. The experimental uncertainties in the estimation of the momentum of the particle is small ($\leq$ 1 %), and can not alter the results. There could not be any error in the identification of the particle also, as we could achieve charge resolution of less than one unit of

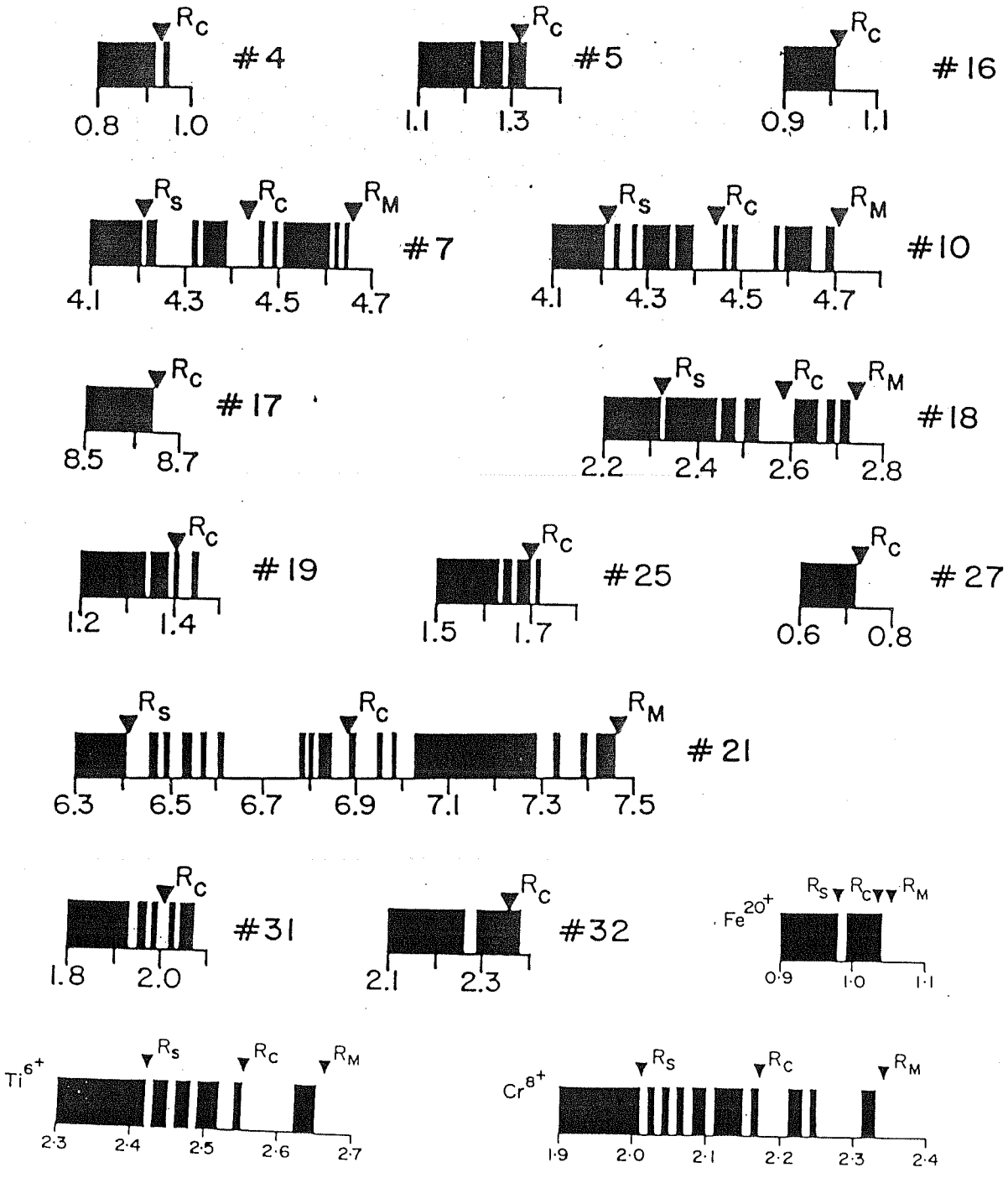

Fig.5-7 The cutoff rigidities R_c (in GV) for all partially ionized events alongwith their penumbra structure are shown. R_M is the main cutoff above which all rigidities are allowed and R_s is the stormer's cutoff below which all rigidities are forbidden. The numbers refer to the individual events (see Table– 5.4).

charge almost routinely, since multiple data points are available for analysis for most of these events.

5.8 Possible Sources for the Partially Ionized Heavy Ions

The clear identification of 16 partially ionized Ti, V, Cr, Mn, Fe and Ni ions among a sample of 46 low energy (≤ 125 MeV/n) events is a completely new observation. We have good confidence in this new result because the use of the same experimental setup and analytical procedure yielded results which showed that the ACR particles are singly ionized and most of the heavy ions are fully ionized, which are in good agreement with our present knowledge about the ionization states of the ACR and GCR components (see chapter-I). The properties of the low energy (20-125 MeV/n) galactic cosmic rays were not studied earlier, as this energy region is generally not accessible to the balloon-borne and most of the spacecraft experiments. Even then the result was entirely unexpected as the theoretical calculations [see *e.g.* Rule and Omidvar, 1979] predict fully ionized state for the GCR iron group particles following their interstellar propagation at energies ≥ 10 MeV/n (fig.5-8). We have therefore made a detailed analysis to make sure that the particles detected are indeed of GCR origin and cannot be sample from any other sources like ACR, SEP and trapped magnetospheric particles.

The ACR particles are now established to have originated from a nearby source, and traverse very little amount of matter as is evident from absence of secondary particles *e.g* ^{3}He [Mewaldt *et al.*,

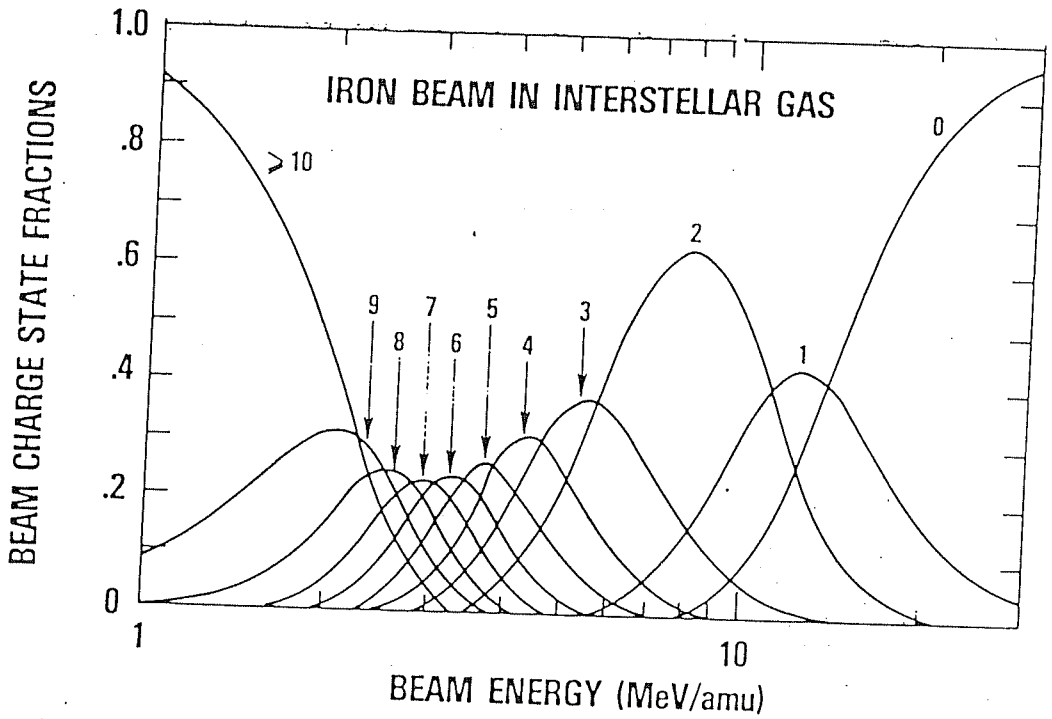

Fig.5-8 Fractions of a beam of Fe ions in interstellar medium with charge states Fe^{+26}-Fe^{+16}, as a function of energy. The curves are labeled by the numbers of electrons on the ion in that charge state. [From Rule and Omidvar, 1979].

1984; Mewaldt, 1988]. Thus secondary sub-iron particles like Ti, V, Cr etc. can not be a part of ACR. Further iron and sub-iron particles do not show any upturn in their spectra at low energies which is also indicative of their absence in the ACR component [Ferrando *et al.*, 1988]. Thus anomalous cosmic rays or quasi-trapped anomalous cosmic rays can not be the source of the observed partially ionized iron group heavy ions.

We next consider whether solar energetic particles could be the source of the partially ionized particles. A small solar flare event did occur on April 24, 1985 five days prior to the space shuttle flight. The IMP-8 and SMM data [Solar Geophysical data, 1987; Goswami *et al.*, 1988; Strong, 1989] showed that >10 MeV proton flux in this flare reached a maximum on April 25 and subsided to the background level by April 27 two days prior to the flight and remained at the background level throughout the experiment duration. The 20-25 MeV/n and 25-90 MeV/n helium fluxes measured by the University of Chicago telescope on IMP-8 show that the maximum flux value of 10^{-3} particles/ (cm^2.sr.sec.MeV/n) was detected on April 26 which decreased to background level by April 28, 1985 [fig.5-9]. As the emission of the solar flare energetic heavy ions are expected to closely follow the emission of helium ions, at the energies of interest (>40 MeV/n), we do not expect any direct contribution from this solar flare event, particularly in the case of the time annotated events which are registered in our detector during 3-6 May, 1985, five days after the flare intensity dropped to the background level. The presence of subiron secondaries like Ti, V, Cr

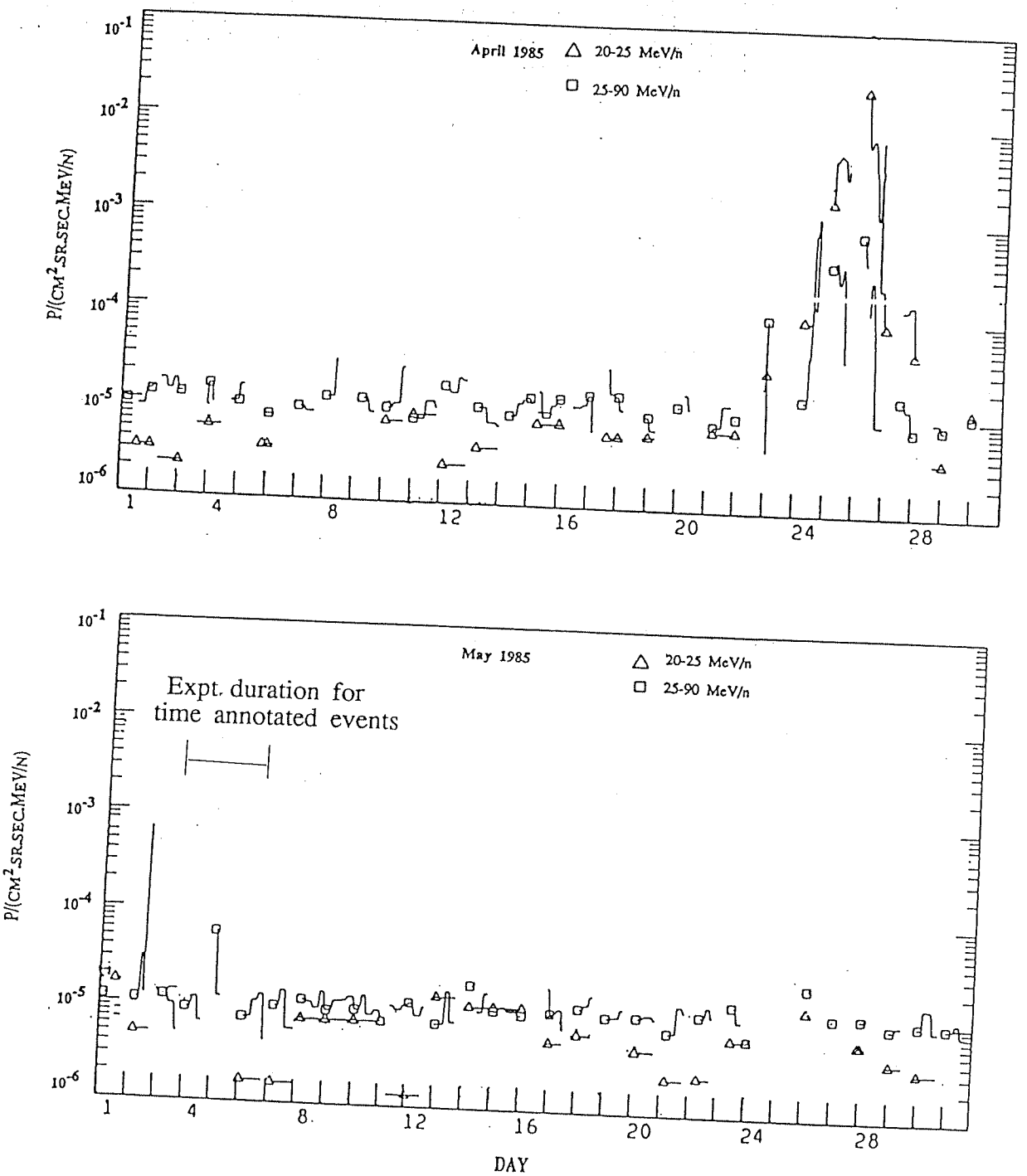

Fig.5-9 The helium fluxes for energies 20-25 MeV/n and 25-90 MeV/n measured by IMP-8 spacecraft at 1 AU during the month of April,1985 (above) and May,1985 (below). [From Solar Geophysical Data, 1987].

etc., whose solar abundance is ~1 % that of iron [Ross and Aller, 1976] also suggest a non solar source for these particles. Further for quite a few events, the upper limit of ionization states are $\leq 10^{+}$, much below the value 15^{+} for normal solar flares and 21^{+} for He^{3}-rich solar flare events, estimated for low energy iron particles (Luhn *et al*,1985; Luhn *et al.*,1987; also see Chapter-I; Section-1.2.1). However, if there are some special process by which solar flare particles could traverse a large amount of matter (several gm cm^{-2}) in the upper atmosphere and hence undergo nuclear interaction and stripping resulting finally in partially ionized trapped iron and subiron particles, then such a process could be examined for its validity. We do not favor such a scenario at present from plausibility considerations and the short decay time of the April 24 event noted above.

We next consider whether geomagnetically trapped particles could be the source of the partially ionized iron group particles. Most of the partially ionized ions are observed within L values of 2 to 4, in the B-L coordinate. There is very little information on the flux of heavier ions ($Z \geq 8$) in this zone, and, although one can consider trapping of solar energetic particles from the April, 24 event, the presence of sub-iron particles will then require further nuclear interaction and fragmentation of SEP before being detected in our experiment. Consideration of SEP as a source would also imply that we may not have a steady source of these particles in the outer radiation belt. It is also not clear if SEP with energies of up to 100 MeV/n could be trapped effectively for almost a week following

the flare event. Direct access of low energy galactic cosmic rays into the magnetosphere is not possible, except perhaps during geomagnetically disturbed conditions, which was definitely not the case during the present experiment. Further, there is no evidence for the presence of any heavy ion component in the outer radiation belt that is compositionally similar to GCR. Nonetheless, we have evaluated the equatorial trapped iron ion flux for the L=2 – 4 zone, necessary to produce the observed flux of partially ionized ions at Spacelab-3 orbit, assuming a isotropic pitch angle distribution. This turns out to be 3.9×10^{-8} p/(cm^2.sr.sec.MeV/n). Thus, although plausibility consideration rules out direct trapping of GCR ions, the requirement of low magnetospheric flux suggests that in-situ measurement of heavy ions (Z>20) in outer radiation belt could be extremely important in the present context.

In view of the above considerations we are finally left with the alternative that galactic cosmic rays are the source of the partially ionized low energy iron-group ions. Here, the composition of the partially ionized particles, particularly the presence of secondary subiron ions, presents no problem if we consider the standard model of cosmic ray propagation. However, as already discussed, it is not possible to have partially ionized GCR ions at energies >10 MeV/n, following their interstellar propagation (see fig.5-8). We therefore, consider here a plausible scenario which can explain the presence of the partially ionized heavy ions in near-earth-space if they are of GCR origin. A two stage process is considered. We propose the presence of a low energy (1-10 MeV/n)

partially ionized iron group GCR in the local interstellar space. These are then accelerated to higher energies in the solar wind termination shock with out any significant change in their ionization state, following which they diffuse into the solar system and are observed as partially ionized ions at energies of 20-125 MeV/n at 1 AU. The low energy partially ionized component postulated by us, may simply represent the lowest energy end of the steady state local interstellar GCR spectra or may be due to the trapping of medium energy (upto a few hundred MeV/n) GCR ions in large molecular clouds in nearby interstellar space resulting in degradation of energy to 1-10 MeV/n for a fraction of these ions. Such low energy iron group ions are expected to be in partially ionized states [Nikoleav, 1965; Rule and Omidvar, 1979]. Thus a mixed population of partially and fully ionized particles finally emerge from this region. The low energy partially ionized iron group particles could be accelerated to tens to hundreds of MeV/n at the heliospheric boundary region, by process similar to those proposed for acceleration of the anomalous cosmic rays [Fisk *et al.*, 1974; Pesses *et al.*, 1981; Potgieter and Moraal, 1988], leading to the observed population of low energy partially ionized galactic cosmic ray ions at 1 AU. We favor the presence of a steady state low energy (1-10 MeV/n) cosmic ray flux in the local interstellar space, since presence of such low energy interstellar cosmic ray component has also been postulated to explain the high C/CO ratios in dense interstellar cloud [Cravens and Dalgarno, 1978; Gradel *et al.*, 1987].

To examine whether the low energy fluxes in the demodulated steady state local interstellar spectrum is sufficient to generate the observed flux of the partially ionized heavy ions, we have calculated the interstellar iron flux at energies 1-10 MeV/n and compared it with the observed flux of partially ionized heavy ions. We have considered the demodulated (ϕ =0) spectrum for GCR iron ions [*e.g* Smart and Shea, 1985] extrapolated down to 1 MeV/n, and calculated the integral flux of particles in the energy interval 1-10 MeV/n. This was estimated to be 2.7×10^{-2} $m^{-2}.sec^{-1}.sr^{-1}$. It is difficult to estimate exactly the flux of the partially ionized heavy ions present in the near-earth-space, since we need to know the geomagnetic transmission factor which is a function of both the ionization state and energy of the particles. We have therefore considered all the particles to have an average ionization state of 10^{+} and calculated the total number of particles in the energy band 20-125 MeV/n. The resultant flux of $\leq 5.9 \times 10^{-3}$ $m^{-2}.sec^{-1}.sr^{-1}$ is ~20% of the integral flux of 1-10 MeV/n iron ion in local interstellar space. Even if the average ionization state of the partially ionized heavy ions in near-earth-space is somewhat higher than 10^{+} we need only a fraction of the low energy (1-10 MeV/n) local interstellar particles to be accelerated in the solar wind termination shock, which then diffuse into the interplanetary space.

If, on the other hand, the low energy partially ionized heavy ions were produced during trapping in large molecular clouds in the neighborhood of the solar system, one can put some constraint on the location of these clouds to within a couple of thousand parsec, so

that electron stripping process is minimal between the escape of these ions from the molecular clouds and their arrival at the solar wind termination shock front. It is also of interest to note that irrespective of the source of the low energy ions the electron capture process may be further aided by the presence of the Oort's cloud in the outer periphery of the solar system (20,000 to 50,000 AU) [Marochnik *et al.*,1988], if we consider the number density in this region to be similar to that for interplanetary space *i.e* ~5 atom/cc [Allen, 1973]. The energy gain factor needed at the SW termination shock is modest, at best a factor of 10-100 even after we consider energy loss by these partially ionized particles in the heliosphere, before reaching 1 AU.

Chapter-VI

CONCLUSIONS

The low energy anomalous and galactic cosmic rays present in the near-earth-space were studied for their ionization states, flux and composition in the *Anuradha* experiment, conducted onboard Spacelab-3 during April-May,1985. The main objectives of this study were i) direct determination of the ionization states of ACR particles and hence to resolve the question of their source and origin, ii) determination of the ionization states of low energy (20-125 MeV/n) heavy ions (Z>10), to see whether they are fully ionized as is expected for GCR particles. The Spacelab-3 orbit-averaged GCR oxygen ion flux in the energy range 50-250 MeV/n was also determined in this work to check on the validity of the trajectory-tracing method used to determine the cutoff rigidity, an important input parameter in determining the ionization state of an energetic particle. The main results obtained in the present work along with their implications are summarized in this chapter. Scopes for further work in this field are outlined along with several suggestions.

6.1 Summary of Results and Conclusions

We have determined the Spacelab-3 orbit-averaged GCR oxygen ion fluxes in the energy range 50-250 MeV/n. The corresponding interplanetary GCR oxygen fluxes are calculated by using the orbit-averaged geomagnetic transmission factors. The average cutoff

rigidities for 5^0 latitude X 5^0 longitude grids are calculated by using the trajectory-tracing method and the 1985 reference geomagnetic field, and the time spent by the Spacecraft in each of these grids were considered in calculating the orbit-averaged geomagnetic transmission factor. To check the validity of the geomagnetic transmission factor, and hence the trajectory-tracing method, we have compared the interplanetary oxygen fluxes derived from our measurement with direct measurement of GCR fluxes outside the magnetosphere. The flux values obtained from our experiment [in unit of $p/(m^2.sr.sec.MeV/n)$] are: $(1.73\pm1.00)\times10^{-3}$ at (45±10) MeV/n, $(3.12\pm1.38)\times10^{-3}$ at (121±37) MeV/n and $(4.96\pm3.46)\times10^{-3}$ at (235±72) MeV/n. These values which compare well with the deduced interplanetary fluxes of $(2.2\pm0.32)\times10^{-3}$, $(4.2\pm0.6)\times10^{-3}$ and $(5.0\pm0.72)\times10^{-3}$ respectively, based on the measured alpha particle fluxes for the same epoch [McDonald and Lal, 1986] and assuming a GCR α/O ratio of (40.2±5.8) in this low energy range [Cartwright *et al.*, 1971]. We have also determined the normalized modulation parameter ($\Phi = \frac{A}{Z} * \phi$) from the interplanetary GCR oxygen fluxes derived from our experiment. This derived value (640±60 MV) is also found to be similar to the Φ values based on proton and helium fluxes (650±20 MV and 670±40 MV respectively) from ISEE-3 experiment [McDonald and Lal, 1986]. The agreement between the flux values and the normalized modulation parameters, gives us good confidence on the validity of the orbit-averaged geomagnetic transmission factors, and hence on the cutoff rigidities obtained by the trajectory-tracing method, which were used extensively in this study for the determination of ionization states of individual ions.

The singly ionized state for the anomalous cosmic ray events proposed earlier by Singh [1990], based on the initial results from this experiment is now further consolidated by the expanded data base, and most of the ACR events are found to be in 1^+ state. As the trajectory-tracing method gives the lower limit on the rigidity of the particle for a specific arrival location and direction, the upper limit of 1^+ for the ionization states of the ACR particles uniquely establish the singly ionized states for ACR. This result supports the model of Fisk *et al.*[1974], who propose the source of ACR particles to be neutral particles in the local interstellar medium and predict the the ACR particles to be uniquely singly ionized. Thus the question of the source and origin of the ACR particles can now be considered as resolved. However, the exact details concerning their acceleration to the observed energies and heliospheric propagation is yet to be understood in their totality.

We have also determined the ionization states of 35 low energy (20-125 MeV/n) heavy ions (Z>10) in this work. Majority of them are found to be in fully ionized states as is expected for galactic cosmic rays. However, 13 of them are found to be in partially ionized states. All the partially ionized events belong to iron group. This substantiates the initial results where three such events were reported [Biswas *et al.*, 1990]. We have good confidence in this new finding, because the use of the same experimental and analytical procedures showed the ACR particles to be singly ionized, and majority of the GCR particles to be in fully ionized, which are

in agreement with the present day knowledge about the ionization states of these particles (section-1.2, Chapter-I). We have examined all the possible sources for these partially ionized heavy ions *e.g* anomalous cosmic rays, magnetospheric particles, solar energetic particles and galactic cosmic rays, and finally conclude them to be of GCR origin. Our results show for the first time the presence of a new component of low energy (20-125 MeV/n) partially ionized heavy ion component in the near-earth-space.

A plausible model for the generation of partially ionized low energy galactic cosmic rays is also presented in this work. We postulate the presence of a low energy (1-10 MeV/n) partially ionized GCR component outside the solar system. This could simply be the low energy component of the steady state local interstellar GCR spectra or could be produced through trapping of high energy (upto a few hundred MeV/n) GCR particles in large molecular clouds in the nearby interstellar space, where a fraction of them suffer degradation in energy to ~1-10 MeV/n and gets partially ionized through electron capture. We favor the low energy steady state local interstellar GCR component as the source, whose presence is also postulated to explain the anomalous C/CO ratio in dense interstellar clouds [Cravens and Dalgarno, 1978; Gredel *et al.*, 1987]. Acceleration of this low energy partially ionized GCR component to the observed energies can take place in the heliospheric boundary as is proposed for the anomalous cosmic rays [Fisk *et al.*,1974; Pesses *et al.*, 1981; Potgieter and Moraal, 1988].

6.2 Suggestions for Improvement and Scope for Further Studies

The experimental and analytical procedures used in the present work can be used as a standard procedure to determine the ionization state of any low energy (≤ few hundred MeV/n) charged particle coming from outside the earth's magnetosphere. However, one can improve the procedures by few ways *viz.* i) better time resolution, to know the arrival information of the particle more precisely, ii) increasing the event statistics. While better time resolution can be achieved by simply reducing the time interval between successive step movement of the detector stack, the limitation in this regard mostly comes from systematic uncertainties during the post-exposure data acquisition period.

The number of events detected in our experiment were too few. More number of events could be observed by increasing the exposure time of the detector. However in the present experiment the constraint of not rotating the bottom stack by more than one revolution, puts a limit to the exposure period. If the rotation of the stack and the orbital period of the spacecraft can be synchronized, one can get rid of this problem. As for example, in the present case the orbital time period of the Spacelab-3 was ~90 min, and it was repeating an orbit after every 31st orbit. Further the time taken for one complete rotation of the bottom stack in this experiment was 90 hr. Therefore if one can synchronize these two parameters in such a manner that as the bottom stack completes one rotation, the spacecraft also starts repeating its 1st orbit, we can

extract the arrival information uniquely and can have more than one rotation of the bottom stack. In such a setup there will not be any constraint on the exposure period and the event statistics can be increased. Such an arrangement can probably be tried during the space-station era. The arrangement of a fixed top stack and single rotating passive detector stack restricts the energy range over which ionization states of different ions can be determined. This impedient can be removed by multiple stack arrangement with alternate fixed and rotating stacks. This will help us to ascertain the ionization states of higher energy GCR particles also.

The presence of partially ionized subiron and iron particles in the near-earth-space has been established in this work. If our hypothesis for the presence of a partially ionized low energy (≤10 MeV/n) component of GCR outside the solar system is correct, we could expect to observe other elements of GCR, like C to Ca in partially ionized states. However, as has been shown by Rule and Omidvar [1979], while the equilibrium charge state for iron beam in interstellar medium could be <26 at energies ≤10 MeV/n, an oxygen beam could be in partially ionized states only at energies ≤1 MeV/n. Thus the possibility of finding partially ionized GCR ions is more in the case of heavy ions and one needs to look for low energy high Z (*e.g* Si, Ca etc) GCR particles rather than lower Z (*e.g* C,O) particles to further investigate this new phenomenon.

One can also attempt variation of the experimental setup in this approach. For example Hertzen and Marenny [1986] proposed

linear movement of two detector stacks to achieve objective similar to our experiment. It is also important to utilize electronic detector in which case the time consuming post-exposure data acquisition procedures needed in case of passive detector can be avoided, and one can use conventional satellites for long duration exposure. Kuznetsov *et al.* [1987] have reported some results on the ionization states of solar flare particles with such an approach. Hovestadt *et al.* [1987] have also proposed an experiment that combines a large area ion drift chamber and a time-of-flight telescope for determination of ionization state of energetic particles. In all these approaches the concept of using geomagnetic field as a rigidity filter has been adopted.

The presence of partially ionized iron group ions may also affect the subiron to iron ratio measured inside the magnetosphere, particularly for small event statistics, if the charge state distribution for both iron and subiron particles are not the same. A detail study of the sub-Fe to Fe abundance ratio within the magnetosphere, spanning the energy range of 50-400 MeV/n, will be useful in this regard.

We have observed few events in this experiment (*e.g* #37, #38, #39 in Table-5.4) which are difficult to explain as the deduced charge state is <1. Two of these events (#37 & #38) with atomic number 12 could be spallation products from aluminum, which was used as a rib structure on the top of the instrument. In such a case the incoming direction of the particles as back-traced from their

records in the detector may not be correct. This may lead to erroneous estimation of cutoff rigidity and hence the ionization states. It will be also interesting to check whether any of the problematic events could be molecular ions like CO^+ as suggested by McGowan [1983]. It is of interest to note that in an experiment with counter telescope conducted in 1981, Saito *et al.* [1990] have observed two geomagnetically forbidden events in a total of 127000 events, which are consistent if we consider them to be partially ionized ($Z^* = 3$) silicon ion or with a particle having atomic number Z ~14, mass A ~350 and energy 450 MeV/n. Because of the high energy of the particle they prefer the second alternative and suggest that these events could be Strange-Quark Matter in GCR. Modified long duration experiment of *Anuradha* type as discussed above, can be used to look for such events in future.

In summary the present work has validated the approach of using geomagnetic field as a rigidity filter for determining the ionization state of low energy particles coming from outside the magnetosphere. The singly ionized state of ACR particles has been conclusively established and we have shown for the first time the presence of a partially ionized low energy heavy ion component in the near-earth-space. The possibility of further work in this area with suitable modification of the present experimental approach seems to be very promising.

REFERENCES

Allen C.W, Astrophysical Quantities, University of London, Athlon Press, 1973

Allen J.W. and Dupree A.K., Calculation of ionization equilibria for oxygen, neon, silicon and iron, Ap.J., 155, 27, 1969

Anglin J.D, Dietrich W.F. and Simpson J.A., Solar flare accelerated isotopes of Hydrogen and Helium, in proc. Symp. High Energy Phenomena on the Sun (NASA SP-342), 315, 1973

Axford W.I., Leer E. and Skadron G., The acceleration of cosmic rays by shock waves, Proc. 15th ICRC (Plovdiv), 11, 132, 1977

Balsubramanyan V.K. and Serlemitsos A.T., Solar energetic particle event with $^{3}He/^{4}He$ >1, Nature, 252, 460, 1974

Bame S.J., Hundhausen A.J., Asbridge J.R. and Strong I.B., Solar wind ion composition, Phys. Rev. Letts., 20, 393, 1968

Bame S.J., Spacecraft observation of solar wind composition, in Solar Wind III, ed. Sonett C.P., Coleman P.J., Jr. and Wilcox J.M., 535, 1972

Benton E.V., A study of charged particle tracks in Cellulose nitrate, Report, USNRDL-TR-68-14, 1968

Binns W.R., Cummings J.R., Garrard T.L., Israel M.H., Klarmann J., Stone E.C. and Waddington C.J., Charge, mass and energy changes during fragmentation of relativistic nuclei, Physical Review C, 39, No. 5, 1785, 1989

Biswas S, Freier P.S. and Stein W., Solar protons and α particles from September 3, 1960 flares, JGR, 67, 13, 1962

Biswas S. and Fichtel C.E., Composition of solar cosmic rays, Sp. Sci. Revs., 4, 736, 1965

Biswas S., Durgaprasad N., Nevatia J., Venkatavardan V.S., Goswami J.N., Jayanthi U.B., Lal D and Mattoo S.K., High fluences of low energy (10-25 MeV/amu) C, N, O and heavier ions at 450 Kms altitude : Results from the Skylab experiments, Astro. Phys. and Sp. Sci., 35, 337, 1975

Biswas S. and Durgaprasad N., Skylab measurements of low energy cosmic rays, Sp. Sci. Revs., 25, 285, 1980

Biswas S., Durgaprasad N. and Trivedi S.S., On the origin of the low energy cosmic rays from stellar sources, Proc. (Ind. Acad. Sci.) Earth Planet Sci., 90, 337, 1981

Biswas S., Durgaprasad N. and Vahia M.N., Energy and nuclear charge dependence of abundance enhancement of solar cosmic ray heavy ions in three large solar events, Solar Physics, 89, 163, 1983

Biswas S., Chakraborti R., Cowsik R., Durgaprasad N., Kajarekar P.J., Singh R.K., Vahia M.N., Yadav J.S., Dutt N., Goswami J.N., Lal D., Mazumdar H.S., Subhedar D.V. and Padmanabhan, Ionization states of cosmic rays: Anuradha (IONS) experiment in Spacelab-3, Pramana, 27, 89, 1986

Biswas S., Durgaprasad N., Mitra N., Singh R.K., Dutta A. and Goswami J.N., Observation of low energy (30-100 MeV nucleon^{-1}) partially ionized heavy ions in galactic cosmic rays, 359, L5, 1990

Blanford R.D. and Ostriker J.P., Supernova shock acceleration of cosmic rays in the galaxy, Ap.J., 237, 793, 1980

Breneman H.H. and Stone E.C., Solar coronal and photospheric abundances from solar energetic particle measurements, Ap.J. Letts., 299, L57, 1985

Cartwright B.G., Garcia-Munoz M. and Simpson J.A., Abundances of the galactic nuclei H through the Fe from satellite measurements, 12th ICRC (Hobart), 1, 215, 1971

Cesearsky C.J., Cosmic ray propagation in the interstellar medium, 20th ICRC (Moscow), 8, 87, 1987

Chapman and Bartels, Geomagnetism, Vol. I and II, 1940

Chan J.H. and Price P.B., Composition and energy spectra of heavy nuclei of unknown origin detected on Skylab, Phys. Rev. Letts., 35, 539, 1975

Christian E.R., Cummings A.C. and Stone E.C., Evidence for anomalous cosmic-ray hydrogen, Ap.J., 334, L77, 1988

Christian E.R., Cummings A.C. and Stone E.C., Evidence for anomalous cosmic ray hydrogen, 21st ICRC (Adelaide), 6, 186, 1990

Cox D.P. and Tucker W.H., Ionization equilibrium and radiative cooling of a low density plasma., Ap.J., 157, 1157, 1969

Cravens T.E. and Dalgarno A., Ionization, dissociation, and heating efficiencies of cosmic rays in a gas of molecular hydrogen, Ap.J., 219, 750, 1978

Cummings A.C., Stone E.C. and Webber W.R., Evidence that the anomalous cosmic-ray component is singly ionized, Ap.J., 287, L99, 1984

Cummings A.C. and Stone E.C., Composition, gradients and temporal variations of the anomalous cosmic-ray component, Solar wind VI proceedings (ed. Pizzo V.J.), 2, 599, 1988

Cummings A.C., Stone E.C. and Webber W.R., Time variation and radial and latitudinal gradients of anomalous cosmic ray oxygen in the outer heliosphere, 21st ICRC (Adelaide), 6, 190, 1990a

Cummings A.C., Mewaldt R.A., Stone E.C. and Webber W.R., Radial and latitudinal gradients of anomalous cosmic ray oxygen and helium from 1 to ~41 AU, 21st ICRC (Adelaide), 6, 206, 1990b

Cummings A.C. and Stone E.C., Elemental composition of the very local interstellar medium as deduced from observations of anomalous cosmic rays, 21st ICRC (Adelaide), 6, 202, 1990c

Dietrich W.F., The differential energy spectra of solar flare ^{1}H, ^{3}He and ^{4}He, Ap.J., 180, 955, 1973

Durgaprasad N., Ionization states and the origin of low energy cosmic ray nuclei, Ap. Space Sci., 47, 435, 1977

Durgaprasad N. and Biswas S., Ionization states and origin of low energy (1-30 MeV/amu) cosmic ray nuclei, 15th ICRC (Plovdiv), 2, 103, 1977

Eichler D., Particle acceleration in collision shocks: regulated injection and high efficiency, Ap.J., 229, 419, 1979

Enge W., Introduction to plastic nuclear track, Nucl. Tracks, 4, 283, 1980

Fanselow J.L. and Stone E.C., Geomagnetic cutoffs for cosmic-ray protons for seven energy intervals between 1.2 and 39 MeV, JGR, 77, No 22, 3999, 1972

Fan C.Y., Gloeckler G. and Hovestadt D., Energy spectrum and charge state of H, He and heavy ions observed in the earth's magnetotail and magnetosheath, Phys. Rev. Letts., 34, 495, 1975

Fermi E., On the origin of the cosmic radiation, Phys Rev., 75, 1169, 1949

Ferrando P., Lal N. and McDonald F.B., Elemental composition of low energy galactic cosmic rays, Proc. Symp. on Cosmic Abundances of Matter (Minneapolis), 1988

Fisk L.A., Kozlovsky B. and Ramaty R., An interpretation of the observed oxygen and nitrogen enhancements in low-energy cosmic rays, Ap.J., 190, L35, 1974

Fisk L.A., ^{3}He-rich flares: A possible explanation, Ap.J., 224, 1048, 1978

Fisk L.A., Private communication, 1983

Fleischer R.L., Price P.B. and Walker R.M., Nuclear Tracks in Solids, Univ. of Cal. Press, 1975

Fluckiger E.O., Effects of asymmetric magnetic currents radiation, Reports, AFGL-TR-82-0177, 1982

Fowler P.H., Redfern R.M. and Swordy S.P., Cometary origin of anomalous cosmic rays, Nature, 279, 622, 1979

Freden S.C. and White R. S., Trapped proton and cosmic ray albedo neutron fluxes, JGR, 67, 25, 1962

Garcia-Munoz M., G.M Mason and Simpson J.A., New test for solar modulation theory: the 1972 May-July low energy galactic cosmic ray proton and helium spectra, Ap.J., 182, L81, 1973

Garcia-Munoz M., Simpson J.A., Guzik T.G., Wefel J.P. and Margolis S.H., Cosmic ray propagation in galaxy and in the heliosphere: The path-length distribution at low energy, Ap.J. Suppl., 64, 269, 1987a

Garcia-Munoz M., Pyle K.R. and Simpson J.A., The anomalous helium component in the heliosphere: The 1 AU spectra during the cosmic ray recovery from the 1981 solar maximum, 20th ICRC (Moscow), 3, 438, 1987b

Garcia-Munoz M., Pyle K.R. and Simpson J.A., Solar modulation in the heliosphere: time and space variations of anomalous helium and galactic cosmic rays, 21 ICRC (Adelaide), 6, 164, 1990

Garrard T.L., Stone E.C. and Vogt R.E., The isotopes of H and He in solar cosmic rays, in Proc. Symp. High Energy Phenomena on the Sun (NASA SP-342), 341, 1973

Gleeson L.J. and Axford W.I., Solar modulation of galactic cosmic rays, Ap.J., 154, 1011, 1968

Gloeckler G., Sciambi R.K., Fan C.Y. and Hovestadt D., A direct measurements of the charge states of energetic iron emitted by the sun, Ap.J. Letts., 209, L93, 1970

Gloeckler G., Compositions of energetic particle populations in interplanetary space, Rev. of Geophys and Space Phys., 17, No. 4, 1979

Goswami J.N., McGuire R.E., Reddy R.C., Lal D. and Jha R., Solar flare protons and alpha particles during last three solar cycles, JGR, 93, 7195, 1988

Gredel R., Lepp S. and Dalgarno A., The C/CO ratio in dense interstellar clouds, Ap.J. Letts., 323, L137, 1987

Henke R.P. and Benton E.V., On geometry of tracks in dielectric nuclear track detectors, NIM, 97, 483, 1971

Henke R.P. and Benton E.V., A program to calculate the range and energy-loss rate of charged particles in stopping media, in 'Solid State Nuclear Track detectors', Pergamon press, 275, 1987

Hertzen G.P. and Marenny A.M., Time resolution equipment for registration of cosmic rays in solid state nuclear track detectors, Nuclear Tracks, 12, 435, 1986

Hovestadt D., Vollmer O., Gloeckler G. and Fan C.Y., Differential energy spectra of low-energy (<8.5 MeV per nucleon) heavy cosmic rays during solar quiet times, Phys. Rev. Letts., 31, 650, 1973

Hovestadt D., Klecker B., Laeverenz P., Seidenschwang E., Mason G.M., Bedini P.B., Gloeckler G., Hamilton D.C., Blake J.B., Chenette D., Experiment for charge determination of cosmic rays of interplanetary and solar origin on the space shuttle, Proc. 21st ICRC (Moscow), 4, 406, 1987

Hoyle F. and Clayton D.D., Nucleosynthesis in white-dwarf atmosphere, Ap.J., 191, 705, 1974

IAGA, International geomagnetic reference field revision 1985, IAGA Division I Working Group 1 (Barraclough D.R.), 1985

Jordon C., The ionization equilibrium of elements between carbon and nickel, Mon. Not. Roy. Astron. Soc., 142, 501, 1969

Kaplon M. F., Peters B., Reynolds H.L. and Ritson D.M., The energy spectrum of cosmic radiation, Phys. Rev., 85, 295, 1952

Klecker B., Hovestadt D., Gloeckler G. and Fan C.Y., On the charge state of the anomalous oxygen component, Geophys. Res. Letts., 7, 1033, 1980

Kocharov L.G. and Kocharov G.E., ^{3}He-rich solar flares, Sp. Sci. Rev., 38, 89, 1984

Kodama M. and Miyazaki Y., Geomagnetic latitude effect of the cosmic ray nucleon and meson components at sea level from Japan to the Antarctic, Rep. of Ionosphere Res. in Japan, 11,99,1957

Kuznetsov S.N., Lutsenko V.N., Vandas M., Fischer S. and Kudela K., Charge state of nuclei accelerated in the February 13, 1978 flare, 21st ICRC (Moscow), 3, 252, 1987

Langel R.A, Estes R.H. and Mead G.D., Some new methods in geomagnetic field modeling applied to the 1960-1980 epoch, J.Geomag. Geoelectr., 34, 327, 1982, 1982

Lin R.P., Observation of suprathermal particles in the interplanetary medium, Solar Wind- IV, (ed. Rosenbaure H.), 463,1981

Luhn A., Hovestadt D., Klecker B., Scholar M., Gloeckler G., Ipavich F.M., Galvin A.B., FAn C.Y. and Fisk L.A., The mean ionic charge of N, Ne, Mg, Si and S in solar energetic particle events, Proc. 19th ICRC (La Jolla), 4, 241, 1985

Luhn A., Klecker B., Hovestadt D. and Mobius E., The mean ionic charge of silicon ^{3}He-rich solar flares, Ap.J., 317, 951, 1987

Marochnik L.S., Mukhin L.M. and Sagdeev R.Z., Estimates of mass and angular momentum in Oort cloud, Science, 242, 547, 1988

McCraken K.G., Rao U.R. and Shea M.A., The trajectories of cosmic rays in a high degree simulation of the geomagnetic field, Teck. Rept. 77, MIT, 1962

McDonald F.B., Study of geomagnetic cutoff energies and temporal variation of the primary cosmic radiation, Phys. Rev., 107, 1386, 1957

McDonald F.B., Teegarden B.J., Trainor J.H. and Webber W.R., The anomalous abundance of cosmic-ray nitrogen and oxygen nuclei at low energies, Ap.J. Letts., 187, L105, 1974

McDonald F.B., Lal N., Trainor J.H., Van Hollebeke M.A.I. and Webber W.R., Observations of galactic cosmic-ray energy spectra between 1 to 9 AU, Ap.J., 216, 930, 1977

McDonald F.B. and Lal N., Variations of galactic cosmic rays with heliolatitude in the outer heliosphere, Geophys. Res. Letts., 13, 781, 1986

McDonald F.B., Lal N., Perko J.S., von Rosenvinge T.T. and Webber W.R., The charge state of the anomalous cosmic-ray component, Ap.J., 333, L109, 1988

McDonald F.B., Lal N. and Perko J.S., Search for the anomalous cosmic ray hydrogen component, 21st ICRC (Adelaide), 6, 185, 1990

McGowan N., A detector to investigate the anomalous component of cosmic rays and its rarer constituents including a possible molecular ion component, in 'Composition and Origin of Cosmic Rays', ed Shapiro M.M., 309, 1983

McGuire R.E., Von Rosenvinge T.T. and McDonald F.B., Energy dependence in solar cosmic ray composition, 17th ICRC (Paris), 10, 33, 1981

McGuire R.E., von Rosenvinge T.T and McDonald F.B., The composition of solar particles, Ap.J., 301, 938, 1986

Mckibben R.B., An experimental test for the charge state of the anomalous helium component, Ap.J. Letts., 217, L113, 1977

Mewaldt R.A., Spalding J.D., Stone E.C. and Vogt R.E., Isotopic measurement of energetic heavy nuclei in solar flares, Bull. Am. Phys. Soc., 24, 694, 1979

Mewaldt R.A., Spalding J.D. and Stone E.C., The isotopic composition of the anomalous low energy cosmic rays, Ap.J., 283, 450, 1984

Mewaldt R.A., The abundances of isotopes in the cosmic radiation, Proc. AIP conference, SRL 88-11, December, 1988

Mewaldt R.A., Temporal variations of anomalous cosmic rays and further evidence for anomalous cosmic ray hydrogen, 21st ICRC (Adelaide), 6, 160, 1990

Mihalov J.D. and White R.S., The low energy proton radiation belts, JGR, 71, 2207, 1966

Mogro-Campero A. and Simpson J.A., Identification and relative abundances of C, N and O nuclei trapped in the geomagnetic field, Phys. Rev. Letts, 25, 1631, 1970

Mogro-Campero A., Geomagnetically trapped carbon, nitrogen, and oxygen nuclei, JGR, 77, 2799, 1972

Neugebaure M. and Snyder C.W., Mariner 2 observations of the solar wind,1,Average properties., JGR, 71, 4469, 1966

Nikoleav V.S., Electron capture and loss by fast ions in atomic collisions, Soviet Physics Uspekhi, 8, 269, 1965

O'Gallagher J.J., A time-dependent diffusion convection model for the long term modulation of cosmic rays, Ap.J., 197, 495, 1975

O'Gallagher J.J. and Masylar G.A. III, A dynamic model for the time evolution of the modulated cosmic ray spectrum, JGR, 81, 1319, 1976

Oschiles K., Beaujean R. and Enge W., On the charge state of anomalous oxygen, Ap.J., 345, 776, 1989

Parker E.N., Dynamics of the interplanetary gas and magnetic fields, Ap.J., 128, 664, 1958

Parker E.N., in "Interplanetary Dynamical Process", Newyork: Intersciences, 1963

Pesses M.E., Jokipii J.R. and Eichler D., Cosmic ray drift, shock wave acceleration and the anomalous component of cosmic rays, Ap.J. (Letts), 246, L85, 1981

Pfotzer G., Proc. Varenna Conference, 1957

Potgieter M.S. and Moraal H., A drift model for the modulation of cosmic rays, Ap.J., 294, 425, 1985

Potgieter M.S. and Moraal H., On the acceleration and modulation of the anomalous cosmic ray component, 20th ICRC (Moscow), 3, 464, 1987

Price P.B., Hutcheon I.D., Cowsik R. and Barber D.J., Enhanced emission of iron nuclei in solar flares, Phys. Rev. Letts., 26, 916, 1971

Quenby J.J. and Webber W.R., Cosmic ray cutoff rigidities and the earth's magnetic field, Phil. Mag., 4, 90, 1959

Ramaty R., Colgate S.A., Dulk G.A., Hoyng P., Knight J.W., Lin R.P., Melrose D.B., Paizis C., Orrall F., Shapiro P.R., Smith D.F. and van Hollebeke M., in Solar Flares, A Monograph from the Skylab Solar Workshop II, ed. Sturrock P.A., 117, 1980

Reams D.V., Energetic particles from impulsive solar flares, Ap.J. (Suppl.), 73, 235, 1990

Rose D.C.,Fenton K.B., Katzman J. and Simpson J.A., Latitude effect on the cosmic ray nucleon and meson component at sea level from the Arctic to the Antarctic, Canad. J. Phys., 34,968, 1956

Ross J.E. and Aller L.A., The chemical composition of Sun, Science, 191, 1223, 1976

Rothwell R. and Quenby J.J., Proc. Varenna Conference, 1957

Rule D.W. and Omidvar K., Charge equilibrium and radiation of low energy cosmic rays passing through interstellar medium, Ap.J., 229, 1198, 1979

Saito T., Hatano Y., Fukada Y. and Oda H., Is there Strange-Quark matter in galactic cosmic rays, Phys. Rev. Letts., 65, 2094, 1990

Sciambi R.K., Gloeckler G., Fan C.Y. and Hovestadt D., Direct measurement of the ionization states of energetic carbon and oxygen emitted by the sun, Ap.J., 214, 316, 1977

Shea M.A., Smart D.F., McCracken K.G. and Rao U.R., Asymptotic directions, Variational coefficients and Cutoff rigidities, Report, AFCRL-68-0030, 1968

Shea M.A., Smart D.F, McCall J.R. and Gumm B.S., Tables of asymptotic directions and vertical cutoff rigidities for a five degree by fifteen degree world grid using the Finch and Leaton geomagnetic field model, Report, AFCRL-TR-75-0042, 1975

Shea M.A. and Smart D.F., Vertical cutoff rigidity of five degree by five degree world grid, private communication, 1988

Silberberg R., Tsao C.H., Letaw J.R. and Shapiro M.M., Distributed acceleration of cosmic rays, Phys. Rev. Letts., 51, 1217, 1983

Simpson J.A., Proc. Varenna Conference, 1957

Simpson J.A., Introduction to the galactic cosmic radiation, in 'Composition and origin of cosmic rays', ed. M.M.Shapiro, 1, 1983a

Simpson J.A., private communication, 1983b

Singer S.F., Radiation belt and trapped cosmic ray albedo, Phys. Rev. Letts., 1, 181, 1958

Singh R.K., Ionization States of Anomalous Cosmic Rays, Ph.D. Thesis, Bombay University, 1990

Skorka S., Breiteneffekt der nukleonen-und mesonenkomponente der ultrastrahlung im meereshohe im Indischem und Atlantischen, Z.phys., 151, 630, 1958

Smart D.F., Shea M.A. and Gall R., The daily variation of trajectory-derived high-latitude cutoff rigidities in a model magnetosphere, JGR, 74, 4731, 1969

Smart D.F. and Shea M.A., Daily variation of electron and proton geomagnetic cutoffs calculated for Fort Churchill, Canada, JGR, 77, No 25, 4595, 1972

Smart D.F. and Shea M.A., Galactic cosmic radiation and solar energetic particles, in 'HandBook of Geophysics and the Space Environment', ed. Jursa A.S., Chapter 6, p 6-8, 1985

Solar Geophysical Data, Prompt Reports, No.491, 1985

Solar Geophysical Data, Part-II, No.510, 1987

Stormer C., Periodische elektronenbahen im felde eines elementarmagnetem und ihre anwendung auf bruches modellversuche und auf eschenhagans elementarwellen des erdmagnetismus, Z. Astrophys., 1, 237, 1930

Strong K., Private communication, 1989

Vahia M.N. and Biswas S., Solar energetic particle studies, in Composition and origin of cosmic rays ,ed. M.M.Shapiro, 155, 1983

Vallarta M.S., On the energy of cosmic radiation allowed by the earth's magnetic field, Phys. Rev., 74, 1837, 1948

Van Allen J.A., Ludwig G.H., Ray E.C. and McIlwain C.E., "Observation of high-intensity radiation by satellites 1958 alpha and gamma", Jet Propulsion, 28, 588, 1958

Van Allen J.A., Randall B.A. and Krimigis S.M., Energetic carbon, nitrogen and oxygen nuclei in the earth's outer radiation zone, JGR, 75, 6085, 1970

Venkatesan D., Cosmic ray picture of the heliosphere, Johns Hopkins APL technical digest, 6, 4, 1985

Vette J.I., Magnetospheric particle population, in 'Earth, Particles and Fields', ed. B.M. McCormac, 1971

Volk H.J., Cosmic ray sources: II. Acceleration, Proc. 17th ICRC (Paris), 13, 131, 1981

Wadditington C.J., Observations on the multiply charged particles of the cosmic radiation, Nuovo Cim. Ser. X, 3, 930, 1956

Wandel A, Eichler D.S., Letaw J.R., Silberberg R. and Tsao C.H., Distributed reacceleration of cosmic rays, Ap.J., 316, 676, 1987

Webber W.R., The spectra of cosmic ray nuclei > 1GeV/nuc - implications for acceleration and propagation, in 'Composition and origin of cosmic rays', ed. Shapiro M.M., 25, 1983

LIST OF PUBLICATIONS

1. The ionization state of oxygen ions in anomalous cosmic rays: Results from the Anuradha experiment in Spacelab-3.

   S.Biswas, N.Durgaprasad, Banashree Mitra, R.K.Singh, M.N.Vahia, J.S.Yadav, **A.Dutta** and J.N.Goswami, **Astrophys. Space Sci., 149**, 357-367, 1988.

2. Studies of anomalous cosmic ray oxygen ions in space and their ionization states in Anuradha experiment in Spacelab-3.

   B.Mitra, S.Biswas, N.Durgaprasad, R.K.Singh, M.N.Vahia, **A.Dutta** and J.N.Goswami, **Adv. Sp. Res., 9**, No.12, 17-20, 1989.

3. Observation of enhanced Sub-iron (Sc-Cr) to iron ratio in low energy cosmic rays of 50-100 MeV/N in Spacelab-3.

   S.Biswas, N.Durgaprasad, Banashree Mitra, R.K.Singh, M.N.Vahia, **A.Dutta** and J.N.Goswami, **Adv. Sp. Res., 9**, No.12, 25-28, 1989.

4. Observation of low-energy (30-100 MeV nucleon^{-1}) partially ionized heavy ions in galactic cosmic rays.

   S.Biswas, N.Durgaprasad, B.Mitra, R.K.Singh, **A.Dutta** and J.N.Goswami, **Ap.J. (Letters), 359, L5,** 1990

5. Ionization states of anomalous cosmic ray nitrogen to neon ions in Spacelab-3 Anuradha experiment.

   Banashree Mitra, S.Biswas, R.K.Singh, M.N.Vahia, **A.Dutta** & J.N.Goswami, **Indian Journal of Physics, 64A(3)**, 201-206, 1990.

6. Cosmic Ray propagation studies from sub-iron and iron abundances in Spacelab-3 Anuradha experiment.

   N.Durgaprasad, S.Biswas, B.Mitra, R.K.Singh, M.N.Vahia, **A.Dutta** and J.N.Goswami, **Indian Journal of Physics, 64A(3)**, 175-181, 1990.

7. Ionization states of the Anomalous Cosmic Rays.

R.K.Singh, S.Biswas, N.Durgaprasad, B.Mitra, **A.Dutta** and J.N.Goswami, **Ap.J.,** To be published in June 10,1991 Issue

8. Ionization states of anomalous cosmic rays in Spacelab-3.

S.Biswas, N.Durgaprasad, **A.Dutta**, J.N.Goswami, D.Lal, R.K.Singh, M.N.Vahia, J.S.Yadav, **Proc. 20th International Cosmic Ray Conf., 3**, 451-453, (Moscow), 1987.

9. Flux and energy spectra of helium and oxygen group ions of anomalous cosmic rays in Spacelab-3.

S.Biswas, N.Durgaprasad, **A.Dutta**, J.N.Goswami, P.J.Kajarekar, D.Lal, R.K.Singh, M.N.Vahia and J.S.Yadav, **Proc. 20th International Cosmic Ray Conf., 3**, 454-457, (Moscow), 1987.

10. Spacelab-3 observations on flux of anomalous cosmic rays of Si group and Fe group nuclei of 10-100 MeV/n.

S.Biswas, N.Durgaprasad, **A.Dutta**, J.N.Goswami, P.J.Kajarekar, R.K.Singh, M.N.Vahia and J.S.Yadav., **Proc. 20th International Cosmic Ray Conf., 3**, 458-459, (Moscow), 1987.

11. Flux, Composition and ionization states of Anomalous cosmic rays in the "Anuradha" in Spacelab-3.

J.N.Goswami, S.Biswas, N.Durgaprasad, **A.Dutta**, R.K.Singh and M.N.Vahia., **In Proc. Fifth National Seminar on Solid State Nuclear Track Detectors**, (Ed.B.B.Baliga), pp.5-13, 1988.

12. Measurements of ionization states of anomalous cosmic rays in Spacelab-3.

R.K.Singh, B.Mitra, N.Durgaprasad, S.Biswas, **A.Dutta** and J.N.Goswami, **Proc. 21st International Cosmic Ray Conf., 6**, 168-171, (Adelaide) 1990.

13. Experimental observation of partially ionized iron group (Z=21-26) ions in the low energy galactic cosmic rays in Spacelab-3.

S.Biswas, N.Durgaprasad, B.Mitra, R.K.Singh, **A.Dutta** and J.N.Goswami, **Proc. 21st International Cosmic Ray Conf., 3**, 23-25, (Adelaide), 1990.

14. Implications of the observation of partially ionized iron group ions in low energy cosmic rays.

S.Biswas, N.Durgaprasad, B.Mitra, R.K.Singh, **A.Dutta** and J.N.Goswami, **Proc. 21st International Cosmic Ray Conf., 3**, 385-388, (Adelaide), 1990.

15. Spacelab-3 observations of enhanced sub-iron (Sc-Cr) to iron abundance ratios in the low energy (30-100 MeV/N) galactic cosmic rays.

N.Durgaprasad, B.Mitra, R.K.Singh, S.Biswas, **A.Dutta** and J.N.Goswami, **Proc. 21st International Cosmic Ray Conf., 3**, 389-392, (Adelaide), 1990.

16. Solar modulation of oxygen ions with energy below 200 MeV/N during last Solar minimum.

Dutta A., Proc. 21st International Cosmic Ray Conf., 6, 384-386, (Adelaide),1990.